Use of small extracellular vesicles for diagnosis of *Mycoplasma bovis*

A thesis presented in partial fulfilment of the requirements for the degree of

Master of Science [MSc] in Genetics

at Massey University, Manawatū, New Zealand.

Joel Thomas Pratt

2022

Abstract

Background: *Mycoplasma bovis* (***M. bovis***) is a pathogenic bacterium responsible for causing numerous production and welfare issues in cattle herds. Eradication efforts worldwide are limited by ineffective antibiotics, intracellular infection of host cells, immune evasion, and insufficient diagnostic tools. Current diagnostic tests are inadequate to assess *M. bovis* infection as they rely upon direct detection of *M. bovis* or indirect detection via serology (*M. bovis*–specific antibodies). Therefore, with aim to improve diagnostics of *M. bovis* infection, small extracellular vesicles (**sEV**s) were utilised. These nanoparticles act as intercellular messengers and contain material representative of their cell of origin. Their use as diagnostic and therapeutic tools has enabled a variety of diseases and infections to be assessed and/or treated.

The aim of this project was to develop an upscaled *in vitro* model of *M. bovis* infection within a bioreactor flask to test the hypothesis that the protein cargo of host cell sEVs were altered in response to *M. bovis* infection.

Methods: A control culture of a bovine endometrial epithelial cell line (**bEEL** cells) and a co–culture of bEEL cells and *M. bovis* were established within bioreactor flasks. Using Size Exclusion Chromatography columns, sEVs were isolated from the harvests of the bioreactor flasks. Liquid Chromatography Tandem Mass Spectrometry assessed the sEV proteome to compare differences created by *M. bovis* infection.

Results: Infection was indicated by a continued presence of *M. bovis* within the co–culture. Changes in the regulation of various proteins, such as inhibition of host cell endopeptidases, was demonstrated in co–culture sEVs as a response to *M. bovis* infection. Adherence of *M. bovis* to bEEL cells was certain, but intracellular infection remained inconclusive.

Conclusion: Data from this study implies that a co–culture can be successfully established within a bioreactor flask, and that the proteome of sEVs is altered in response to infection by *M. bovis*.

Acknowledgments

First and foremost, I would like to thank my supervisors.

Axel, the chance you took taking me on initially as your intern has meant everything. Thank you for providing me with such an incredible opportunity and all your advice on how to become a better scientist.

Mal, your tips and tricks for writing has influenced the entirety of my thesis. Thank you for having me as your student and setting the standards that I am continually striving to achieve.

Alice, without your enormous efforts in mentoring me, I would not be the capable scientist that you have shaped me into. Thank you for keeping me sane throughout the many hours of experiments and being the continued voice of encouragement within every research decision.

Rao, your immunology lectures set me on the path that I wanted to become as a scientist. Thank you for being the initial inspiration and what that has eventuated into.

Secondly, to Dr. Evelyne Maes and the proteomics team at Lincoln. Without your considerable efforts, the entire project would have stalled significantly. Thank you all immensely for the many hours spent processing and analysing our complex samples.

Thirdly, I would like to thank Professor Murray Mitchell for providing the bovine cell line. Without these cells, my ability to create the infection model would still only be a dream. Likewise, I want to thank Hector Goodoy and Daniel Maxwell (Auckland Biosciences) for providing the porcine serum. Your timely supply aided the progression of our project greatly.

My deepest appreciation is to the New Zealand Ministry for Primary Industries for providing the funding and supply of *Mycoplasma bovis* isolates that enabled our project to commence. Wanting to improve the diagnostics of *Mycoplasma bovis* has continued to be a substantial factor in my strive for success.

Last, but by no means least, I would like to thank my partner and all my family.

Michaela, your support has been instrumental in allowing me to develop into who I am today. Thank you for being the calm within the storm and helping me to balance the weight of all things in life.

Mum, Dad, and Kelsie, without you all I would not be the person that I am. Thank you all so much for always being there and giving me the means that I needed to grow, learn, and succeed.

Table of Contents

i. List of Figures

ii. List of Tables

iii. List of Abbreviations

Aβ	Amyloid–beta
ACN	Acetonitrile
ADP	Adenosine diphosphate
Ambic	Ammonium bicarbonate
ALK	Anaplastic lymphoma kinase
APP	Amyloid Precursor Protein
ARF6	ADP–ribosylation factor 6
aRPMI	Advanced Rosewell Park Memorial Institute 1640 medium
BCA	Bicinchoninic acid
bEEL cells	Bovine Endometrial Epithelial cell Line
BRD	Bovine Respiratory Disorder
CCU	Colour Change Units
CFU	Colony Forming Units
CO2	Carbon dioxide
Da	Dalton
DAPI	4′,6–diamidino–2–phenylindole
DNA	Deoxyribonucleic acid
dNTP	Deoxynucleoside triphosphate
EGFR	Epidermal Growth Factor Receptor
ELISA	Enzyme–Linked Immunosorbent Assay
EM	Electron Microscopy
EML4	Echinoderm Microtubule–associated protein–Like 4
ESCRT	Endosomal Sorting Complex Required for Transport
FA	Friis Agar
FB	Friis Broth
FBS	Foetal Bovine Serum
FDR	False Discovery Rate
FITC	Fluorescein isothiocyanate
g	Grams
GTPase	Guanosine triphosphatase
Hz	Hertz

ILV	Intraluminal Vesicle
IU/mL	International Units/millilitre
kDa	Kilodaltons
L	Litre
LC–MS/MS	Liquid Chromatography Tandem Mass Spectrometry
M	Molar
mbar	Millibar
M. bovis	*Mycoplasma bovis*
mg/mL	Milligram/millilitre
MISEV (2018)	Minimal Information for Studies of Extracellular Vesicles (2018)
mL	Millilitre
mm	Millimetre
mM	Millimolar
MOI	Multiplicity of Infection
M. ovi	*Mycoplasma ovipneumoniae*
MSC	Mesenchymal Stromal Cells
M. tuberculosis	*Mycobacterium tuberculosis*
MVB	Multivesicular Body
MVE	Multivesicular Endosome
nA	Nanoampere
ng/µL	Nanogram/microlitre
nm	Nanometre
NZ	New Zealand
PC2	Physical Containment level 2
PC3	Physical Containment level 3
PCA	Principal Component Analysis
PCR	Polymerase Chain Reaction
ppm	Parts per million
qPCR	Quantitative Polymerase Chain Reaction
R18	Octadecyl Rhodamine B Chloride
RAB	Ras-associated binding protein
RAL–1	(Ras–related GTPase) homolog

rcf	Relative centrifugal force
RIPA	Radioimmunoprecipitation Assay
RNA	Ribonucleic acid
rRNA	Ribosomal Ribonucleic acid
rpm	Rotations per minute
RPMI 1640	Rosewell Park Memorial Institute 1640 medium
SARS–CoV–2	Severe Acute Respiratory Syndrome Coronavirus 2
sbsp.	Subspecies
SDC	Sodium deoxycholate
SEC	Size Exclusion Chromatography
S. enterica	*Salmonella enterica* serovar Typhimurium
SNAP23	Synaptosomal–associated protein 23
SNARE	Soluble N-ethylmaleimide-Sensitive Factor Attachment Receptor
sp.	Species
ssp.	Species (plural)
sEV	Small Extracellular Vesicles
SYX–5	Syntaxin 5
T75	Nunc EasYFlask 75 cm^2
TBS–T	1x Tris–Buffered–Saline Tween 20
TEM	Transmission Electron Microscopy
TGN	Trans–Golgi network
TNF–α	Tumour Necrosis Factor α
TRPS	Tunable Resistive Pulse Sensing
US	United States
USA	United States of America
V	Volts
v/v	Volume to volume
VAMP3	Vesicle–associated membrane protein 3
W	Watt
w/v	Weight to volume

1x PBS	1x Phosphate Buffered Saline
°C	Degrees Celsius
µg	Microgram
µg/mL	Microgram/millilitre
µg/µL	Microgram/microlitre
µL	Microlitre
µm	Micrometre

1 Introduction and Literature Review

On the 22nd of July 2017, samples taken from cattle on a South Canterbury dairy herd tested positive for *Mycoplasma bovis* (***M. bovis***). Until this point, *M. bovis* had not been detected in New Zealand cattle (Government, 2017).

A joint announcement on the 28th May 2018 by the New Zealand government, alongside the dairy and beef industries, stated that an attempt would be made to eradicate *M. bovis* from New Zealand (Biosecurity, 2020).

The *M. bovis* Science Plan was released in October 2018, with aim to identify the priority sciences needed to eradicate *M. bovis* from New Zealand farms (Government, 2018). Research is currently occurring in seven specific areas (epidemiology, diagnostics, direct impacts of the disease, entry pathways, behaviour drivers and incentives, social impacts, and economic impacts), with five areas focused on gathering information to understand disease development, which further supports *M. bovis* eradication efforts.

The Animal Health Laboratory team have tried to ensure an accurate assessment of infected properties by assessing blood and milk samples for measuring *M. bovis* infection.

Tests with high specificity and sensitivity from the commercially available enzyme–linked immunosorbent assays (**ELISA**) and real–time quantitative PCR (**qPCR**) tests are currently being used (Dudek et al., 2020).

The *M. bovis* Science Plan identified that a novel assay was necessary to identify cases of disease in the absence of seroconversion or *M. bovis* shedding (Government, 2018).

A team at AgResearch, led by Dr. Mallory Crookenden, has been awarded funding from the New Zealand Ministry for Primary Industries for development of a new assay for diagnosing *M. bovis* infection. If successful, the proposed assay would provide an alternative tool to aid assessment of *M. bovis* in the absence of bacterial shedding or if any of the currently used assays failed to detect an anti-*M. bovis* antibody response.

The test would involve identifying bacterial protein signatures within circulating nanoparticles known as small Extracellular Vesicles (**sEV**s) in the serum of healthy/infected cows and within a cell culture model of *M. bovis* infection. In diseased animals, it is thought that sEVs secreted from cells containing *M. bovis* will contain proteins that are specific to infection and enable identification of *M. bovis* without prior exposure of the bacterium to the host immune system. The research presented in this thesis contributed to this project.

1.1 Mycoplasma bovis

Mycoplasma spp. represent a range of prokaryotes that infect numerous animal species throughout the world. All *Mycoplasma* ssp. are formed as a gram–negative coccus bound by a triple–layered plasma membrane; however, as they lack a cell wall, they are classed as Mollicutes (Razin, 2018).

Mycoplasma spp. are classified amongst the smallest self–replicating anaerobic bacteria, ranging in size from 0.2–0.8 µm, with a limited genome (0.58–2.2 megabases) as a result of their size (Rosenberg et al., 2014; Labroussaa et al., 2016). Likewise, cellular machinery that are responsible for metabolic growth and replication of mycoplasma cells are minimal, limited to structures such as ribosomes and plasma membranes (Borchsenius et al., 2020).

Mycoplasma ssp. exist as a parasitic bacterium *in vivo*, requiring a host cell for their continued survival (Breuer et al., 2019). For example, *M. bovis* is a *Mycoplasma* sp. that infects bovine animals.

Mycoplasma ssp. interact with their host cell either by adherence to the cell surface or by intracellular infection (Hoelzle et al., 2020). It is currently unknown if either method is solely responsible for infection of host cells, or if a combination of these processes is required for successful infection.

1.1.1 Incidence and economic impact

First isolated from a dairy cow with mastitis on a farm in the United States of America (**USA**) in 1961 (Hale et al., 1962), *M. bovis* has since been observed worldwide and now affects every major cattle–rearing country (Dudek et al., 2020). *Mycoplasma bovis* causes bovine mycoplasmosis, which manifests as mastitis (Timonen et al., 2017), bronchopneumonia (Oliveira et al., 2021), arthritis (Nishi et al., 2021b), a range of fertility/genital issues (Peippo et al., 2020), keratoconjunctivitis (Kneipp, 2021), and increased animal fatigue (Calcutt et al., 2018).

It is also a substantial factor that aids in development of bovine respiratory disorder (**BRD**), a disease complex that presents as a high fever and increased coughing (Oliveira et al., 2020). Whilst many bovine pathogens can cause mastitis, co–infection of *M. bovis* increases the occurrence of mastitis symptoms in more than one udder quarter, resulting in an increased somatic cell count in bulk milk (Al-Farha et al., 2017).

Cattle infected with *M. bovis* are most prevalent in the USA, with rates of infection increasing in European and Middle Eastern countries (Nicholas et al., 2016). In England and Wales, *M. bovis* is the most frequently identified pathogenic organism in cattle (Deeney et al., 2021).

Severe issues arise regarding animal welfare and production, where economic loss for farmers can be substantial. In the USA, annual costs associated with treating *M. bovis*–induced BRD have been estimated to be 55 million US dollars (Johnson & Pendell, 2017).This estimate excluded production costs associated with morbidity and mortality of cattle, meaning the loss associated with *M. bovis* is likely greater. Loss was associated with costs such as treatment, reduced rates of fertility and premature culling of calves (Maunsell & Donovan, 2009; Perez-Casal, 2020).

If *M. bovis* infection had continued to spread uncontrollably throughout New Zealand, a billion dollar loss was estimated over a ten–year period (O'Connor, 2020). Compared to compensation to farmers for their loss of cattle and production, which is currently 212 million NZ dollars over a three–year period (Biosecurity, 2021), eradication of *M. bovis* from New Zealand farms reduced the economic impact that *M. bovis* would create. More importantly, it mitigates long–term effects on animal welfare that a widespread *M. bovis* outbreak would cause.

1.1.2 Transmission and zoonosis

Risk of zoonosis caused by a species of Mollicutes is low, with only a few cases reported of human infection (Heller et al., 2015; Matet et al., 2020). However, there are limited reports demonstrating *M. bovis* infection occurs in other ruminant species such as bison, deer, and pronghorns (Register et al., 2019; Malmberg et al., 2020).

Risk of infection can be significant for naïve farms in terms of international cattle trade and is dependent on hygienic farming practices (Amram et al., 2013). Contamination by *M. bovis* occurs within several bovine products, such as milk, semen, and meat, which increases losses associated with discarding products. Infected semen is a major source of *M. bovis* transfer between countries, increasing prevalence of disease when imported to countries with low rates of infection (Haapala et al., 2018).

On farm, calves raised on milk contaminated with *M. bovis* demonstrated increased rates of BRD with disease development resulting in major economic impact and animal loss (Arcangioli et al., 2021). Loss of replacement heifers as a consequence of *M. bovis* infection contributes to further economic losses and reduces the ability of farmers to genetically improve their herds (Hazelton et al., 2020b).

There are many challenges attributed to complete eradication of *M. bovis* from cattle herds. Resistance in *Mycoplasma* ssp. to many previously effective antibiotics has developed continually, with *M. bovis* not an exception, (Ledger et al., 2020). Challenges associated with eradication are partially related to *M. bovis* size or its route of infection, enabling *M. bovis* to excel in avoiding immune cells. This leads to a reduction in measurable immune responses required for detection of *M. bovis*.

All age groups of cattle can be infected by *M. bovis,* facilitated by bacterial shedding/increased animal stress, and results in persistence of *M. bovis* within cattle herds months following initial infection (Vähänikkilä et al., 2019; Becker et al., 2020).

1.1.3 Diagnosis of *M. bovis*

Currently, no vaccine exists for aiding resistance to *M. bovis* infection within cattle herds (Dudek et al., 2021). Therefore, a heavy reliance on diagnostic assays is the only way to assess infection status and subsequently reduce spread of *M. bovis*. Current commercial detection kits of *M. bovis* infection rely upon Polymerase Chain Reaction (**PCR**), ELISA, or bacteriological culturing (Mehmet Akan et al., 2014; Parker et al., 2018)

1.1.4 Polymerase Chain Reaction (PCR)

Using PCR, *M. bovis* deoxyribonucleic acid (**DNA**) is amplified from swabs taken directly from tissue or milk of infected animals. Both the type of tissue swabbed and prevalence of bacterial shedding within this tissue can drastically alter detection of *M. bovis* (Hazelton et al., 2018).

In a comparison using a variety of commercially available DNA extraction and PCR kits, *M. bovis* detection from the same samples were comparable between independent laboratories (Wisselink et al., 2019). However, PCR test results (cycle–threshold values) frequently represented weak positive results of non–target *Mycoplasma* ssp., with a laboratory alternatively diagnosing *Mycoplasma agalactiae* instead of *M. bovis*. This false positive diagnosis cemented a substantial issue related to many real–time and end–point PCR methods for detection of *M. bovis*.

Some of these tests target ribosomal ribonucleic acid (**rRNA**) 16S sequences, which is genetically similar between many ruminant *Mycoplasma* ssp. (Pettersson et al., 1996). Though detection occurred, sensitivity was a problem.

Substantial issues arise in relation to detection of subclinical infection. Detection often follows observation of one or more related disease symptoms and cattle lacking visible symptoms mean a correct diagnosis is less likely. It was demonstrated that testing for subclinical infection by PCR is ineffective (Hazelton et al., 2020c).

Therefore, it is often problematic separating asymptomatic infected cattle from uninfected animals before infection spreads, as was evident in two American case studies (Fox et al., 2008; Punyapornwithaya et al., 2010).

There have been improvements in sensitivity for *M. bovis* diagnosis using PCR. For example, primers designed using genes from membrane–protein 81 of *M. bovis* (Foddai et al., 2005; Mehmet Akan et al., 2014). There are conserved sections of the endonuclease gene *uvrC* that have aided *M. bovis* diagnostics. Successful amplification from infected samples improved sensitivity of real–time PCR assays (Behera et al., 2018). More recently, the *uvrC* gene has improved rapid detection of *M. bovis* using isothermal recombinase polymerase amplification with fluorescence enabling real–time detection (Li et al., 2021).

Despite these promising diagnostic assays, issues still exist for PCR–based evaluation of *uvrC* as gene insertions within conserved regions of the gene can result in diagnosis being false negatives (Register et al., 2018).

Swabs taken from tonsils of post–mortem calves provided a greater detection rate than from swabs of bronchial tissue of the same calves, demonstrating that detection of *M. bovis* is dependent on tissue type selected and that tonsil tissue provides a greater rate of PCR detection (~90 %) (Buckle et al., 2020). However, detection using tonsil tissue occurs through loss of life.

Farmers and herds are affected by loss of any animal, which eventuates into substantial economic issues for these farms without control or treatment of *M. bovis*. Again, this reinforced an issue regarding reliance upon only using PCR for evaluation of an *M. bovis* outbreak. Depending on the swabbed tissue, PCR may not identify *M. bovis* infection. Relying on a single swabbed tissue for guaranteed presence of *M. bovis* can be disastrous, as misdiagnosing a single animal can ensure a continued infection of a herd for months or even years.

There have been recent advances aimed at improving current diagnostic methods, including a highly specific multiplex–quantitative–PCR assay that uses genes with greater specificity to *M. bovis* rather than other *Mycoplasma* ssp. (Chauhan et al., 2021). Alternatively, developments in isothermal DNA amplification methods have enabled a more rapid diagnosis of *M. bovis* to occur than standard PCR methods (Li et al., 2021).

1.1.5 Serology

An alternative to PCR is a serological evaluation using ELISA. Whilst PCR can be used for direct detection of bacterial DNA from tissue or culture, ELISA can be used for indirect detection by measuring *M. bovis* antibodies in blood, serum, or bulk milk samples (Wawegama et al., 2014; McCarthy et al., 2021).

Serological evaluation of *M. bovis* infection provides mixed results. For example, collection of blood/serum or milk samples can be easier than a swab taken from tissue, especially those taken from bronchoalveolar lavage or tonsil tissue (Thomas et al., 2002). However, many disadvantages are associated with use of these assays. These include how varied commercially available assays are in providing a concordant result. For example, two ELISAs that were tested independently between six laboratories demonstrated a very different diagnostic ability (Andersson et al., 2019). Results between alternative ELISA tests cannot be compared as *M. bovis* antibodies were detected at different concentrations in sera previously established as *M. bovis* positive, (Petersen et al., 2018).

Issues of sensitivity are widespread throughout ELISA tests, with some tests not reaching a sensitivity estimate above 30% (Wawegama et al., 2016), and the sensitivity of western blotting outperforming the ELISAs used to confirm infection (Schibrowski et al., 2018).

Age is a substantial factor that reduces overall precision of these assays. Infection was assessed in *M. bovis*–positive calves and was vastly different between three–week–old, three–month–old, and six–month–old calves. Sera from three–week–old calves was assessed using ELISA and results were below the recommended optical–density measurement cut–off (37 %) that would indicate positive infection (Petersen et al., 2018; Schibrowski et al., 2018).

1.1.6 Bacterial culture

Culturing *M. bovis* functions as a reliable method to diagnose infection. Growth of *Mycoplasma* ssp. *in vitro* results in changes to the liquid culture growth medium.

For example, *Mycoplasma* ssp. undertake fatty acid metabolism using cholesterols provided by serum within a complete growth medium (Awadh et al., 2021). Metabolism results in an altered pH, indicated by differences in the colour of the medium from red to orange to yellow, which enables assessment of the growth of a variety of *Mycoplasma* ssp. (Bottinelli et al., 2020).

However, *in vitro* culture does not occur without issues. It takes time for colonies to form on solid agar, sometimes taking weeks for signs of growth to occur (Szacawa et al., 2016). Diagnosis becomes dependent on the strain/isolate of *M. bovis* being cultured.

Other issues include contamination by other infectious *Mycoplasma* ssp., which cause a colour change in growth medium or colony growth on agar that could be confused with a positive *M. bovis* infection (Ayling et al., 2015).

1.1.7 Summary

In summary, commercially available methods to reliably detect *M. bovis* lack sensitivity and an ability to identify animals with subclinical infection. Diagnosing infection remains the only reliable method to reduce spread of *M. bovis*.

Therefore, there is an opportunity for development of an alternative diagnostic tool that is dependable and can be assessed from a variety of biological sources.

1.2 Treatment

Resulting from the absence of a cell wall, most *Mycoplasma* ssp. are intrinsically resistant to a variety of commonly used antibiotics (Gautier-Bouchardon, 2018). These include, but are not limited to, β–lactams/glycopeptides that are designed to target cell wall synthesis (Pereyre & Tardy, 2021; Khaledi et al., 2022), and sulfadimethoxine that acts to prevent folate synthesis essential for DNA replication. *Mycoplasma* ssp. lack their own folic acid pathways making treatment with sulfadimethoxine antibiotics ineffective (Schultz et al., 2012).

Broad spectrum antibiotics, designed to prevent protein or DNA synthesis, such as tetracyclines, fluoroquinolones and lincosamides are most effective in treating infection by *Mycoplasma* ssp. (Cai et al., 2019; Ahn et al., 2021). However, tetracycline use can be detrimental in pregnant/paediatric patients (Enabulele et al., 2020). Their overuse as a treatment has meant that antibiotic resistance to tetracyclines is developing in *Mycoplasma* ssp. worldwide (Ahmadi, 2021). *Mycoplasma* ssp. have also been reported to develop resistance to alternative antibiotics, such as macrolides (Yin et al., 2017; Dumke & Ziegler, 2019).

Susceptibility to these antimicrobials varies between *Mycoplasma* ssp./strains, with various mutations aiding resistances to a broad spectrum of treatments (Hata et al., 2019; Kakiuchi et al., 2021). Improved assays have been designed to assess mutations in *Mycoplasma* ssp. involved in antibiotic susceptibility (Sulyok et al., 2018). However, mitigating the effects of such mutations, i.e., rising ineffectiveness of the individual antibiotics, can only be achieved by prescribing multiple antibiotics.

Without development of a novel antibiotic, difficulties in treating infection created by *Mycoplasma* ssp. will continue to increase. Detection of *M. bovis* before a major outbreak occurs is essential to prevent widespread development of an ineffectively treated disease, as current vaccine developments have not demonstrated viable efficacy for commercial use (Dudek et al., 2021).

1.3 Extracellular Vesicles

Early observations of cells and their surrounding extracellular matrix using electron microscopy (**EM**) revealed the presence of a variety of minuscule, rounded structures (Porter et al., 1945).

These structures, initially termed 'vesicles', 'granules' or 'particulates', were identified within the ground substance of the extracellular matrix, which is amorphous gelatinous substance in the extracellular space that contains all components of the extracellular matrix except for fibrous materials such as collagen and elastin. They were within a size range of 30–150 nm, with majority ranging between 80–100 nm.

Considered as artefacts of EM staining, understanding of these vesicles has developed substantially since their discovery. Initially, cytolysis (cellular disintegration) was considered as the cause for vesicle release, thus explaining their similarities to secretions from the cytoplasm or endoplasmic reticulum (Porter, 1953).

These initial observations were subsequently developed by Palade (1955a) who observed the cytoplasm of cells in rat and chicken tissues, identifying particulates sized between 80–300 nm. Palade (1955b) deduced that these particulates existed *in vivo* by examining a variety of cell types and noted differences in their intracellular/extracellular positioning.

Pan and Johnstone (1983); Johnstone et al. (1987) provided the first evidence regarding membrane invagination and subsequent exocytosis of membrane–bound vesicles, terming them extracellular vesicles, by observing antibody–tagged transferrin receptors within reticulocytes.

Research regarding extracellular vesicles remained a relatively niche topic until the late 2000's. Research by Valadi et al. (2007) detailed exchange of functional ribonucleic acid (**RNA**) molecules from mouse mast–cells to mouse or human recipient mast cells through endocytic transfer by extracellular vesicles.

A report by Skog et al. (2008) demonstrated functional microvesicles shed by tumour cells contained viable RNA and proteins that represented a mechanism of cell–to–cell communication, providing an extensive number of potential uses and functions for these vesicles.

1.3.1 Biogenesis, Composition, and Function of small Extracellular Vesicles (sEVs)

Since their initial discovery, understanding of the formation of extracellular vesicles and their involvement in the endocytic pathway has progressed greatly.

Endosomal sorting pathways provide support regarding development of a *M. bovis* diagnostic assay as representative nuclear material is encapsulated within intracellular vesicles and sorted accordingly.

1.3.1.1 Early Endocytosis

The endocytic pathway is involved in recycling or degrading transmembrane proteins for maintenance of cellular homeostasis by responding to fluctuations in proteins (Estadella et al., 2020). Transmembrane proteins, such as transient–receptor potential vanilloid 5 calcium–ion–selective channels, can be localised to important membrane–bound clathrin–coated pits (van de Graaf et al., 2008). These clathrin–coated pits eventually bud internally, trapping surface receptor proteins within a variety of single intracellular vesicles through invagination of the plasma membrane (Yoshida et al., 2018).

Fusion of these singular vesicles is essential for formation of dynamic early/sorting endosomes (Karim et al., 2018; Cruz & Kim, 2019). Processing of transmembrane cargo is facilitated by two endocytic methods: Rab11 guanosine triphosphatase (**GTPase**)–mediated movement that aids protein recycling, or, further invagination of early endosomes (Horgan et al., 2010; Baetz & Goldenring, 2014).

Invagination of the lumen within the maturing endosome results in formation of intra–luminal vesicles (**ILV**s). Acidification of early endosomes occurs through an absorbance of hydrolytic enzymes, with change in luminal pH representative of endosome maturation (Elkin et al., 2016).

A true marker of endosomal development is a change in responsibility of regulatory proteins. Early endosome function was identified by activity of an endocytic master regulator, GTPase Rab5, whereas a shift to GTPase Rab7 activity was a key indication of endosome maturation (Kaur & Lakkaraju, 2018).

Internalised transmembrane proteins are sorted by a system of tubulovesicular compartments within the trans–Golgi network, termed the endosomal sorting complex required for transport (**ESCRT**) (Huang et al., 2019).

Organisation of nascent ILVs by the ESCRT was aided by, but not limited to, post translational modifications such as ubiquitin–labelling (Raiborg & Stenmark, 2009; Jones et al., 2020). Late endosome maturation was a direct consequence of continual ILV formation with the ESCRT implemented in many trafficking pathways.

To illustrate ESCRT functionality, Edgar et al. (2015) demonstrated that alterations in sorting of Amyloid Precursor Protein (**APP**) into ILVs lead to APP accumulation.

Trafficking of APP was linked to a population of Multivesicular Bodies (**MVB**s) containing epidermal growth factor receptor (**EGFR**).

Many MVBs containing EGFR are allocated for lysosome fusion as majority are designated for protein degradation (Van Niel et al., 2018).

If the ESCRT was fully operational, accumulated APP and its cleavage product (Amyloid–beta (**Aβ**) would be reduced as would be designated for lysosomal fusion/ subsequent degradation (Gireud-Goss et al., 2020).

Severe consequences of an unfunctional ESCRT system, which causes APP accumulation, have been linked with initiating development of Alzheimer's Disease (Uddin et al., 2020).

However, an existence of ESCRT–independent pathways was provided by Stuffers et al. (2009). A recent study by Wei et al. (2021) described previously unknown enzyme functions within these ESCRT–independent pathways.

Phosphorylated Rab31 aided EGFR uptake within ILVs and occurred within ESCRT–depleted cells (Wei et al., 2021).

Tetraspanin proteins that are enriched on the membrane of extracellular vesicles, such as CD63, were linked in regulating ESCRT–independent pathways (Gauthier et al., 2017).

Though understanding of these pathways remains limited, there is potential for packaging of a specific *Mycoplasma* sp. protein marker within ILVs given there are two independent pathways functioning to sort proteins encapsulated within cells.

1.3.1.2 Late Endocytosis

Multivesicular Bodies (**MVB**s) or late endosomes are termed so owing to numerous intraluminal invaginations (Mir & Goettsch, 2020).

Proteins in MVBs that could not be degraded or were involved in intercellular signalling were processed differently than proteins delegated for degradation/reuse.

Ubiquitination is a key factor in aiding protein sorting in MVB maturation (Ageta & Tsuchida, 2019) For example, ubiquitination predestined CD81 proteins for lysosomal fusion during endocytosis (Hosokawa et al., 2020).

Primarily, MVBs fuse with lysosomes as is dictated by their nuclear content (Van Niel et al., 2018). As cells contained extracellular vesicles throughout their cytoplasm, it demonstrated that there were mechanisms for avoiding lysosomal degradation using alternative endocytic pathways.

Discovery of the syntenin–syndecan–(ALG–2–interacting protein X) (**ALIX**) pathway provided evidence of a specific small extracellular vesicle (**sEV**) secretion route (Baietti et al., 2012).

Differences in post–translational modifications dictate secretion of sEVs and it determined some of their downstream functions (Atukorala & Mathivanan, 2021).

Fusion of ILVs with the plasma membrane releases completed sEVs through exocytosis (Van Niel et al., 2018). Within the extracellular environment, sEVs are involved in a variety of functions.

Encountering recipient cells is a priority objective for sEVs, which enables intercellular communication through macropinocytosis–mediated intake of sEVs by recipient cells (Verdera et al., 2017).

Once internalised within recipient cells, sEVs are lysed to release their cargo. Lysis of sEVs elicits responses matching sEV content, with examples including secretion of immunoregulatory cytokines (Fitzgerald et al., 2018).

A summary of the endocytic process, the RAB GTPases involved in intracellular protein sorting and formation of extracellular vesicles is provided by **Figure 1**.

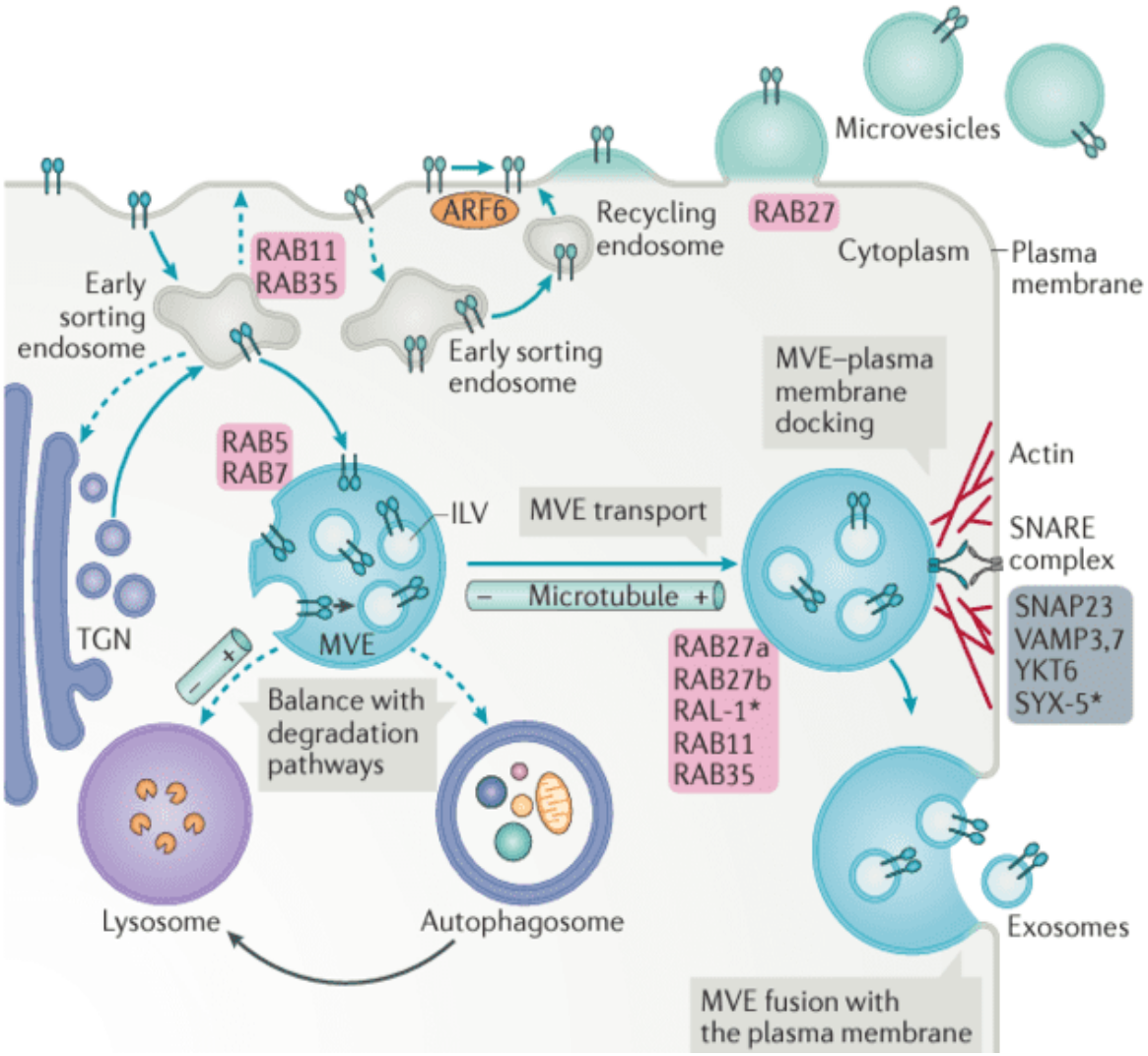

***Figure 1*: Interdependency of intracellular trafficking routes in the generation of extracellular vesicles (Van Niel et al., 2018)**

"The generation of exosomes and microvesicles requires regulation of multiple intracellular trafficking steps (blue arrows for exosomes, green arrows for microvesicles) that influence cargo targeting to the site of extracellular vesicle biogenesis and, for exosomes, the fate of Multivesicular Endosomes (**MVE**s)/Multivesicular Bodies (**MVB**s) from which these vesicles originate.

Cargoes targeted to MVEs/MVBs originate from endocytosis at the plasma membrane and are directly targeted to MVEs/MVBs or to early sorting endosomes via the biosynthetic pathway (from the trans–Golgi network (**TGN**)).

Retrograde transport towards the TGN or recycling back to the plasma membrane will divert cargoes from their targeting to the MVE/MVBs (dashed arrows) and, therefore, their incorporation into intraluminal vesicles (**ILV**s).

These sorting processes are regulated by various RAS–related protein (**RAB**) GTPases.

Once matured, MVEs/MVBs that are not targeted to lysosomes or autophagosomes for degradation are transported along microtubules to the plasma membrane.

At this step, docking and fusion are the two final processes required for exosome release.

Actin, RABs, and Soluble N-ethylmaleimide-Sensitive Factor Attachment Receptor (**SNARE**) proteins are involved in exosome release steps.

In the case of microvesicle biogenesis, endocytic uptake (dashed arrow) and recycling will, respectively, decrease and increase the targeting of membrane (and membrane–bound) cargoes to microvesicles.

Of note, as the release of exosomes requires tightly regulated steps of transport, tethering, and fusion of MVE/MVBs to the plasma membrane (apart from cargo sorting), this could account for the time difference between the generation and release of the two types of extracellular vesicles.

Protein abbreviations: **ARF6**, ADP–ribosylation factor 6; **RAL–1**, RAL (Ras–related GTPase) homolog; **SNAP23**, synaptosomal–associated protein 23; **SYX–5**, syntaxin 5; **VAMP3**, vesicle–associated membrane protein 3."

1.4 Use of sEVs as Diagnostic Tools

Over the past ten years, an increasing number of published studies have used sEVs as analytical tools for monitoring disease development. Particularly in cancer diagnostics, sEVs have enabled an alternative diagnostic method that reliably provides an indication of cellular health (Zhou et al., 2020).

As the initial formation of sEVs within cells encapsulates a variety of nuclear material such as proteins, messenger RNA, and microRNAs, secreted sEVs are representative of their cell of origin (Sork et al., 2018). For example, sEVs released upon antigen presentation by immune cells carry representative markers that elicit downstream responses, which aid in reactions against foreign bodies (Mathieu et al., 2019).

In contrast, pathogenic influence on cells creates altered nucleic material that is captured within sEVs. Changes in sEV proteins elicit inhibitory responses that reduces the detection of pathogens, demonstrating the complex and conflicting abilities of sEVs within intercellular communication (Armstrong et al., 2020).

1.4.1 Cancer

Production of sEVs is not limited to healthy cells. Diseased cells, such as those involved in tumour development or pathogenically–infected cells, make use of sEV intercellular communication pathways to promote disease progression (Yu et al., 2021).

Diseased cells shed sEVs containing unique proteins that represent their cytoplasmic environment, with several biomarkers identified within sEVs in studies investigating progression of cancer or infection.

'Liquid biopsies' allow for measurements of biomarkers including circulating nucleic acids, proteins and associated sEV proteins from blood (or other bodily fluids); they present a non–invasive method of diagnosis as compared to tissue biopsy (Alix-Panabieres, 2020; Ignatiadis et al., 2021).

Results using liquid biopsy are very promising. For example, an assessment of genes encoding for echinoderm microtubule–associated protein–like 4 (**EML4**) and anaplastic lymphoma kinase (**ALK**) using liquid biopsy revealed that a fusion or rearrangement of these genes augmented development of non–small–cell lung cancer (Zhu et al., 2014; Sabir et al., 2017).

Liquid biopsy of non–small–cell lung cancer patients provided the first commercially validated test using sEVs, the ExoDx Lung (ALK) (sEV Diagnostics Inc., MA, USA), achieved by analysis of a specific protein biomarker (Sheridan, 2016; Brinkmann et al., 2018).

The ExoDx Lung (ALK) test demonstrated some of the first validated evidence that RNA and circulating tumour DNA, encapsulated within sEVs, represented progression of genetic mutations associated with tumorigenesis. As such, changes in EML4–ALK RNA were demonstrated in developing lung carcinomas, with tumour progression tracked by RNA packaged within sEVs (Reclusa et al., 2019).

Improved detection and an increased understanding of these mutations contributes to prescription of ALK–inhibitors: drugs that perform favourably in patients with EML4–ALK mutations in comparison to chemotherapy (Golding et al., 2018). As tumour–mediated mutations created altered RNA, it demonstrated that modifications to sEV cargo are generated in cells as a response to disease.

Further research has been undertaken to develop additional sEV diagnostic tests. As lung cancer has remained the leading cause of cancer–related mortality worldwide (Sung et al., 2021), more sEV–based tests for detection of alternative lung–tumour–promoting mutations have become available.

Liquid biopsy using sEVs has improved detection of a mutation in EGFR, which is related with an increased risk of developing non–small–cell lung cancer. Detection occurred regardless of copy number with a high sensitivity (Castellanos-Rizaldos et al., 2018). These tests represent critical advancements regarding cancer diagnostics.

Serum–based assays provide a non–invasive diagnostic method for early detection of cancer using specific biomarkers, as compared with more invasive alternatives such as tissue biopsy.

Use of tissue biopsy limits an ability for early detection of diseases to occur through reduced precision (Macías et al., 2018). Tissue biopsy can be difficult to repeat, painful for patients and does not provide a means for longitudinal assessment of disease progression (Russano et al., 2020).

Successful diagnosis using sEVs expanded the ability of researchers to detect disease, with sEVs used effectively to assess development of cancers in tissues other than the lungs. For example, tumorigenesis of pancreatic cancer (Takahashi et al., 2020; Reese & Dhayat, 2021). Proteins and RNA within sEVs, derived from pancreatic ductal adenocarcinomas, were attributed to promotion of angiogenesis and development of diabetes in pancreatic cancer patients (Javeed et al., 2015; Baj-Krzyworzeka et al., 2020; Shang et al., 2020).

Advancements in understanding of sEV biology have indicated that sEVs are useful targets for analysing or inhibiting cancer progression. Advancements have included development of an ELISA for analysis of breast cancer progression that quantified a Glypican–1 biomarker by magnetic bead–based immunocapture (Liu et al., 2018a).

Another successful analytical assay using sEVs enables concentrations of a urine biomarker to be assessed to understand the progression of prostate cancer (Øverbye et al., 2015; Tutrone et al., 2020).

1.4.2 Infectious Disease

In context of our own research aims, an understanding of changes to sEV cargo in response to infection by pathogenic microorganisms (especially gram–negative bacteria) was required.

Pathogens can generate host sEV changes that promote pathogenesis of the infectious microorganism with modifications in protein cargo comparable to changes in sEVs generated by tumorigenesis (Geller et al., 2017; Gopalakrishnan et al., 2018; Pleguezuelos-Manzano et al., 2020).

Secretion of sEVs is an evolutionarily conserved method of intercellular communication, which is used by a substantial variety of organisms within each kingdom of life (Woith et al., 2019).

Various gram–negative bacteria (i.e., *M. bovis*) shed their own sEVs for inter–cellular communication, which complicates separation of sEV cargo.

Bacterial sEVs act to dampen or exacerbate immune responses, which confounds development of diagnostic methodologies (Hasegawa et al., 2015; Pérez-Cruz et al., 2015; Roier et al., 2016).

Recent research in other pathogenic microorganisms, such as severe acute respiratory syndrome coronavirus 2 (**SARS–CoV–2**), demonstrated that sEV secretion pathways were utilised for increased pathogenesis in hosts. Slight alterations in sEV protein cargo enabled spread of the virus and aided SARS–CoV–2 uptake in naïve cells (Hassanpour et al., 2020).

Use of sEVs in tuberculosis research is currently preliminary. However, promising studies using macrophage cells infected with *Mycobacterium tuberculosis* (***M. tuberculosis***) identified twenty proteins altered in sEV cargo as a result of infection (Kruh-Garcia et al., 2014). Identified proteins, such as Antigen 85B and a catalase–peroxidase enzyme, were considered to be involved in *M. tuberculosis* adhesion and virulence (Forrellad et al., 2013). Proteins were localised to sEV membranes, suggesting an involvement in aiding an increased adherent/intracellular infection of *M. tuberculosis* in host cells.

Further assessment by Diaz et al. (2016) of the sEV cargo from *M. tuberculosis*–infected macrophages supported previous changes in the sEV proteome.

Interestingly, Kruh-Garcia et al. (2014) alluded that sEV composition was dependent on the clinical manifestation of tuberculosis within a host, be it pulmonary or extra–pulmonary, with sEVs altered according to the stage of disease.

Preliminary data using ELISA–based detection revealed differences in the concentration of mammalian and bacterial heat shock proteins within serum sEVs, which was attributed to either active or latent infection by *M. tuberculosis* (Shekhawat et al., 2016; Castro-Garza et al., 2017).

Alternatively, urinary sEVs were representative of stages in *M. tuberculosis* infection, with concentrations of protein biomarkers within sEVs altered accordingly (Dahiya et al., 2019). In the context of *M. bovis*, differentiating subclinical/clinical infection would aid disease diagnosis as detection of hidden *M. bovis* and *M. bovis*–symptoms could occur.

Yet, sEVs are not limited by their role in increasing pathogenesis. Experimental evidence provided by a *M. tuberculosis* infection model in mice demonstrated that sEVs produced *in vitro* were substantial promotors of T–cell activity (Smith et al., 2017).

Release of bone–marrow–derived dendritic cells was amplified by presentation of sEVs derived from *M. tuberculosis*–infected macrophage cells. Antigen presentation intensified activation of specific CD4+ and CD8+ T–cells (Giri & Schorey, 2008). Immune responses reduced development of infection and remained an integral part in preventing active infection.

Another gram–negative bacterium, *Salmonella enterica* serovar Typhimurium (***S. enterica***), was used to establish an *in vitro* macrophage infection model (Hui et al., 2018). An exposure of sEVs derived from *S. enterica*–infected macrophages released greater concentrations of tumour necrosis factor α (**TNF–α**) from naïve macrophages as compared to exposure of sEVs from non–infected control macrophages.

Pro–inflammatory cytokines like TNF–α are vital factors in inducing signal cascades for promotion of apoptosis/necrosis in *S. enterica*–infected cells (Rydström & Wick, 2007; Pham & McSorley, 2015).

Post–translational modifications have been linked to sEV secretion pathways meaning microorganisms, such as *Legionella pneumophila*, can take advantage of this secretion system to increase their pathogenesis in host cells (Shinde & Maddika, 2018).

An addition of adenosine monophosphate to Rab1 led to changes in MVB pathways by preventing GTPase activity of Rab1.

Exploiting Rab proteins in a host cell can alter endocytic trafficking and change MVB maturation pathways, which can enable increased pathogenesis of infectious microorganisms (Homma et al., 2021).

Production and functionality of sEVs can differ depending on what cell type receives the sEV cargo that is representative of infection.

As an example, a comparison of the pro–inflammatory responses of naïve immune cells to sEVs derived from *S. enterica*–infected primary dendritic cells revealed that further production of dendritic sEVs was low, directly contrasting a greater production of macrophage sEVs following presentation of *S. enterica*–containing sEVs (Hui et al., 2018).

In response to detection of a foreign body, sEV production differs in recipient cells and demonstrates how sEV processing/disease progression can be altered in response to infection.

Infectious microorganisms do create changes within host cells that aid in their increased pathogenesis. It is thought that *M. bovis* will influence sEV secretion/cargo in a bovine cell line.

1.4.3 Other Diseases

Diagnostics using sEVs are not limited to cancer research. Cardiovascular disease and neurodegenerative/pregnancy–associated disorders are amongst those where early detection using sEV cargo is becoming a possibility. In accordance, a recently developed magnetic bead–based immunocapture assay enabled sEV–based detection demonstrating that that micro–RNA packaged into sEVs could be isolated from human serum and were altered in response to progression of cardiovascular disease (Chen et al., 2020).

Preeclampsia can be a critical factor during pregnancy in increasing chances of maternal–foetal mortality (Burton et al., 2019). Clinical symptoms associated with this syndrome, for mothers/babies, can be severe and early detection lessens or eliminates effects of disease. A greater concentration of a placental alkaline phosphatase biomarker was present in placental–derived sEVs and these were linked with development of placental hypoxia, a symptom related to preeclampsia (Pillay et al., 2016). In support, alterations in sEV micro–RNA cargo were linked to complications caused by preeclampsia and restrictions in foetal growth (Li et al., 2020).

In patients diagnosed with Alzheimer's Disease, changes to sEV cargo occur (Malm et al., 2016). Extracellular plaques form as result of Aβ deposition within neural tissue (Perl, 2010). An ability to rid cells of accumulated Aβ are affected by loss of function mutations in endosomal–lysosomal pathways, which in turn alter sEV cargo (Goetzl et al., 2015). In neural cells, fusion of MVBs containing a larger concentration of accumulated Aβ with the plasma membrane of the cell occurs more frequently than fusion of other MVBs, thus releasing sEVs with a greater potential to cause neurodegenerative harm (Lakshmi et al., 2020). It remains unknown if sEV function is beneficial or detrimental, as sEV contribution can be ambiguous. For example, developments in therapeutics using sEVs has demonstrated recovery of neural tissue within an *in vivo* rat model (Drommelschmidt et al., 2017).

As no current long–term cure exists for Alzheimer's Disease, with medication only lessening symptoms, sEVs derived from mesenchymal stem–cells could provide a viable ongoing treatment for restoration of white matter function. Examples of sEV shedding from diseased cells demonstrate that sEVs can be used as biomarkers for estimating of progression of a variety of diseases. Disease progression can be traced by changes in a variety of different sEV factors that are associated with the same clinical disease.

1.5 Hypothesis, Aim and Objectives

An opportunity provided by our government–funded project enabled novel research involving analysis of sEVs from a *M. bovis* co–culture infection model for eventual development of an sEV–based diagnostic test for *M. bovis* infection.

Our hypothesis was that sEV protein cargo would be altered by an infection by *M. bovis*. To investigate this, we aimed to develop an *in vitro* model of *M. bovis* infection using bovine endometrial epithelial cells and use this model to assess resulting proteomic changes in sEVs.

The specific objectives were as follows:

1. Culturing of bEEL cells and/or *M. bovis* (3.1).
2. Assessment of small Extracellular Vesicles (sEVs) (3.2).
3. Assessing composition and regulation of sEV proteins using Liquid Chromatography Tandem Mass Spectrometry (LC–MS/MS) (3.3).

Our *in vitro* infection model might uncover novel proteins that are candidate biomarkers for a new diagnostic test. Additionally, it might provide a greater understanding of *M. bovis* pathogenesis in bovine cells.

2 Materials and Methods

2.1 Overview of Experiments

Individually, the culture conditions of bEEL cells (see 2.3.1) and *M. bovis* (2.3.4) were developed/verified for cell growth.

Any contaminating sEVs resulting from an input of FBS were reduced through adaptation of bEEL cells (2.2.1) to an Exosome–Depleted FBS in aRPMI medium.

Bioreactor flasks containing a control bEEL cell culture (2.6.1) and a co–culture infection model (2.6.2) were established.

Harvesting (2.6.3) and concentrating (2.6.5) of sEV fractions isolated from each cell culture condition enabled their subsequent characterisation using Tunable Resistive Pulse Sensing (**TRPS**) (2.7.1), Transmission Electron Microscopy (**TEM**) (2.7.2), Western Blotting (2.7.3.1) and an Exo–Check Exosome Antibody array (2.7.3.2).

Survival and/or infection of *M. bovis* was confirmed using colour change assays (2.3.5), gentamicin protection assays (2.3.7) and epi–fluorescent microscopy (2.5).

Selection and validation of a *M. bovis* sterilisation method was required to enable transfer of sEV preparations from the Physical Containment level 3 (**PC3**) facility (2.4).

Finally, the sEV cargo of each culture condition was analysed using Liquid Chromatography Tandem Mass Spectrometry (**LC–MS/MS**) (2.8).

An overview of the methods used for analysis of the infection model is summarised in **Figure 2**.

All methods, experiments, and analyses described within this thesis were performed by myself (unless specifically stated otherwise).

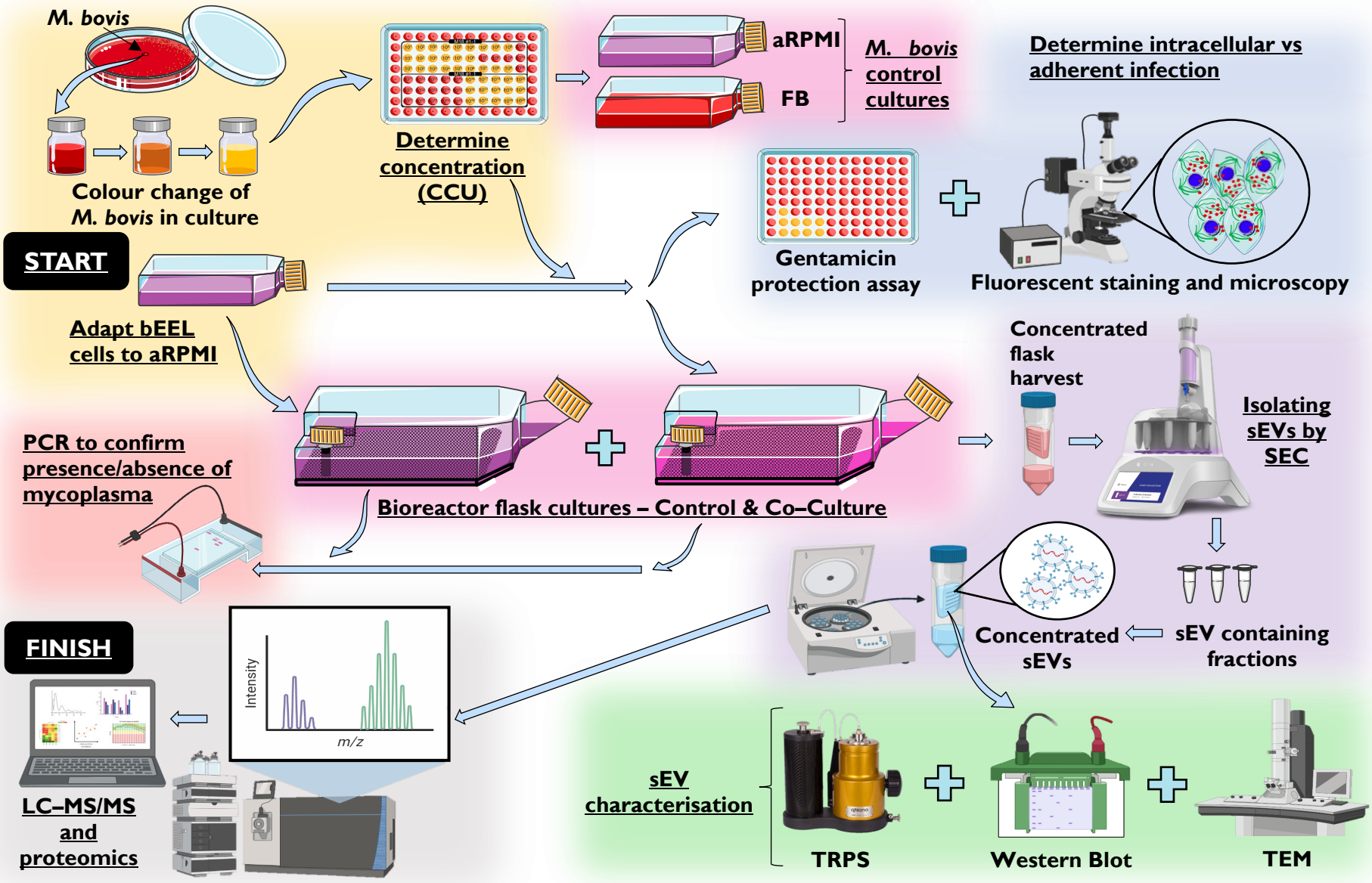
M. bovis
Colour change of M. bovis in culture
Determine concentration (CCU)
aRPMI
FB
M. bovis control cultures
Determine intracellular vs adherent infection
START
Adapt bEEL cells to aRPMI
Gentamicin protection assay
Fluorescent staining and microscopy
PCR to confirm presence/absence of mycoplasma
Bioreactor flask cultures – Control & Co–Culture
Concentrated flask harvest
Isolating sEVs by SEC
Concentrated sEVs
sEV containing fractions
FINISH
Intensity
m/z
LC–MS/MS and proteomics
sEV characterisation
TRPS
Western Blot
TEM

Figure 2*: Overview of all experiments to analyse a *Mycoplasma bovis* (*M. bovis*) infection model and the small extracellular vesicles produced *in vitro

At the START point (denoted by the yellow background), two methods were utilised concurrently.

Mycoplasma bovis (***M. bovis***) was grown on Friis Agar and a single colony was transferred into Friis Broth (**FB**). Colour change of FB from red to orange to yellow was representative of *M. bovis* growth (denoted by the yellow background).

A colour change assay was used to assess the concentration of *M. bovis* in culture using Colour Change Units (**CCU**).

Two *M. bovis* controls were created, with *M. bovis* grown in FB and Advanced Rosewell Park Memorial Institute Medium (**aRPMI**) (denoted by a pink background).

Concurrent to the growth of *M. bovis*, a bovine endometrial epithelial cell line (**bEEL cells**) was adapted to aRPMI (supplemented with 4.5 % Exosome–Depleted foetal bovine serum, 2x GlutaMAX and 1x Penicillin/Streptomycin) (denoted by the yellow background).

The adapted bEEL cells were seeded into a CELLine AD1000 bioreactor flask as an uninfected **control** flask.

Another CELLine AD1000 bioreactor flask was seeded with bEEL cells, and *M. bovis* was inoculated into the flask at a multiplicity of infection of 5, which created the **co–culture** flask.

All flasks used to create small extracellular vesicles (both bioreactor flasks and both *M. bovis* controls) are denoted by a pink background.

The ability of *M. bovis* to infect bEEL cells was assessed using a gentamicin protection assay and fluorescent microscopy, which is denoted by a blue background.

The presence/absence of *M. bovis* in either bioreactor flask was assessed using Polymerase Chain Reaction (**PCR**), which is denoted by a red background.

The medium of each bioreactor flask (and *M. bovis* controls) was concentrated using Size Exclusion Chromatography (**SEC**) qEV10 columns. All eluted fractions were collected using an Automatic Fraction Collector. All fractions containing small extracellular vesicles (**sEVs**) were concentrated, with all sEV isolation/concentration denoted by a purple background.

The sEVs were characterised using Tunable Resistive Pulse Sensing (**TRPS**), Western Blotting and Transmission Electron Microscopy (**TEM**). These methods assessed the size/concentration of sEVs, presence of sEV–specific proteins, and were denoted by the green background.

Finally, at the FINISH point, all sEVs were processed using Liquid Chromatography Tandem Mass Spectrometry (LC–MS/MS), and proteomic analysis of sEV proteins assessed differences between the control and treatment groups (denoted by a grey background).

Created/modified using Servier Medical Art, licensed under a Creative Commons Attribution 3.0 Unported License (https://smart.servier.com/), and BioRender (https://biorender.com/).

2.2 Content of Media and Buffers

2.2.1 Media to culture bEEL cells

Initially, bEEL cells were cultured in Nunc EasYFlask 75 cm^2 (**T75**) with filter lids (Nunc, Thermo Fisher Scientific) containing RPMI 1640 medium (Gibco, Thermo Fisher Scientific) supplemented with 10 % FBS (Gibco, Thermo Fisher Scientific) and 1x Penicillin/Streptomycin (Gibco, Thermo Fisher Scientific).

Adaptation of bEEL cells to a secondary growth medium also occurred. Advanced RPMI 1640 (**aRPMI**); Gibco, Thermo Fisher Scientific) was enriched for cell growth using 4.5 % Exosome–Depleted FBS (Gibco, Thermo Fisher Scientific), 2x GlutaMAX Supplement (Gibco, Thermo Fisher Scientific) and 1x Penicillin/Streptomycin. A serum–free aRPMI alternative was also required and was termed 'nutrient–only aRPMI'.

2.2.2 Friis Broth (FB)

Complete Friis Broth (**FB**) required a prior preparation of Friis Base (Tully, 2012). Friis Base was formulated by combining 50 mL of Hanks Balanced Salt Solution (Sigma–Aldrich, Merck–Millipore), 8.2 g of Difco™ Bacto™ Brain Heart Infusion (BD BioSciences, Thermo Fisher Scientific), 8.7 g of Difco™ pleuropneumonia–like organisms Broth (BD BioSciences, Thermo Fisher Scientific) and 1200 mL of sterile Milli–Q water.

This solution was adjusted to a pH of 7.6, dispensed into 200 mL aliquots and autoclaved at 121 °C for five to ten minutes. These 200 mL aliquots of Friis Base were frozen at –20 °C.

Completion of FB required combination of a thawed 200 mL aliquot of Friis Base with 10 mL of a 16 % solution of Bacto™ yeast extract (Gibco, Thermo Fisher Scientific), 25 mL of heat–inactivated horse serum (Gibco, Thermo Fisher Scientific), 25 mL of heat–inactivated porcine serum (Auckland BioSciences, New Zealand); both sera were inactivated at 56 °C for forty–five minutes, 0.3 mL of a 1 % solution of phenol red (Sigma–Aldrich, Merck–Millipore), 0.0234 g of bacitracin (Sigma–Aldrich, Merck–Millipore) and 500 µL of a 100,000 IU/mL solution of penicillin (Sigma–Aldrich, Merck–Millipore).

2.2.3 Friis Agar (FA)

Friis Agar (**FA**) was generated through an addition of 2.5 g of Bacteriological agar (Sigma–Aldrich, Merck–Millipore) to a thawed 200 mL aliquot of Friis Base, which was then autoclaved at 121 °C for fifteen minutes and cooled to 56 °C using a pre–heated water bath. All ingredients required for formation of complete FB were added to this molten agar solution, creating complete FA. In sterile 6 mm petri dishes, ~5 mL of FA was poured and cooled for thirty minutes in a sterile environment. Finally, completed FA plates were stored at 4 °C.

2.2.4 Western Blotting

Complete Radioimmunoprecipitation Assay (**RIPA**) buffer was prepared using 500 µL of 1 M Tris–hydrochloride buffer (pH 7.6) (Merck–Millipore), 600 µL of 5 M sodium chloride (Thermo Fisher Scientific), 200 µL of NP–40 Surfact–Amps™ Detergent Solution (Thermo Fisher Scientific), 0.4 g of Sodium Deoxycholate (**SDC**) detergent (Thermo Fisher Scientific), 200 µL of a 10 % (w/v) UltraPure™ SDS Solution (Invitrogen, Thermo Fisher Scientific) and 18.5 mL of sterile Milli–Q water. An addition of 5 µL of Halt™ Protease Inhibitor Cocktail (100x) (Thermo Fisher Scientific) was included in 495 µL aliquots of RIPA buffer prior to their use.

2.2.5 Lysis Buffer

Lysis buffer was made fresh for each batch of sEV isolations. Lysis buffer consisted of 7 M Urea (Avantor, VWR International), 2 M Thiourea (Avantor, VWR International) and 1 % SDC in 100 mM Ammonium bicarbonate (**Ambic**; (Sigma–Aldrich, Merck–Millipore). Lysis buffer was adjusted according to volume required using sterile Optima™ LC–MS/MS–grade water (Thermo Fisher Scientific).

2.2.6 Fixative

2.2.6.1 Fixation of sEVs for Transmission Electron Microscopy

Samples were fixed in 3 % (v/v) glutaraldehyde (Thermo Fisher Scientific) in 0.1 M sodium cacodylate buffer (pH 7.2; (Sigma–Aldrich, Merck–Millipore).

2.2.6.2 Fixation of bEEL cells and M. bovis for Epi–fluorescent microscopy

Samples were fixed in 10 % (v/v) Neutral Buffered Formalin (~4 % formaldehyde), which was followed by permeabilization with 0.05 % (v/v) Triton X–100 in 1x Phosphate Buffered Saline (**1x PBS**; pH 7.4, without Mg2+ and Ca2+ (Gibco, Thermo Fisher Scientific).

2.3 Culture Techniques

2.3.1 Culturing bEEL cells

Previous research indicated that bovine epithelial cell lines were susceptible to infection using *M. bovis* (Josi et al., 2018) and that bovine uterine tissue could be infected (Ghanem et al., 2013; Guo et al., 2014). Therefore, bEEL cells (Fortier et al., 1988) were selected for our study.

Initially, this cell line was a kind donation from Professor Michel A. Fortier (Université Laval, Québec) to Professor Murray Mitchell (Queensland University of Technology, Australia), who then generously provided samples for our own use.

All bEEL cell cultures were maintained at 37 °C in a humidified 5 % CO_2 incubator. Cells were grown to ~70–80 % confluency and then passaged to maintain cellular health. Passaging involved an initial removal of old culture medium from T75 flasks using suction. Cells were washed with 7 mL of 1x PBS, which was replaced with 1.5 mL of TrypLE® (Gibco, Thermo Fisher Scientific).

Cells were incubated for five to ten minutes or until cells were free floating. Light microscopy aided visualisation of cell rounding. An additional 5.5 mL of medium was added following incubation creating a total of 7 mL of resuspended bEEL cells, which was transferred into a fresh 15 mL conical tube.

Centrifugation at 300 rcf for five minutes pelleted bEEL cells. Cells were resuspended in 4 mL of fresh medium following removal of the supernatant. Typically, bEEL cells were split $^1/_4$ with 1 mL of resuspended bEEL cells transferred into a T75 flask from the 4 mL within the conical tube. However, splitting was dependent on bEEL cell growth rate.

Finally, to complete splitting of bEEL cells, 14 mL of fresh medium was added to the T75 flask (totalling 15 mL of a bEEL cell suspension within the T75 flask). The T75 flask was transferred into a 37 °C/5 % CO_2 humidified incubator for bEEL cell growth.

A T75 flask could be reused a maximum of three times and, if reused, required an additional wash step with 7 mL of 1x PBS to remove remnants of TrypLE® following cell dissociation.

Use of a 40x objective on a light microscope, and an EVOS™ XL Core Imaging System (Life Technologies, Thermo Fisher Scientific), enabled imaging of growing bEEL cells.

2.3.2 Cell counting

Viability of bEEL cells was assessed using a TC20 Automated Cell Counter (BioRad), with 30 µL of a 0.4 % Trypan Blue Solution (Gibco, Thermo Fisher Scientific) combined with 30 µL of a resuspended bEEL cell pellet. A 10 µL aliquot of Trypan Blue–stained cells was loaded into a cell counting cartridge. Two individual cell counts, gated between 8 µm and 30 µm, were averaged as an estimate of live bEEL cells.

2.3.3 Assessing contamination

Any cell culture containing bEEL cells was consistently assessed for *Mycoplasma* ssp. contamination. A variety of *Mycoplasma* ssp., including *M. bovis* and commensal human *Mycoplasma* ssp., were assessed using a LookOut Mycoplasma PCR Detection Kit (Sigma–Aldrich, Merck–Millipore). Although PCR was mainly used for confirming an absence of *Mycoplasma* ssp. within control bEEL cultures, as to prevent their potential influence on bEEL growth, its usefulness also extended to confirming presence of *M. bovis* in co–culture bioreactor harvests.

Cell culture medium was clarified by centrifugation to remove larger cellular debris at 500 rcf for ten minutes, then at 10,000 rcf for ten minutes. Deoxyribonucleic acid (**DNA**) was extracted from clarified cell culture media using a DNeasy kit (Qiagen).

Aliquots of 200 µL from clarified co–culture harvest 1, clarified co–culture harvest 6, clarified co–culture harvest 7 and a clarified control bEEL harvest were combined with 20 µL of an included proteinase–K solution.

Samples were subsequently combined with 200 µL of Buffer AL and 200 µL of 96 % analytical–grade ethanol. Each sample was transferred to a DNeasy Mini Spin column and spun at 6000 rcf for one minute. Flow–through was collected in 2 mL tubes, discarded, and each tube replaced. Buffer AW1 (500 µL) was spun through each column at 6000 rcf for one minute, flow–through discarded, and each tube was replaced. Buffer AW2 (500 µL) was spun through each column at 20,000 rcf for three minutes, flow–through discarded, and each tube was replaced.

Buffer AE (200 µL) was added directly onto the membrane of each column. Columns were incubated at room temperature for one minute and, finally, were spun at 6000 rcf for one minute to elute DNA. Eluted DNA from each column was stored at 4 °C.

A LookOut Mycoplasma PCR Detection Kit was used to assess contamination of *Mycoplasma* ssp. Rehydration of all test reaction tubes (containing lyophilised dNTPs and primers) was necessary and required use of 22.5 µL of rehydration buffer in combination with 0.5 µL of a Jumpstart Taq DNA Polymerase (Sigma–Aldrich, Merck–Millipore). Subsequently, 2 µL of eluted DNA (extracted from clarified cell culture samples) or 2 µL of nuclease–free water (negative control) was transferred into their respective tubes to make a total volume of 25 µL. However, rehydration of an individually included mycoplasma positive control instead required 24.5 µL of rehydration buffer and 0.5 µL of a Jumpstart Taq DNA Polymerase.

Tubes were incubated using a 5331 MasterCycler Gradient Thermal Cycler (Eppendorf AG) for forty cycles of 94 °C for thirty seconds, 55 °C for thirty seconds and 72 °C for forty seconds. A 1.5 % agarose gel was loaded with 8 µL of a GeneRuler 50 bp DNA ladder (Thermo Fisher Scientific) and PCR products (5 µL from the positive/negative controls and 5 µL from each prepared sample).

Gel electrophoresis occurred for fifty minutes at 100 V. Gels were imaged using the Ethidium bromide setting on a ChemiDoc MP Imaging System (BioRad).

2.3.4 Culturing *Mycoplasma bovis*

Discovery of *M. bovis* infection on New Zealand farms is relatively new. Therefore, culturing *M. bovis* required approval under various sections of the Hazardous Substances and New Organisms Act 1996 for use in a PC3 facility (Crookenden, 2020). Approval was obtained with expectation that *M. bovis* would be nonviable prior to removal from PC3. Therefore, multiple techniques were tested to balance effects caused by sterilisation upon *M. bovis* viability and sEV biology.

Isolates of a New Zealand strain of *M. bovis* were tested and were recorded with accessions: W18_04866 (#1) (collected in 2018), W18_06150 (#5) (collected in 2018) and W20_06790 (#3) (collected in 2020).

Stocks of these individual isolates were stored at –80 °C on cryobeads. All isolates were cultured in FB and were incubated at 37 °C in a humidified 5 % CO_2 incubator. Quality control of each FB aliquot was required before *M. bovis* inoculation occurred. A positive control *Mycoplasma mycoides* subsp. *mycoides* (LC), a negative control *Acholeplasma laidlawii* and an uninoculated FB negative control, were used to confirm viability of each FB aliquot.

A single cryobead of each isolate was streaked onto FA, alongside controls of *Mycoplasma mycoides* subsp. *mycoides* (LC) and *Acholeplasma laidlawii*, with an intention of separating single colonies. A single colony was transferred from FA to 4 mL of FB using a pipette tip. Subcultures of each isolate were generated using 10 µL of culture inoculated into 4 mL of fresh FB.

Colour change of FB from red to orange/yellow was used to indicate success of a *M. bovis* subculture, through assessing bacterial growth over nine days using light absorbance spectrophotometry at wavelengths of 415 nm and 560 nm (as phenol red was used as the pH indicator (Held, 2018). Daily comparison to an uninoculated FB control, which was utilised as a colour reference, provided a growth pattern for both isolates of *M. bovis*.

Isolate W18_04866 (#1) was inoculated (375 µL in 15 mL) into either aRPMI (stress sEVs) or FB (*M. bovis* sEVs), which created *M. bovis* sEV controls. Cultures were maintained in T75 culture flasks and were harvested concurrently with bioreactors.

2.3.5 Colour change assay

Colour change assays enabled *M. bovis* concentration to be estimated using Colour Change Units (**CCU**), with the plate layout demonstrated by **Figure 7**.

Within each well of a 96–well flat–bottomed cell culture plate (Thermo Fisher Scientific), 180 µL of FB was loaded. In column 2 of the 96–well plate, rows B, C and D were inoculated with 20 µL of an *M. bovis* isolate.

Using these three inoculated wells, 20 µL from column 2 (10^1 CCU) was diluted 10–fold within each column across the plate until column 11 (10^{10} CCU) was reached.

Further 10–fold dilutions using 20 µL from rows A, B and C of column 11 were created within rows E, F and G of column 2 (10^{11} CCU) and were similarly diluted within wells across the plate, which enabled a final concentration (10^{20} CCU) to be reached in column 11.

Risk of colour change resulting from CO_2 absorption was reduced by using a barrier of wells, containing uninoculated FB, that surrounded all wells containing inoculated FB.

Plates were sealed with parafilm and, over a two–week period, colour change from red to orange to yellow was assessed daily.

The concentration of *M. bovis* was identified by the change in FB colour within wells containing the greatest dilution factor (i.e., in column 9 of rows A, B and C, colour change of FB indicated a *M. bovis* concentration of 10^8 CCU). Colour change assays were repeated daily over a week and were compared to a spectrophotometry–generated growth curve of an equivalent period.

Despite assay limitations, such as formation of carbonic acid (from absorbance of CO_2 present within the incubator) altering pH, colour change remained a viable assessment of *M. bovis* growth. Colour change from red to orange/yellow represented increased fatty acid metabolism and, subsequently, a greater concentration of *M. bovis* in culture (Garcia-Morante et al., 2018).

Light absorbance spectrophotometry at wavelengths of 415 nm and 560 nm evaluated colour change of FB, enabling a better growth assessment than directly observing colour change.

2.3.6 Recovery of *Mycoplasma* ssp. in aRPMI

Survival of each *M. bovis* isolate in aRPMI provided understanding of whether *M. bovis* isolates survived independently from bEEL cells or did not survive without presence of a host.

Our hypothesis meant that any sEV production by extracellular *M. bovis* was considered as an influential factor for downstream proteomic analysis. Therefore, sEVs isolated from control groups (FB–grown *M. bovis* and aRPMI–grown *M.* bovis) were considered within our final proteomic analysis as changes in their protein regulation could be compared for discovery of biomarkers unique to a *M. bovis* co–culture.

Mycoplasma ovipneumoniae (***M. ovi***), another ruminant *Mycoplasma* sp., acted as an initial model for survival of *Mycoplasma* ssp. in aRPMI. Frey's medium (Merck–Millipore) was used for growth of *M. ovi* until colour change from red to orange/yellow was observed.

Dr. Benjamin Bridgeman must be acknowledged for providing *M. ovi* isolates that enabled initial modelling of a *Mycoplasma* sp.

Four–day old cultures of New Zealand *M. ovi* isolate 90 (Bridgeman et al., 2020) and New Zealand *M. ovi* isolate 103 (Bridgeman, 2021) were inoculated into aRPMI (300 µL into 3 mL). At time 0, bijous containing aRPMI were inoculated with *M. ovi*.

From each bijou, 30 µL was inoculated into 3 mL of Frey's medium at one, two, three, four, five, six and seven–days post inoculation. A replicate of each isolate was created at each time point, with recovery of *M. ovi* indicated by colour change of Frey's medium up to two weeks post inoculation.

Two isolates of *M. bovis* were assessed for survival in aRPMI. Isolates W18_04866 (#1) and W20_06790 (#3) were inoculated into aRPMI (300 µL into 3 mL) Each *M. bovis* isolate was inoculated into aRPMI alongside two repeats of each condition.

Uninoculated FB and aRPMI were used as negative controls, and positive controls of each *M. bovis* isolate were grown in FB. Additionally, three repeats using 30 µL aliquots of each isolate were included as initial *M. ovi* modelling indicated that reducing the concentration of *M. bovis* inoculated would represent survival of a *Mycoplasma* sp. more reliably.

A 10 µL aliquot of each aRPMI culture was inoculated weekly into 4 mL of FB for four weeks post inoculation. Light wavelength microscopy at 415 nm and 560 nm assessed recovery of *M. bovis* in FB, as compared to the included controls.

2.3.7 Gentamicin protection assay

Gentamicin protection assays evaluated the ability of each *M. bovis* isolate to infect bEEL cells and provided a crude analysis of *M. bovis* survival; be it through an intracellular route or limited to only adherence of bacteria to host cells (Raymond et al., 2018).

Gentamicin is an aminoglycoside antibiotic that is effective against gram–negative *Mycoplasma* ssp. by altering their protein translation (Lysnyansky & Borovok, 2021).

Gentamicin can struggle to penetrate the cell membrane of eukaryotic cells, therefore, internalised *Mycoplasma* ssp. are protected from antibiotic treatment (Bürgi et al., 2018).

However, concerns were raised about the reliability of how impenetrable eukaryotic cell membranes are to aminoglycoside antibiotics (VanCleave et al., 2017). Therefore, gentamicin concentrations were modified from previously reported assays.

In a 24 well flat–bottomed cell culture plate (Thermo Fisher Scientific), bEEL cells were seeded in sixteen wells at 2 x 10^5 cells/well. Eight wells did not contain bEEL cells as were kept as *M. bovis*–only controls.

Treatment positions are described within the provided plate map (**Figure 3**).

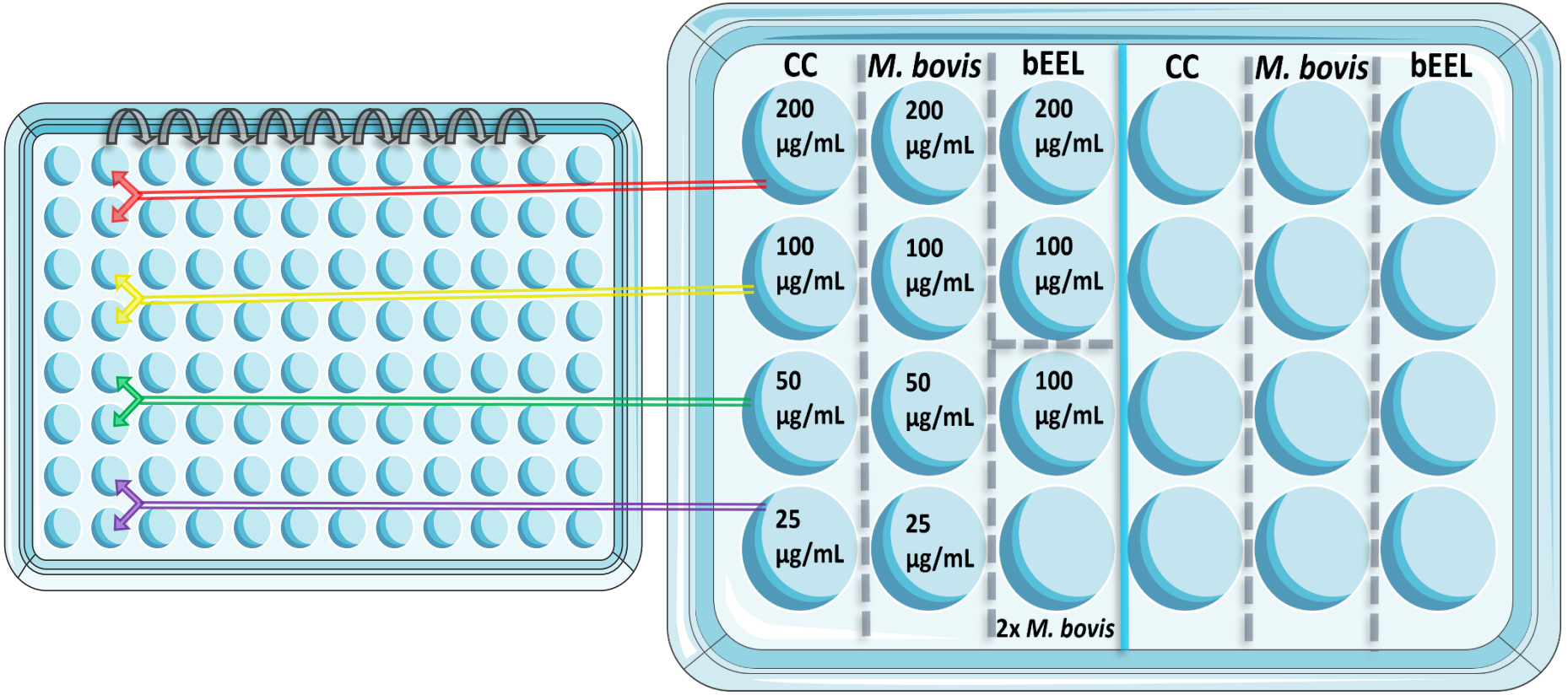
CC
M. bovis
bEEL
CC
M. bovis
bEEL
200 µg/mL
200 µg/mL
200 µg/mL
100 µg/mL
100 µg/mL
100 µg/mL
50 µg/mL
50 µg/mL
100 µg/mL
25 µg/mL
25 µg/mL
2x M. bovis

***Figure 3*: A gentamicin protection assay assessed the differences in adherence and intracellular infection of *Mycoplasma bovis* (*M. bovis*)**

A 24–well cell culture was seeded with a bovine endometrial epithelial cell line (**bEEL cells**) in Advanced Rosewell Park Memorial Institute 1640 (**aRPMI**) medium at 2 x 10^6 cells/mL within the specified wells: co–culture (**CC**), **bEEL** and **2x *M. bovis***.

The co–culture (**CC**) was inoculated with *Mycoplasma bovis* (***M. bovis***) isolate W18_04866 (#1) at a multiplicity of infection of 5.

In wells specified by ***M. bovis***, 20 µL of isolate W18_04866 (#1) was inoculated into 1 mL of aRPMI. In the wells specified by **2x *M. bovis***, 20 µL from each isolate, W18_04866 (#1) and W20_06790, were inoculated into 1 mL of aRPMI.

Infection of bEEL cells with *M. bovis* occurred for twenty–four hours post inoculation.

Wells were washed five times with 1 mL of 1x Phosphate Buffered Saline (**1x PBS**) following infection.

200 µg/mL, **100 µg/mL**, **50 µg/mL**, and **25 µg/mL** refer to concentrations of the antibiotic gentamicin (diluted from a stock solution of 10 mg/mL in 1 mL of aRPMI).

Wells not specified with a concentration of gentamicin were not treated with the antibiotic and were used as controls for each condition/treatment.

Gentamicin treatment occurred for three hours post 1x PBS washes. Wells were washed five times with 1 mL 1x PBS post gentamicin treatment.

TrypLE® was used to disassociate adherent cells within each well.

20 µL from each well of a column of the 24–well plate was transferred separately into column 2 of 96–well cell culture plates, as indicated in the figure, with all wells of the 96–well plate pre–filled with 180 µL of Friis Broth (**FB).**

Two repeats (from each well of the 24–well plate) were transferred to column 2 of a 96–well plate.

Column 1 of the 24–well plate is used as an example. Red arrows depict the two repeats of 200 µg/mL. Yellow arrows depict the two repeats of 100 µg/mL. Green arrows depict the two repeats of 50 µg/mL. Purple arrows depict the two repeats of 25 µg/mL.

Six columns of the 24–well plate created six individual 96–well plates.

The FB within column 2 of each 96–well plate was serially diluted 10–fold (depicted as grey arrows) across the plate, with column 11 being the final point for dilution.

Colour change of FB indicated *M. bovis* survival, with the final column of the 96–well plate to demonstrate colour change representative of the concentration of *M. bovis*.

A schematic diagram was required as, in compliance with the regulations set by the Physical Containment level 3 facility, images of any experiments could not be caputured.

Created/modified using Servier Medical Art, licensed under a Creative Commons Attribution 3.0 Unported License (https://smart.servier.com/).

Using a four–day old culture of W18_04866 (#1), bEEL cells were infected at a Multiplicity of Infection (**MOI**) of 5.

MOI was calculated using this equation:

$$'MOI' = \frac{Volume\ of\ M.bovis\ culture\ (\mu L) \times Concentration\ of\ M.bovis\ Culture\ (CCU)}{Number\ of\ bEEL\ cells\ to\ infect\ (cells/m\ L)}$$

Where CCU = Colour Change Units (*M. bovis* concentration),

M. bovis = *Mycoplasma bovis* isolate W18_04866 (#1), and

bEEL cells = a bovine endometrial epithelial cell line.

The plate was shaken for five minutes and then centrifuged at 300 rcf for five minutes to ensure an 'even' infection of bEEL cells. Each well was washed five times with 1 mL of 1x PBS, twenty–four hours post *M. bovis* inoculation. A 10 mg/mL stock gentamicin reagent (Gibco, Thermo Fisher Scientific) was diluted to 200 µg/mL, 100 µg/mL, 50 µg/mL, or 25 µg/mL as required within wells of the plate using 1 mL of aRPMI. Subsequently, the plate was incubated for three hours at 37 °C/5 % CO_2 following addition of gentamicin.

Three–hours post gentamicin treatment, aRPMI was removed by suction and each well was washed five times with 1 mL of 1x PBS per wash. Each well containing cells was then filled with 20 µL of TrypLE®, followed with incubation of the plate at 37 °C/5 % CO_2 for five to ten minutes. Wells were scrapped using a 10 µL inoculation loop to remove any remaining adherent cells.

Each well (of six 96–well flat–bottom cell culture plates) was loaded with 180 µL of FB. According to the plate map (**Figure 3**), each well of the 24–well cell culture plate corresponded to specified positions within column 2 of six individual 96–well cell culture plates. Four wells per column from the 24–well cell culture plate became eight wells per column within a 96–well cell culture plate, as two repeats of each treatment were included.

Accordingly, content of each of the six individual 96–well cell culture plates varied by treatment. Comparable to the colour change assay, the entirety of column 2 (10^1 CCU) was diluted 10–fold across the plate by transferring 20 µL between each column until column 11 (10^{10} CCU) was reached.

Plates were sealed with parafilm and incubated at 37 °C/5 % CO_2 for two weeks, with the colour change of FB assessed daily to validate *M. bovis* survival.

2.4 Sterilisation

2.4.1 Heat inactivation

A 1 mL aliquot of New Zealand *M. ovi* isolates 90 and 103 were individually heated at 80 °C, 90 °C and 100 °C for five minutes and ten minutes, with a technical replicate created for each individual treatment.

Heat–treated *M. ovi* was inoculated into Frey's medium at a $^{1}/_{4}$ dilution (1 mL of *M. ovi* into 3 mL of Frey's medium). An inclusion of an untreated positive control for both isolates of *M. ovi* was required for a comparison of colour change. Likewise, an uninoculated Frey's medium negative control was required, as was pre–heating and post–heating controls created from uninoculated Frey's medium for colour change comparison.

Samples were checked daily for a minimum of two weeks to confirm if colour change had occurred within heat treated samples.

Inactivation of *M. bovis* was adapted from modelling inactivation using *M. ovi.* However, instead of 1 mL of culture, 100 µL aliquots of *M. bovis* isolates W18_04866 and W20_06790 were heated in a heat block at either 56 °C for two hours, 80 °C for ten minutes, or 90 °C for ten minutes.

Within individual bijous, 50 µL from each heat–treatment was inoculated into 3.95 mL of FB at a $^{1}/_{80}$ dilution. Bijous were incubated at 37 °C/5 % CO_2 in a humidified incubator for two weeks. Using light absorbance spectrophotometry at wavelengths of 415 nm and 560 nm, colour change of heat–treated samples was compared to positive controls of each isolate/an uninoculated FB negative control.

Colony Forming Units (**CFU**) provided an alternative means to assess inactivation, with 10 µL of each heat treatment individually spread onto FA. Likewise, untreated W18_04866 (#1) and W20_06790 (#3) positive controls and an uninoculated FB negative control were spread onto FA plates.

Inactivation was confirmed by little to no formation of colonies, with a log10 difference in CFU between heat–treated samples and negative controls indicating that inactivation had occurred.

Three technical replicates were created from each of the three experimental temperatures, which established an average growth pattern of *M. bovis* using FB cultures and/or FA plates to determine if inactivation had occurred.

2.4.2 Fixation/Lysis

Prior to an addition of lysis buffer, 10 % from the total volume of concentrated sEV fractions (see 2.6.7) was aliquoted for downstream applications.

From this 10 % volume, 6 µL was combined at a 1:1 ratio with 3 % glutaraldehyde fixative (see 2.2.6.1) for subsequent TEM analysis of *M. bovis*–containing samples.

Only the remaining volume of control bEEL fractions were used for TRPS on the qNANO (IZON, Christchurch, NZ) as fixation of *M. bovis*–containing fractions caused aliquots to be unmeasurable on the qNANO.

Fixative was used to create TEM samples of concentrated sEVs that could be removed from the PC3 facility.

Lysis buffer was combined with concentrated sEV fractions at a ratio of 2:1, as the volume of each concentrated sample varied. Each solution was heated at 95 °C for ten minutes following addition of lysis buffer. All lysed sEV samples were stored at –80 °C.

Inactivation of *M. bovis* using lysis buffer and/or fixative was assessed in a similar way to inactivation using heat–treatment.

Three replicates of each condition were grown in FB and on FA, alongside positive/negative controls, for comparison of colour change/colony growth.

2.5 Epi–Fluorescent Microscopy

Epi–fluorescent microscopy expanded the evidence provided by the gentamicin assays regarding *M. bovis* infection. Pre–stained *M. bovis* was compared to post–stained *M. bovis* and bEEL cells, which demonstrated any differences in fluorescent dye uptake within nuclear/cellular membranes.

Whilst not specifically relevant to our hypothesis regarding sEV cargo changes, epi–florescent imaging demonstrated that the positioning of *M. bovis* was directly relative to the positioning of bEEL cells on the slides.

Round glass coverslips (22 mm) were sterilised in 70 % acetone, then 70 % ethanol, and were left to dry prior to their placement within each well of a 12–well cell culture plate (Nunc, Thermo Fisher Scientific). In aRPMI, bEEL cells were grown to ~80 % confluency, split (see 2.3.1) and seeded at 2 x 10^6 cells/mL using 1 mL of the cell suspension.

Twenty–four hours post–seeding, bEEL cells were infected with a four–day old subculture of W18_04866 (#1). Cells were infected at an MOI of 100 by combining 200 µL of *M. bovis* and 1 mL of FB within each well.

Prestaining of *M. bovis* involved an addition of Octadecyl Rhodamine B Chloride (**R18**) diluted to 5 µg/mL from a stock solution (2 mg/mL), and/or an addition of 4',6–diamidino–2–phenylindole (**DAPI**) diluted to 2 µg/mL from a stock solution (2 mg/mL). Both dyes were used separately and in combination to pre–stain *M. bovis* or bEEL cells.

Twenty–four hours post infection, FB was removed with each coverslip subsequently washed three times with 1 mL of 1x PBS. Cells were fixed with 200 µL of 10 % (v/v) Neutral Buffered Formalin (see 2.2.6.2) for fifteen minutes, then washed with 1 mL of 1x PBS.

Fixed cells were permeabilised using 0.05 % (v/v) Triton X–100/1x PBS for five minutes at room temperature with a final wash using 1 mL of 1x PBS.

Experimental coverslips were post–stained in a dark humidified chamber. Post–stains included Fluorescein isothiocyanate (**FITC)**–Phalloidin diluted $^1/_{500}$ from 0.5 mg/mL, DAPI diluted $^1/_{1000}$ from 2 mg/mL, and R18 diluted $^1/_{500}$ from 2 mg/mL. FITC–Phalloidin was combined with DAPI or used individually at mentioned concentrations for six experimental coverslips.

Individual post–stain control coverslips were created concurrently. A single additional coverslip was post–stained with FITC–Phalloidin combined with R18 at previously mentioned dye concentrations.

An additional two separate coverslips were post–stained with FITC–Phalloidin, which was combined with DAPI (diluted at $^{1}/_{500}$ or $^{1}/_{100}$).

Three coverslips were generated for each *M. bovis* or bEEL–only condition and were post–stained according to the fluorescent dye concentrations mentioned first (i.e., FITC–Phalloidin at $^{1}/_{500}$, DAPI at $^{1}/_{1000}$ and R18 at $^{1}/_{500}$).

Within the chamber, all coverslips were inverted into 50 µL of their respective post–stain on parafilm, left for thirty minutes in complete darkness and were subsequently washed five times using 1 mL of 1x PBS.

Each coverslip was mounted onto a microscope slide using ProLong™ Gold Antifade Mountant (ThermoFisher).

All coverslips were imaged using a 20x long–working objective on an Eclipse Ti–U inverted epi–fluorescent microscope (Nikon).

Texas Red, FITC and DAPI filters were utilised for imaging. All images were processed using ImageJ (Fiji).

2.6 Harvesting sEVs from Bioreactors

CELLine AD1000 bioreactor flasks (Merck–Millipore) were used to maximise sEV production from adapted bEEL cells.

The design of bioreactor flasks enables amplified bEEL cell growth through constant nutrient and waste diffusion between separated medium chambers.

Any sEVs produced by bEEL cells were prevented from diffusing throughout the flask by a semi–permeable membrane. A secondary separate membrane aided in cell respiration.

Bioreactor flasks were utilised over a prolonged culturing period to maximise production of sEVs, which enabled effective downstream analysis of the sEV proteome.

Figure 4 demonstrates a schematic of the CELLine AD1000 bioreactor flask.

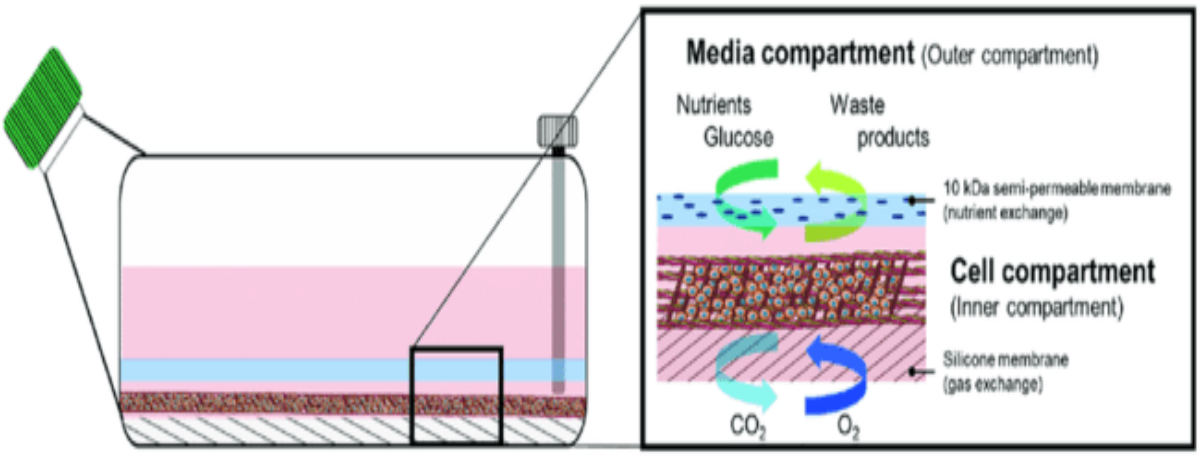

Figure 4*: Schematic illustration of the CELLine AD1000 flask (Guerreiro et al., 2018)

"This is a two–compartment culture system with an inner (cell) compartment designed to sustain cell growth at high densities, and an outer (media) compartment where cell–free culture medium is used.

Here, the outer and inner compartments are separated by a semi–permeable membrane which allows a continuous exchange of nutrients and waste.

A woven polyethylene terephthalate mesh inside the cell compartment provides cells with support for adherence and growth.

A silicone membrane at the bottom allows for direct oxygenation and gas exchange. Each compartment is accessed by a specific port.

The media compartment reservoir is reached through the green cap and the inner cell compartment through the white cap."

*Illustration and legend taken/adapted from (Guerreiro et al., 2018), https://journals.plos.org/plosone/article?id=10.1371/journal.pone.0204276, an open access article distributed under the terms of the Creative Commons Attribution License.

2.6.1 Control bEEL bioreactor

The cell compartment of the control bioreactor flask was seeded with adapted bEEL cells (19 x 10^6 viable cells suspended in 15 mL of aRPMI). The media compartment of each bioreactor contained 1 L of nutrient–only aRPMI.

A single control bEEL bioreactor flask was maintained to harvest sEVs, which required consistent replacement of each alternative medium once weekly.

The control bioreactor flask was harvested over approximately three months.

2.6.2 Co–culture bioreactor

The cell compartment of the co–culture bioreactor flask was seeded with adapted bEEL cells (29.25 x 10^6 viable cells suspended in 15 mL of aRPMI).

The media compartment of the co–culture bioreactor flask was filled with 1 L of nutrient–only aRPMI.

A single co–culture bioreactor flask was maintained to harvest sEVs, which required consistent replacement of each alternative medium once weekly.

In contrast to the control flask, the co–culture flask was inoculated with *M. bovis* isolate W18_04866 (#1) at an MOI of 5 (with bEEL cell growth estimated at 400 x 10^6 viable cells after two weeks of maintaining the bioreactor).

Isolate W18_04866 (#1) was inoculated into the aRPMI taken from the cell compartment (2 mL of *M. bovis* into 13 mL of aRPMI), which was then replaced into the cell compartment.

After a week to allow for infection to occur, sEVs were harvested from the co–culture bioreactor flask.

Weekly co–culture bioreactor harvests coincided with weekly control bioreactor harvests. Isolate W18_04866 was not reinoculated into the cell compartment following the initial inoculation.

The co–culture bioreactor flask was harvested over approximately three months.

2.6.3 Harvesting sEVs from bioreactor flasks

Weekly harvesting of each bioreactors' cell compartment required initial removal of 1 L of nutrient–only aRPMI from the media compartment.

For removal, a bioreactor flask was inverted over a beaker, with the neck of the flask facing down, enabling nutrient–only aRPMI to be poured out into the beaker.

The cell compartment lid was kept tightly closed and was pointed toward the ground following flask inversion.

The lid of the media compartment remained loose after removal of nutrient–only aRPMI, ensuring that proper harvesting of the cell compartment could occur without rupturing the polyethylene terephthalate matrix that bEEL cells were growing upon.

Harvesting 15 mL of aRPMI from the cell compartment required use of a 25 mL serological pipette.

The aRPMI was carefully mixed within the cell compartment three times before it was transferred to a sterile 15 mL conical tube.

By rocking the flask slightly whilst pipetting, bubbles were prevented from occurring between the polyethylene terephthalate matrix and the semi–permeable membrane.

2.6.4 Resetting each bioreactor

Each compartment of the bioreactor was restored using freshly prepared medium, which enabled the continual growth of bEEL cells and their subsequent production of sEVs.

Initially, 50 mL of nutrient–only aRPMI was used to wet the semi–permeable membrane within the media compartment. The cell compartment was then filled with 15 mL of aRPMI.

Continually, flasks were slightly rocked throughout medium replacement as it reduced potential introduction of bubbles between the membranes.

Finally, the media compartment was filled with 1 L of fresh nutrient–only aRPMI.

2.6.5 Clarifying and concentrating sEV harvests

Each bioreactor harvest was centrifuged to remove cellular debris, which created a clarified medium that could be processed for isolation of sEVs.

Clarified aRPMI was generated from the medium collected from the cell compartment of each bioreactor, which was spun at 500 rcf for ten minutes followed by a subsequent centrifugation at 10,000 rcf for ten minutes.

Clarified aRPMI was then concentrated using an Amicon Ultra–15 Centrifugal Filter Unit with an Ultracel–100 membrane (Merck–Millipore). Filter units were primed before use with a 5 mL wash of 0.1 M sodium hydroxide, followed immediately by two individual washes using 5 mL of LC–MS/MS–grade water.

As Size Exclusion Chromatography qEV10 columns (IZON, Christchurch, NZ) required 10 mL of medium to accurately isolate sEVs, a 6 mL aliquot from the previously clarified aRPMI was spun at 4000 rcf for eight to twelve minutes.

The retentate (1 mL) of the filter unit was added to the remaining 9 mL of unconcentrated, but clarified, aRPMI creating a concentrated 10 mL harvest. All harvests were frozen at –20 °C until sEV isolation occurred.

2.6.6 Setting up an Automatic Fraction Collector

Size Exclusion Chromatography (**SEC**) qEV10 columns (IZON, Christchurch, NZ) with 35 nm pores were used for consistent isolation of minimally damaged sEVs sized between 30–150 nm (Yang et al., 2020).

Other sEV isolation methods, such as differential ultracentrifugation, can be limited by resulting low purity and yield (Shirejini & Inci, 2021). Additionally, IZON is a New Zealand–based company, which was extremely useful for training, troubleshooting, and purchasing equipment locally.

Each qEV10 column was flushed three times prior to an addition of sample. First, columns were flushed with 140 mL of 1x PBS (previously degassed in a sonic bath for five minutes at 94 % power and 75 Hz), followed by a 2 mL flush of 0.5 M sodium hydroxide and, finally, another 140 mL flush of 1x PBS.

The final flush was used to remove any traces of sodium hydroxide or of sodium azide, which is present in the column storage buffer.

A total of 10 mL of clarified and concentrated medium was loaded into the reservoir of a qEV10 SEC column and passed into the column by gravity flow.

A volume of 1x PBS, altered accordingly to how many fractions were required, was loaded into the column reservoir once the medium had passed through the column frit.

Each 5 mL fraction was collected in Protein LoBind Tubes (5.0 mL; PCR Clean (Eppendorf AG) loaded onto the Automatic Fraction Collector and were stored at 4 °C prior to concentrating.

The first and fifth use of each column required a quality control check. These checks ensured a comparable flow rate and confirmed there were no blockages.

Twelve fractions, fractions 1–12, were isolated to analyse the relative positions of sEVs using light absorbance spectrophotometry at wavelengths of 350 nm and 600 nm.

Columns could be reused and were flushed prior to their storage with 140 mL of 1x PBS, followed by 2 mL of 0.5 M Sodium hydroxide and finally, a storage flush using of 140 mL of 1x PBS/sodium azide 0.05 % (w/v).

2.6.7 Concentrating sEV–containing fractions

Fractions 5–7 (sEV–containing fractions) were concentrated using primed Amicon Ultra–15 Centrifugal Filter Units.

Each individual 5 mL fraction was combined within a single filter unit, which was subsequently centrifuged at 4084 rcf for ten to fifteen minutes. Potentially, further centrifugation was required depending on sample viscosity.

All samples were spun until ~500 µL of retentate was achieved. The retentate was then transferred to a 1.5 mL Protein LoBind Tube (PCR Clean, Eppendorf AG) for subsequent lysis and inactivation.

2.7 Analysis of sEVs

2.7.1 Tunable Resistive Pulse Sensing (TRPS)

Tunable Resistive Pulse Sensing (**TRPS**) provided a means to assess sEV concentration and size. Only sEVs isolated from the control bEEL bioreactor were assessed.

Diluted sEV samples were forced through a nanopore with any resulting blockage inducing a current, which was interpreted as sEV size and concentration using the qNANO (IZON, Christchurch, NZ) (a machine that utilised TRPS to measure sEVs).

The concentration of sEVs was estimated solely using TRPS as Nanoparticle Tracking Analysis was unavailable during the current COVID–19 pandemic.

The qNANO was initialised according to manufacturer's recommendations.

A 100 nm polyurethane nanopore, NP100 (Izon Science), was freshly coated in coating solution (Izon Science) prior to each series of measurements.

The qNANO was calibrated using 100 nm polystyrene calibration particles, CPC100 (Izon Science), diluted $^{1}/_{1000}$ in 1x PBS/0.05 % (v/v) Tween–20.

Pore stretching, voltage and applied pressure were adjusted to ensure a baseline current of > 100 nA and background noise (root mean square) of < circa 15 pA. Calibrations and measurements were evaluated using two positive pressures, 5 mbar and 10 mbar.

A minimum of 500 blockade events were required for each measurement. Re–calibration occurred after each sample measurement to ensure pore stability and no blockages.

Data was analysed using an Izon Control Suite 3 software (Izon Science).

2.7.2 Transmission Electron Microscopy (TEM)

Transmission Electron Microscopy (**TEM**) was utilised effectively to contrast fixed samples of each sEV harvest.

Negatively stained sEVs from *M. bovis*, bEEL and co–culture samples were imaged as distinctive cup–shaped vesicles. Approximate sEV size and concentration was compared between treatments using TEM.

Fixation of sEV–containing samples occurred for twenty–four hours prior to imaging in 2x volume of 3 % glutaraldehyde fixative (see 2.2.6.1). Each treatment was diluted $^{1}/_{5}$ prior to fixation.

Preparation for TEM required inversion of 2 mm Formvar/Carbon coated size–200 mesh copper grids (Sigma–Aldrich, Merck–Millipore) into 10 µL of a fixed sample for four and a half minutes at room temperature. Grids were washed once with Milli–Q water.

A 10 µL droplet of an aqueous 4 % (w/v) uranyl acetate solution was used to negatively stain the samples on each grid.

Negative staining required four and a half minutes of incubation at room temperature, with excess stain blotted off using filter paper.

Images were captured using a Tecnai G2 Spirit BioTWIN Transmission Electron Microscope (Field Electron and Ion Company, ThermoFisher Scientific). Measurements of sEVs were generated by ImageJ (Fiji).

2.7.3 Analysis of sEV proteins

Presence of sEV–specific and exclusion proteins were confirmed within isolated fractions using Western Blotting and an Exosome Antibody array (Exo–Check; (System Biosciences).

Western Blotting compared positions of sEVs and larger proteins relative to each isolated fraction. Protein concentration was not established in our study using these techniques.

Importantly, both techniques demonstrated the viability of SEC columns to isolate sEVs correctly.

Dr. Alice Lake must be acknowledged for her considerable efforts in capturing all sEV images using TEM.

2.7.3.1 Western Blotting

Aliquots of ~120 µL from fractions 2–11 were added to an equal volume of complete RIPA buffer (see 2.2.4). Each fraction was vortexed, then agitated for thirty minutes at 4 °C.

Samples were sonicated twice for two second pulses at a maximum energy of 1,000,000 J and maximum amplitude of 40 %.

After sonication, each fraction was spun at 12,000 rcf for twenty minutes in a pre–cooled 4 °C centrifuge to pellet insoluble proteins.

The supernatant of each sample was transferred to pre–chilled 1.5 mL LoBind tubes. Lysates were stored at –80 °C.

Lysates of fractions 2–11 were concentrated to ~120 µL using a CentriVap Benchtop Vacuum Concentrator (Labconco Corporation, MO, USA).

Instead of estimating protein concentration (see 2.7.3.1.1), the variation in lysate concentrations of each fraction was normalised by combining 10 % of the total lysate volume with 4 µL of NuPAGE™ LDS Sample Buffer (4x) (Invitrogen, Thermo Fisher Scientific) and 2.5 % β–mercaptoethanol. Samples were heated at 90 °C for five minutes and kept on ice until loaded into gels.

Bis–Tris Gels (15–well 1.5 mm 4–12 %; (Thermo Fisher Scientific) were loaded into a NuPAGE mini tank filled with 200 mL of 1x MES/SDS running buffer within the inner chamber.

To prevent overheating, 50 µL of a NuPAGE antioxidant (Invitrogen, Thermo Fisher Scientific) was included.

Additionally, the outer compartment of the mini– tank was half filled with MES/SDS running buffer for this purpose.

In lane 1 of each gel, 7 µL of SeeBlue™ Plus2 pre–stained Protein Standard (Invitrogen, Thermo Fisher Scientific) was loaded.

In each subsequent well, 16 µL was loaded from sEV lysate fractions 2–11. Gels were run at 120 V for ninety minutes.

Once gel electrophoresis was finished, each gel was transferred onto a Nitrocellulose iBlot™ Transfer Stack (Invitrogen, Thermo Fisher Scientific). An iBlot® Gel Transfer Device (Invitrogen, Thermo Fisher Scientific) was used for seven minutes on program three to transfer proteins from each gel onto a nitrocellulose membrane.

Each nitrocellulose membrane was washed with sterile Milli–Q and stained with 0.1 % Ponceau S in 5 % acetic acid for ten minutes at room temperature using a shaker set at 75 rpm. Membranes were washed using sterile Milli–Q until each membrane was changed from red to pink.

Over–washing membranes required another ten–minute stain in Ponceau as reduced sensitivity and made protein bands less visible. Membranes were imaged using the Ponceau S setting on a ChemiDoc MP Imaging System (BioRad).

Membranes were washed with sterile Milli–Q water to remove Ponceau S. Membranes were blocked in 5 mL of either 5 % BSA (w/v) or 5 % trim milk (w/v) in 1x Tris–Buffered–Saline Tween 20 (0.1 %) (**TBS–T**) for one hour at room temperature, whilst shaken at 75 rpm.

Post–blocking, membranes were separated into individually labelled 50 mL conical tubes and were washed twice with 5 mL TBS–T (0.1 %). Anti–protein rabbit primary antibodies against CD63, CD9, Heat Shock Protein 70 (Exo–Ab–Kit–1, System Biosciences), Syntenin–1 (Ab19903, Abcam) and Calnexin (Ab22595, Abcam) were diluted $^{1}/_{1,000}$ in blocking solution.

Membranes were continually agitated using a Rotator Multi–mix with adjustable adaptors (Avantor, VWR International) in primary antibody overnight at 4°C

Twenty–four hours post–primary antibody, membranes were washed five times with 5 mL of TBS–T for two minutes each wash. Each membrane was transferred to a fresh 50 mL conical tube containing secondary antibody: anti–rabbit goat antibody conjugated with horse radish peroxidase, which was diluted $^{1}/_{10,000}$ in 5 mL of blocking solution. Membranes were constantly agitated in secondary antibody for an hour at room temperature. Finally, membranes were washed five times for two minutes each wash in TBS–T (0.1 %).

Proteins were visualised with Clarity™ ECL Western Blotting Substrate (BioRad) using a 1:1 ratio of luminol–enhancer solution and peroxide solution, which was kept in the dark. Each membrane and 1 mL of the Clarity™ ECL Western Blotting Substrate was sandwiched between two clear acetate sheets.

Membranes were imaged using a ChemiDoc MP Imaging System (BioRad). Protein ladders were imaged using automatic optimal colorimetric settings. Protein bands were imaged using chemiluminescence settings. Bands were initially auto exposed but required adjusting using Signal Accumulation Mode to achieve better clarity. All ladder and protein band images were merged/processed using ImageLab (BioRad).

2.7.3.1.1 Bicinchoninic acid (BCA) assay

A Bicinchoninic acid (**BCA**) assay was required to estimate protein concentration of fractions 5–7 (sEV–containing fractions) that were loaded into a Bis–Tris Gel.

Lysates were diluted $^1/_5$ in fresh RIPA buffer, creating a total volume of 25 µL. Bovine Serum Albumin standards of 12.5 µL were added in duplicate over two columns to a 96–well, flat–bottom plate alongside a duplicate of each sample being measured within two columns of the plate.

Part B and part A of a Pierce™ BCA Protein Assay Kit (Thermo Fisher Scientific) were combined $^1/_{20}$, with 100 µL of the working reagent added to each well. Plates were shaken for thirty seconds, incubated at 37 °C for thirty minutes, and read at 562 nm using a plate reader to estimate protein concentration.

2.7.3.2 Exo–Check: Exosome Antibody array

Fractions 5–7, from two harvests of the control bEEL bioreactor, were concentrated using a Amicon Ultra–15 Centrifugal Filter Unit with an Ultracel–100 membrane to maximise sEV concentration. A BCA assay was used according to the previously described method to estimate protein concentration (see 2.7.3.1.1).

A 10x stock solution of lysis buffer was combined with 6 µg of protein to create a 1x solution, which was then vortexed for fifteen to thirty seconds. The Exo–Check™ Exosome Antibody Array (System Biosciences) provided a labelling agent, and 1 µL was added to each lysate solution. Lysates were then vortexed and incubated at room temperature for thirty minutes with constant agitation.

Columns provided by the Exo–Check kit were used to remove excess labelling agent. Columns were prepared by an initial centrifugation at 800 rcf for one minute to remove storage buffer. Five separate washes using 400 µL of column buffer (provided by the Exo–Check kit) at 800 rcf followed the initial removal of storage buffer.

Finally, lysates were added directly into the middle of a column and, if required, total volume was adjusted to 140 µL using column buffer. Labelled sEV proteins were eluted through centrifugation at 800 rcf for two minutes in a fresh collection tube. Eluted proteins were combined with 5 mL of blocking buffer (provided by the Exo–Check kit) in a 15 mL conical tube.

Initially, a fresh Exo–Check membrane (pre–conjugated with antibodies) needed to be wet using sterile Milli–Q water for two minutes. The water was removed, and the membrane positioned 'face–up' so that the notched corner was orientated to the upper left–hand side.

For capture of antigens, 5 mL of the eluted protein/blocking buffer solution was transferred onto the moistened membrane. The membrane was incubated overnight at 2–8 °C with constant rocking.

Twenty–four hours post–incubation, the membrane was washed twice for two minutes in 5 mL of wash buffer. Coincidingly, detection buffer was prepared by combining 5 mL of reagent A and 1.5 µL of reagent B per membrane.

The washed membrane was incubated at room temperature in 5 mL of prepared detection buffer for thirty minutes. Detection buffer was removed, and wash buffer was used three times for five minutes to wash the membrane using agitation.

The membrane was developed using a Clarity™ ECL Western Blotting Substrate (BioRad) as previously described (see 2.7.3.1). The membrane was imaged using ChemiDoc MP Imaging System (BioRad) as previously described (see 2.7.3.1). The membrane image was processed using ImageLab (BioRad).

2.8 Liquid Chromatography Tandem Mass Spectrometry (LC–MS/MS) preparation of sEV lysates

2.8.1 Processing of sEV proteins

Eighteen sEV lysates were removed from a –80 °C freezer and were thawed at room temperature with a 250 µL aliquot taken to enable lysates to be refrozen. Each aliquot was concentrated using a CentriVap Benchtop Vacuum Concentrator.

Lysates were sonicated three times for five seconds using a VC–50 Vibra Cell Ultrasonic Processor (Sonics & Materials Inc., Newtown, CT, USA) at an output of 30 W. Insoluble proteins were pelleted in a pre–cooled 4 °C centrifuge at 12,000 rcf for ten minutes. The supernatant of each sample was then transferred into fresh PCR Clean 1.5 mL Protein LoBind Tubes (Eppendorf AG).

For initial precipitation, solvents were added to each sample in subsequent order. Four volumes of methanol (400 µL), one volume of chloroform (100 µL) and three volumes of LC–MS/MS grade water (300 µL) were added to 100 µL of each lysate. Each tube was vortexed thoroughly between addition of each solvent.

Samples were spun in a pre–cooled 4 °C centrifuge at 15,000 rcf for ten minutes. Without breaking the methanol/chloroform precipitation interface, the top aqueous layer of each solution was aliquoted out.

Initially, a secondary methanol precipitation step was included, using four volumes of methanol (400 µL) spun in a pre–cooled 4 °C centrifuge at 15,000 rcf for ten minutes. However, in subsequent protein precipitations, this additional step was excluded as it reduced protein concentration.

Supernatant was removed without disturbing the pellet of each sample. Protein pellets were air–dried in a fume cupboard at room temperature. Once dried, pellets were resuspended in 100 µL of 10 mM Ambic, then vortexed and placed in a sonication bath for five minutes.

2.8.2 Protein concentration

Attempts were made to measure protein concentration using Direct Detect Assay–free cards (Merck–Millipore) on a Direct Detect Spectrophotometer (Merck–Millipore), with 10 mM Ambic used as a blank comparison control. Protein concentration was unreadable using 2 µL of a trial sample (bEEL control sample #1).

Concentrated lysate aliquots were combined in duplicate to maximise protein concentration. Each duplicate sample was separately resuspended in 20 µL of 10 mM Ambic.

Test samples from a duplicate pair of lysate samples were measured prior to combining them. Both samples were within a difference of 0.1 mg/mL. Therefore, each duplicate lysate sample was combined, making a total solution of 40 µL.

Initially, lysates were measured in triplicate using analysis method 1 on a Direct Detect Spectrophotometer but it was unable to provide an accurate measurement. Instead, a Qubit 1.0 Fluorometer (Invitrogen, Thermo Fisher Scientific) and a QuDye Protein Quantification Kit (Lumiprobe) were used.

A total volume of 200 µL was required for each Qubit measurement. By diluting QuDye Protein Reagent $^{1}/_{200}$ with provided QuDye Protein buffer, a working solution of QuDye Protein dye was formed. Each protein standard was created at 0 ng/µL, or 200 ng/µL, or 400 ng/µL of Bovine Serum Albumin in TE buffer.

Each tube was incubated at room temperature for at least fifteen minutes to ensure protein staining had occurred. Each tube was vortexed prior to staining and again before they were measured. Measurement of each lysate occurred within ten minutes of each protein standard being read.

Each duplicate sample was read twice to increase accuracy. Protein concentration was averaged, and each sample was normalised to 3 µg/µL in a total of 50 µL of 10 mM Ambic. This enabled quantifiable protein measurements to be obtained using LC–MS/MS/MS.

2.8.3 Digestion of proteins to peptides

Using 1 µL of 200 mM Dithiothreitol enabled protein reduction through diminishing disulfide bonds. It was mixed thoroughly into each precipitated protein sample and left in the dark at 56 °C for forty–five minutes in a Thermomixer (Eppendorf AG).

Using 1 µL of 200 mM Iodoacetamide enabled alkylation of proteins to prevent reformation of disulfide bonds. It was mixed thoroughly into each sample and left in the dark at room temperature for thirty minutes in a Thermomixer (Eppendorf AG).

Proteins were digested using a Pierce™ Trypsin/Lys–C Protease Mix, MS–Grade (Thermo Fisher Scientific), which was dissolved in 20 µL of 100 mM of Ambic at a concentration of 1 ug/µL. To each tube, 1 µL of Trypsin/Lys–C was added and, to aid in digestion/prevent proteins sticking together, 5 µL of Acetonitrile (**ACN**) was included within this digestion mixture. Digestion occurred overnight at 37 °C in a Thermomixer (Eppendorf AG).

Finally, peptides were desalted following digestion, and were eluted through use of Pierce™ 100 µL C18 Tips (Thermo Fisher Scientific). Each tip containing monolithic C18 reversed–phase sorbent was activated by loading 50 µL of 50 % ACN three times. Each tip was equilibrated following activation using 50 µL of 0.1 % formic acid.

From each peptide sample, 48 µL was transferred into fresh 0.5 mL PCR Clean Protein LoBind Tubes (Eppendorf AG). To increase retention of peptides, peptide mixtures were aspirated three times. Peptides remained trapped in each C18 tip.

All tips containing peptides were washed once with 50 µL of 0.1 % formic acid, which was discarded after use. Peptide elution occurred twice using 50 µL of 70 % ACN into fresh 0.5 mL PCR Clean Protein LoBind Tubes.

All eluted peptides were frozen at –80 °C. Three individual aliquots from each peptide sample were processed using LC–MS/MS.

Dr. Evelyne Maes and Ancy Thomas must be acknowledged for their outstanding effort in processing peptide samples for LC–MS/MS and identifying the resulting proteins.

2.9 Peaks X Pro Studio

Each LC–MS/MS–generated protein peak representing sEV treatment group was assessed using PEAKS (Bioinformatics Solutions Inc). It enabled their differentiation and subsequent grouping of comparable proteins.

Consequently, the regulation of analogous proteins between treatments and constitutively expressed sEV proteins could be contrasted to enable discovery of a representative biomarker.

2.9.1 Protein identification

The Peaks X Pro Studio software package (Bio informatic Solutions Inc) was used to analyse the LC–MS/MS data.

The raw data were refined by a built–in algorithm, including only ions with a charge 2+ to 5+ and allowing chimeric spectra. The proteins and peptides were identified with the following parameters: a precursor mass error tolerance of 10 ppm and fragment mass error tolerance of 0.05 Da were allowed, an *in–house* database containing bovine protein sequences and Uniprot *M. bovis* protein sequences were used, the *Saccharomyces* uniport database was used as contaminant database, Trypsin/LysC was specified as digestive enzyme and up to 2 missed cleavages were allowed.

Carbamidomethylation of cysteine was set as a fixed modification. Oxidation (M), deamidation (NQ), carbamylation, acetylation (N–terminal), pyroglutamate from Q and methylation were chosen as variable modifications. A maximum of three post–translational modifications per sample were permitted.

False discovery rate (**FDR**) estimation was made based on decoy–fusion. An FDR of < 1 % at peptide level was considered adequate for confident peptide and protein identification. At least one unique peptide per protein was required for both identification and quantification purposes.

Dr. Evelyne Maes and Ancy Thomas must be acknowledged for their outstanding effort in processing peptide samples for LC–MS/MS and identifying the resulting proteins.

2.9.2 Label free quantification

To quantify the protein expression levels, label–free quantification was performed using Peaks Studio X Pro software.

The following parameters were set: a mass tolerance error of 15 ppm and a retention time shift tolerance of two minutes were allowed.

To determine the relative protein abundances in the Liquid Chromatography retention–time–aligned samples, peptide feature–based quantification was performed.

Comparison of the relative levels of each protein identified in the samples was based on the peak areas of all unique peptides per protein. Total ion count was used to normalise across samples and batches.

2.10 Statistical Analyses

Analyses regarding *M. bovis* recovery or inactivation were performed using either an unpaired students t–test or a One–Way ANOVA. The significance values were indicated as * = $p < 0.05$, ** = $p < 0.01$, *** = $p < 0.001$, **** = $p < 0.00001$, or ns = not significant. Analysis of *M. bovis* growth was performed using a repeated measures ANOVA.

The Correlation Coefficient is a statistic value used to show how the scores from one measure relate to scores on a second measure for the same group of individuals. A high value (approaching +1.00) is a strong direct relationship, values near 0.50 are considered moderate and values below 0.30 are considered to show weak relationship. A low negative value (approaching -1.00) is similarly a strong inverse relationship, and values near 0.00 indicate little, if any, relationship.

Principle Component Analyses (**PCA**) were performed on the protein abundance levels using the PCA function of the mixOmics package (Rohart et al., 2017).

Prior to calculating the PCA loadings, the proteins were filtered to only include proteins with an abundance estimate of at least 25 % required in the samples.

Protein differential abundance analyses were calculated by fitting a negative binomial model (glm.nb from the R package MASS (Core Team, 2013; Venables & Ripley, 2013) to estimate the abundance as an interaction between the protein and sample group, followed by the adjusted p–value calculation for each individual protein in each group using the R package predictmeans (version 1.0.6, (Dongwen, 2021).

All analysis was performed in R version 4.0.2.

Dr. Charles Hefer and Dr. Alasdair Noble must be acknowledged for their considerable efforts in statistically analysing all LC–MS/MS samples.

3 Results

3.1 Culturing of bEEL cells and/or M. bovis

3.1.1 Adaptation of bEEL cells to aRPMI

For investigation of sEVs produced from a bovine cell culture, successful adaptation of bEEL cells to aRPMI medium (supplemented with Exosome–Depleted FBS, GlutaMAX and penicillin/streptomycin) was required to reduce interfering bovine sEVs that were present within standard FBS.

Adaptation was achieved by slowly reducing the concentration of Exosome–Depleted FBS in aRPMI from 10 % to 4.5 % over eight weeks, equivalent to approximately fifteen passages.

Survival of bEEL cells for three consecutive passages in 4.5 % Exosome–Depleted FBS within aRPMI indicated adaptation was successful. Adaptation transiently altered growth patterns of bEEL cells.

Cells grown in RPMI 1640 medium grew in a 'cobblestone'–like appearance throughout tissue culture flasks (**Figure 5Ai** and **Figure 5Aii**), with bEEL cells grouping together to create patches.

Following adaptation to aRPMI, patterns of bEEL cell growth were altered. Changes in bEEL cell growth indicated that bEEL cells associated less with each other during early growth, with cells growing in 'eyelet shapes' rather than 'cobblestone–like' patches (**Figure 5B**).

Adapted cells required an additional medium change before they were split as compared to unadapted bEEL cells.


Aii


Ai

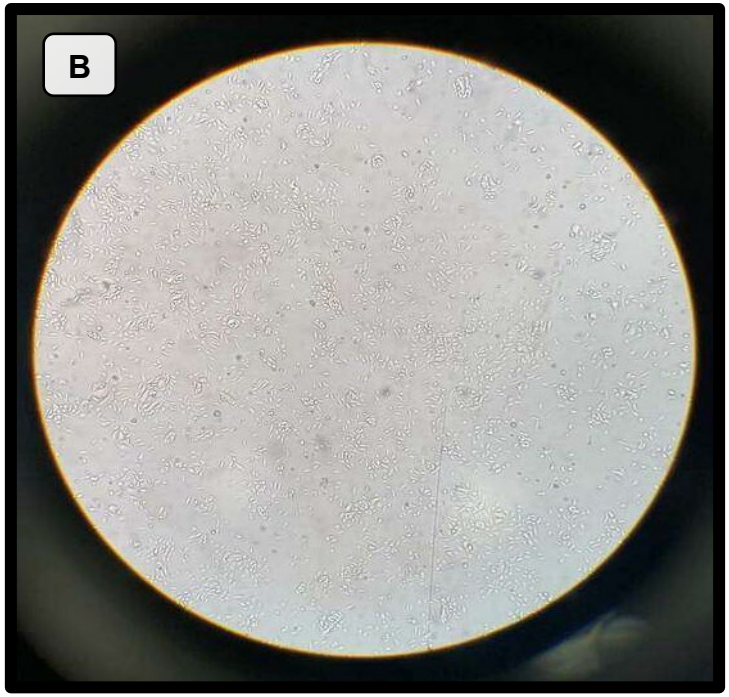
B

Figure 5: Growth pattern of a bovine endometrial epithelial cell line (bEEL cells) was altered through adaptation to a new medium

Initial bovine endometrial epithelial cell line (**bEEL cell**) cultures (Images **Ai and Aii**) were grown in Rosewell Park Institute Memorial 1640 (**RPMI 1640**) medium supplemented with 10 % foetal bovine serum (**FBS**) and 1 % penicillin–streptomycin.

Adaptation to an Advanced Rosewell Park Memorial Institute 1640 (**aRPMI**) medium (Image **B**), supplemented with 4.5 % Exosome–Depleted FBS, 2x Glutamax and 1x penicillin/streptomycin, altered bEEL growth as bEEL cells grouped together less and formation of cell patches was reduced.

Images (**Ai**) and (**B**) were captured using a 40x objective on a light microscope, with (**Ai**) imaged at ~70 % confluency and (**B**) imaged at ~50 % confluency.

Image **Aii** was captured using an EVOS™ XL Core Imaging System using a 40x objective at ~40 % confluency.

All bEEL cells were grown at 37 °C in a humidified 5 % CO_2 incubator for the entirety of cell culturing.

3.1.2 Stable growth of two separate *M. bovis* isolates was established and characterised

To investigate the ideal growth conditions of *M. bovis* and choose the isolate used for infection of bEEL cells, two separate isolates, W18_04866 (#1) and W20_06790 (#3), were assessed.

Small creamy–coloured colonies formed on Friis Agar (**FA**) and were observed macroscopically. Microscopic examination at 40x magnification revealed bacterial cocci with a central inner ring.

Growth of each isolate was associated with changes in colour/acidity of FB. An increased concentration of *M. bovis* was indicated by a colour change from phenol red to light orange and then to a bright yellow.

Colour change was semi–quantitively measured using spectrophotometry at 415 nm (**Figure 6A**) and 560 nm (**Figure 6B**). Three independent subcultures of each *M. bovis* isolate were assessed for growth.

An increased absorbance at 415 nm (as compared to a uninoculated FB negative control), was interpreted as growth of each *M. bovis* isolate. Absorbance at 415 nm initially increased, peaked, and then continued to increase after a slight drop.

Each day, absorbance was normalised against the uninoculated FB negative control kept at the same conditions as the *M. bovis* isolates.

A decrease in absorbance at 560 nm was interpreted as growth of each *M. bovis* isolate. The change in absorbance of 560 nm was represented as a 'bell curve' with the curve going down, peaking, and then going back up to zero change in absorbance.

Each day, absorbance was normalised against the uninoculated FB negative control kept at the same conditions as the *M. bovis* isolates.

An absence of a sustained change in average absorbance at 560 nm (i.e., day 0 compared to day 9) indicated that leaving the uninoculated FB negative control untouched for nine days had caused the pH of FB to decrease through absorbance of CO_2 (formation of carbonic acid) that was present within the incubator.

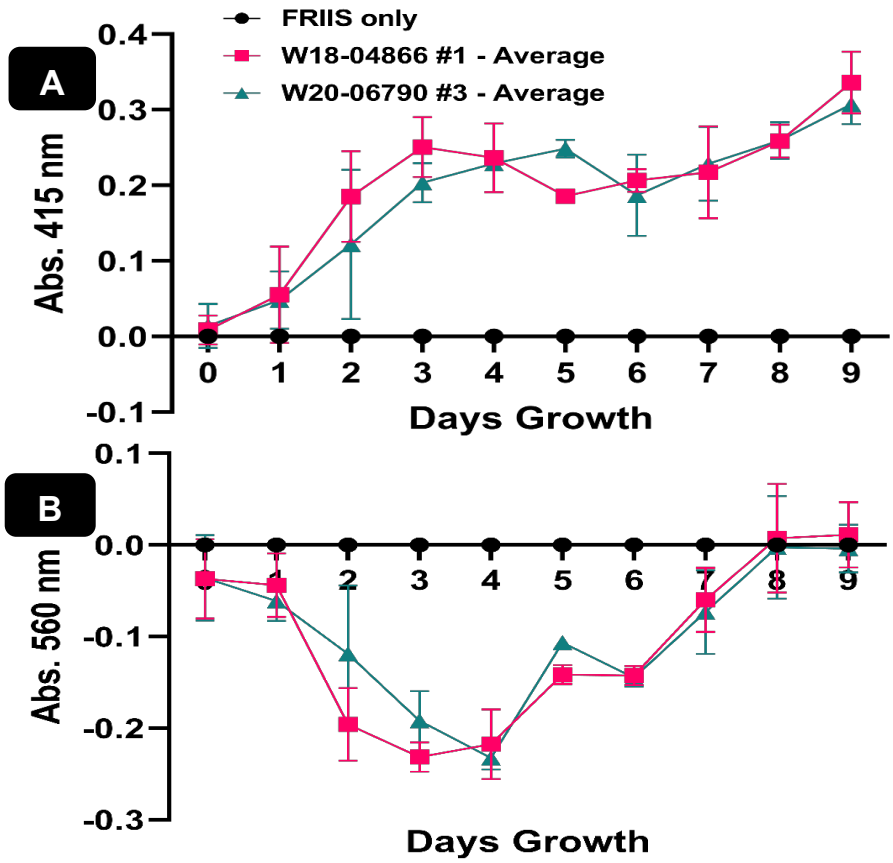

***Figure 6*: Two isolates of *Mycoplasma bovis* (*M. bovis*) reached exponential growth four–days post–subculturing**

Both *M. bovis* isolates peaked at Day 4 growth, with the average absorbance at 415 nm and 560 nm comparable at Day 4 in each curve. The growth patterns of each *M. bovis* isolate were comparable with no significant differences between independent subcultures.

Average absorbance of W18_04866 (#1) and W20_06790 (#3) overlap at Day 4 in both curves, with slight differences in absorbance between isolates at Day 3 and Day 5 in each absorbance curve.

Therefore, a four–day old subculture of a *M. bovis* isolate was used for infection or downstream analysis.

Light absorbance of three independent subcultures of two *Mycoplasma bovis* (***M. bovis***) isolates, W18_04866 (#1) and W20_06790 (#3) was measured daily using light absorbance spectrophotometry at wavelengths of 415 nm (**A**) and 560 nm (**B**).

Daily assessment was normalised against daily assessment of the uninoculated Friis Broth (**FB**) control that was measured at both wavelengths, and was represented as black dots.

Isolate W18_04866 (#1) is represented as pink squares and isolate W20_06790 (#3) as light blue triangles. All spectrophotometry was normalised to an uninnoculated FB control, which was created at the point of initial inncoulation of *M. bovis* isolates.

The FB control and subcultures were incubated at 37 °C in a humidified 5 % CO_2 for the length of days grown indicated in the figure. Analysis was performed using a repeated measures ANOVA. Both *M. bovis* isolates were significantly different ($p > 0.05$) from the FB control.

3.1.3 Cultures of *M. bovis* reached peak growth between day 3 and 5 post inoculation

Further investigation of *M. bovis* isolates estimated their concentration (Colour Change Units (**CCU**) in culture through changes in the colour of FB (**Figure 7**), which provided a necessary part of the formula required for infection of bEEL cells.

Initially, using a colour change assay, *M. bovis* concentration was estimated through 10–fold serial dilutions in FB using a four–day old subculture of isolate W18_04866 (#1). Dilutions were repeated in three wells.

Three 96–well culture plates containing the same series of dilutions were used to estimate the concentration of W18_04866 (#1). The FB of each repeat changed colour at a concentration of at least 10^6 CCU/mL in all plates.

However, using light microscopy, *M. bovis* colonies were observed within the 96–well culture plate at a concentration of 10^9 CCU/mL. At a concentration of 10^9 CCU/mL, at least two out of the three wells containing W18_04866 (#1) changed colour in each plate. As colonies of W18_04866 (#1) were observed at a greater concentration than 10^6 CCU/mL, the concentration of a four–day old subculture of W18_04866 (#1) was estimated to be 10^9 CCU/mL.

Although W20_06790 (#3) was not used for co–culturing, the concentration of W20_06790 (#3) in FB was estimated to be at least 10^5 CCU/mL.

To further assess *M. bovis* growth, colour change assays were used to estimate the concentration of W18_04866 (#1) subcultures created on each day over nine days, with three replicates of each daily condition generated.

Subcultures were similarly assessed by 10–fold serial dilution, with the final dilution indicating the concentration of W18_04866 (#1) for that specific day. Colour change of FB and visualising any growth of *M. bovis* colonies within 96–well culture plates were used to assess concentration.

Three 96–well culture plates were generated for each condition. Day 1 and 2 subcultures grew to ~10^2 CCU/mL. Concentrations of Day 3, 4 and 5 subcultures were greater, reaching ~10^9 CCU/mL. Seven–days post inoculation, the concentration of W18_04866 (#1) was reduced to ~10^4–10^5 CCU/mL. The concentration of any subsequent daily subculture remained at a concentration of ~10^4–10^5 CCU/mL for the remainder of the daily subcultures.

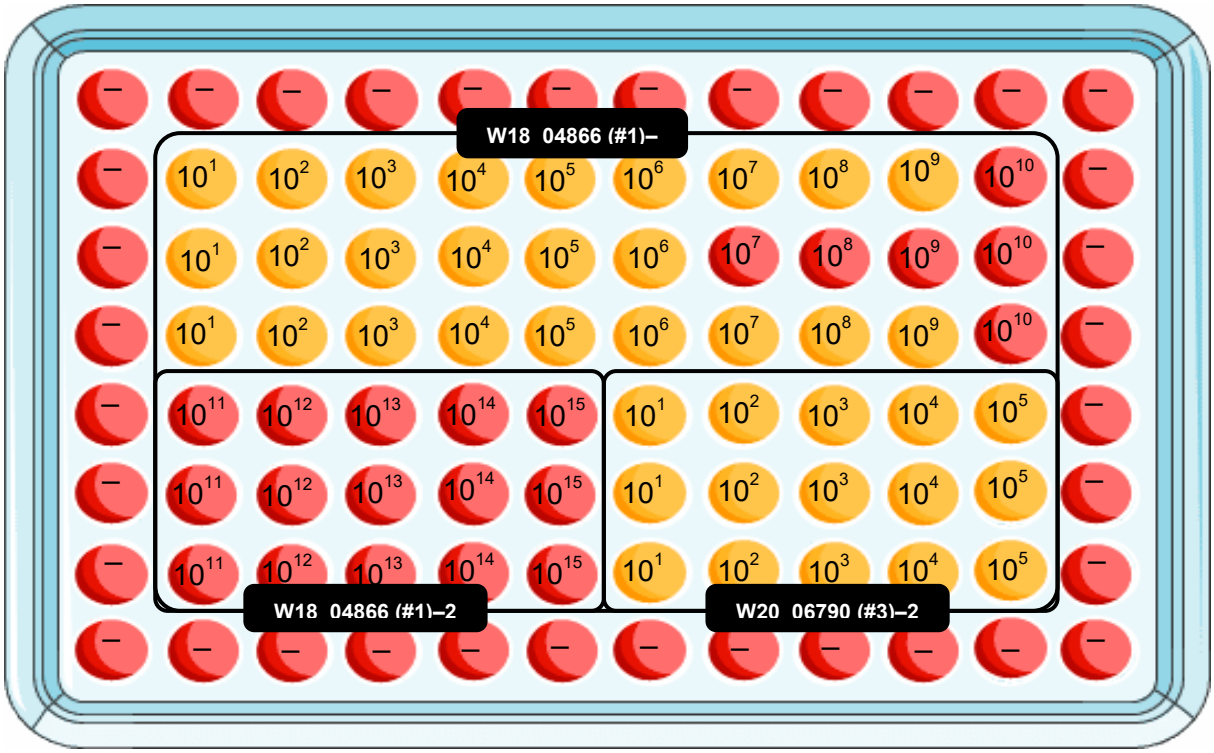

Figure 7: **Colour change assays estimated concentration of two isolates of *Mycoplasma bovis* (*M. bovis*) in culture**

Isolates W18_04866 (#1) and W20_06790 (#3) of *M. bovis* were serial diluted across a 96–well plate using Friis Broth (**FB**).

Isolate W18_04866 (#1) was inoculated into rows B, C and D of column 2 and W20_06790 (#3) was inoculated into rows E, F and G of column 7.

Colour Change Units (**CCU**) indicated the concentration of each *M. bovis* isolate, with the final column to change colour used as an experimental concentration of *M. bovis* isolates.

Each column was subsequently diluted 10–fold across the plate (**10^x** where x indicates the dilution factor) from column 2 (W18_04866 (#1) or column 7 (W20_06790 (#3) until the end of the plate was reached (i.e., column 11 (10^{10} CCU (W18_04866 (#1)) or column 11 (10^5 CCU (W20_06790 (#3)).

From rows A, B and C of column 11, isolate W18_04866 (#1) was further 10–fold diluted using rows E, F and G of column 2 to reach a CCU of 10^{15} (column 6). Inoculated wells were surrounded with a barrier of uninoculated FB (indicated by a **–**).

Plates were sealed and *M. bovis* growth was observed over a two week period, with signs of FB yellowing attributed to *M. bovis* growth.

A schematic diagram was required to demonstrate colour change assays as, in compliance with the regulations set by the Physical Containment level 3 facility, images of any experiments could not be caputured.

Created/modified using Servier Medical Art, licensed under a Creative Commons Attribution 3.0 Unported License (https://smart.servier.com/).

3.1.4 Recovery of *M. bovis* from aRPMI was comparable to FB

It was necessary to assess growth of *M. bovis* in aRPMI to prepare for potential downstream impacts that extracellular *M. bovis* had upon co–culture sEVs. Growing *M. bovis* in aRPMI did not prevent recovery of the bacterium after transfer to FB (**Figure 8**).

Triplicate replicates of *M. bovis* isolates W18_04866 (#1) and W20_06790 (#3) in aRPMI were generated and left for fourteen, twenty–one and twenty–eight days.

Each *M. bovis* isolate, grown in aRPMI or FB, was subcultured in fresh FB following their lengthy incubation.

After a week had passed to allow for recovery of aRPMI or FB–grown *M. bovis* to occur, light–wavelength spectrophotometry at 415 nm (**Figure 8A**) and 560 nm (**Figure 8B**) was used to measure the absorbance of each replicate against an uninoculated FB negative control.

Three replicates were created for each condition and averaged to assess recovery. An uninoculated aRPMI negative control was included, which indicated slight differences in absorbance between an uninoculated FB control and an uninoculated aRPMI control.

There was no difference in recovery between either *M. bovis* isolate grown in aRPMI or FB, with *M. bovis* recovered successfully in FB after twenty–eight days in aRPMI.

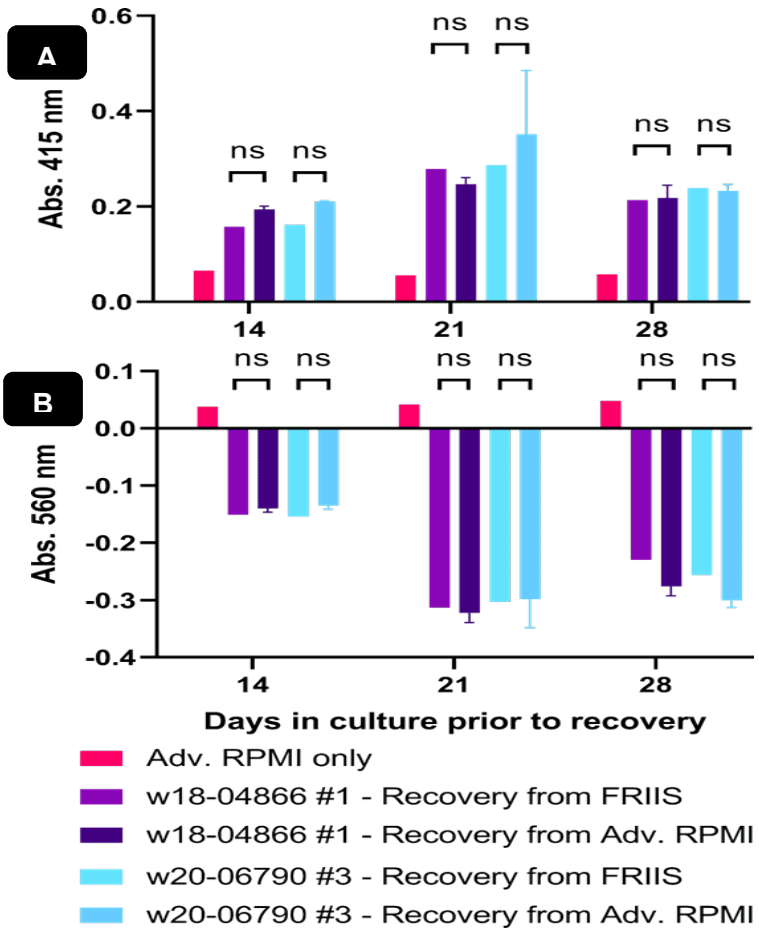

***Figure 8*: Recovery of *Mycoplasma bovis* (*M. bovis*) from Advanced Rosewell Park Memorial 1640 (aRPMI) medium was comparable to control Friis Broth (FB) cultures at least twenty–eight days post inoculation**

Isolates W18_04866 (#1) and W20_06790 (#3) of *M. bovis* were inoculated into Advanced Rosewell Park Memorial Institute (**aRPMI**) medium (dark purple=W18_04866 (#1) and light blue=W20_06790 (#3)) and Friis Broth (**FB**) (light purple=W18_04866 (#1) and darker blue=W20_06790 (#3)) separately at day zero.

Subcultures were created at fourteen– , twenty–one– and twenty–eight–days post inoculation using fresh FB.

Light absorbance spectrophotometry at wavelengths of 415 nm (**A**) and 560 nm (**B**) assessed isolate survival/growth seven–days post–subculturing by comparing uninoculated aRPMI and FB controls.

All spectrophotometry was normalised to an uninnoculated FB control, which was created at the point of initial inncoulation of *M. bovis* isolates.

Analyses were performed using a One–Way ANOVA. At each wavelength, no significant differences (**ns**) in absorbance occurred between treatments.

3.1.5 Heat treatment did not fully inactivate *M. bovis*, but fixation and lysis enabled successful inactivation of *M. bovis*

In New Zealand, inactivation of *M. bovis* was required to prevent a potential outbreak. Inactivation preceded transfer of any samples out of the PC3 facility.

Various inactivation methods were compared to determine an ideal technique that would be able to concurrently maintain sEV biology and cause inactivation of *M. bovis*; all inactivation results are summarised in **Table 1**.

The SEC columns used for downstream isolation of sEVs did not cause inactivation of *M. bovi*s (**Figure 9**). Each SEC fraction, fractions 2–13, was inoculated into FB and assessed for colour change to indicate survival of *M. bovis*. Each fraction generated a colour change in FB one–week post inoculation, which demonstrated that *M. bovis* was isolated alongside sEVs by SEC and that generating *M. bovis* sEV controls would be essential to enable downstream analysis of co–culture–specific sEVs.

Therefore, an additional inactivation step was required for removal of any sEV samples from the PC3 laboratory as *M. bovis* remained viable following SEC isolation. Hence, multiple temperatures were tested for inactivation of *M. bovis* with an intention of also maintaining sEV biology (**Figure 10**).

Inactivation at 56 °C for thirty minutes produced viable *M. bovis* colonies in FB and on FA (**Figure 10A** and **Figure 10B**).

At 80 °C, a colour change occurred after a week following separate inoculation of each heat–treated *M. bovis* isolate in FB (**Figure 10C** and **Figure 10D**). Also, colonies formed on FA and the difference in growth between untreated and heat–treated samples was minimal.

At 90 °C, colour change occurred after a week following separate inoculation of each heat–treated *M. bovis* isolate in FB (**Figure 10C** and **Figure 10D**). However, in contrast to heating *M. bovis* at 80 °C, growth of *M. bovis* colonies on FA was reduced. Heat treatment reduced *M. bovis* colony numbers from a bacterial lawn (untreated W18_04866 (#1)) to ~10–20 colonies. Growth of viable *M. bovis* colonies on FA, especially from a 10 µL aliquot, meant that heat treatment was a non–viable inactivation technique.

Instead, an inclusion of a glutaraldehyde (**Figure 11A** and **Figure 11B**), formalin or a Mass Spectrometry lysis buffer (**Figure 11C** and **Figure 11D**) in culture enabled sterilisation of SEC fractions and inactivation of *M. bovis*.

Treating *M. bovis* isolates with these solutions generated no colour change in FB (except at 415 nm for the Mass Spectrometry lysis buffer). Colour change was less representative of inactivation than in previous treatments, as the acidity of the lysis buffer affected absorbance (**Figure 11C**).

Compared to an untreated control W18_04866 (#1), no growth of *M. bovis* colonies occurred on FA (i.e., a bacterial lawn was reduced to 0 CFU/mL). The use of FA provided a better representation that inactivation caused by a Mass Spectrometry lysis buffer, formalin and/or glutaraldehyde had occurred (compared to colour change of FB).

Inactivation was repeated separately with at least three replicates. Each replicate provided a consistent result, which confirmed sterilisation of *M. bovis*–containing SEC fractions.

***Table* 1: Summary of all inactivation experiments used to treat *Mycoplasma bovis* (*M. bovis*)**

Experiments	Growth		Results	Replicates
	FRIIS Broth (FB)	FRIIS Agar (FA)		
Heat inactivation at 56 °C for two hours.	Yes	Yes	Both isolates of *M. bovis* survived heat inactivation at 56 °C for two hours and were subcultured into FB or grown on FA successfully with growth detectable after four days.	4 Technical 2 Experimental 2 Biological
Heat inactivation at 80 °C for ten minutes.	Yes	Yes	Both isolates of *M. bovis* survived heat inactivation at 80 °C for ten minutes and can be subcultured into FB or grown on FA successfully with growth detectable after four days.	4 Technical 1 Experimental 2 Biological
Heat inactivation at 90 °C for ten minutes.	No	Yes	Both isolates of *M. bovis* survived heat inactivation at 90 °C for ten minutes. They grew on FA with growth detectable after four days. However, FB subcultures did not demonstrate growth after seven days.	4 Technical 1 Experimental 2 Biological
Survival in Mass Spectrometry lysis buffer.	No	No	Both isolates of *M. bovis* did NOT survive lysis using Mass Spectrometry buffer. No growth was detected in FB or on FA after seven days.	3 Technical 1 Experimental 2 Biological
Survival in 3 % glutaraldehyde/ 0.1 M sodium cacodylate buffer.	No	No	*M. bovis* did NOT survive fixation using 3% Glutaraldehyde. No growth was detected in FB or on FA after seven days.	3 Technical 1 Experimental 2 Biological
Survival in 10 % formalin.	No	No	Both isolates of *M. bovis* did NOT survive fixation in 10 % formalin. No growth was detected in FB or on FA after seven days.	3 Technical 1 Experimental 2 Biological

***Footnote*: Three or four technical replicates indicated the number of repeats created for the specific experiment using the same conditions. Two experimental replicates indicated that the specific experiment was repeated twice independently (using the same number of technical and biological replicates. A single experimental replicate indicated that the specific experiment was not independently repeated. Two biological replicates indicated use of two *M. bovis* isolates, W18_04866 (#1) and W20_06790 (#3), for the specific experiment.**

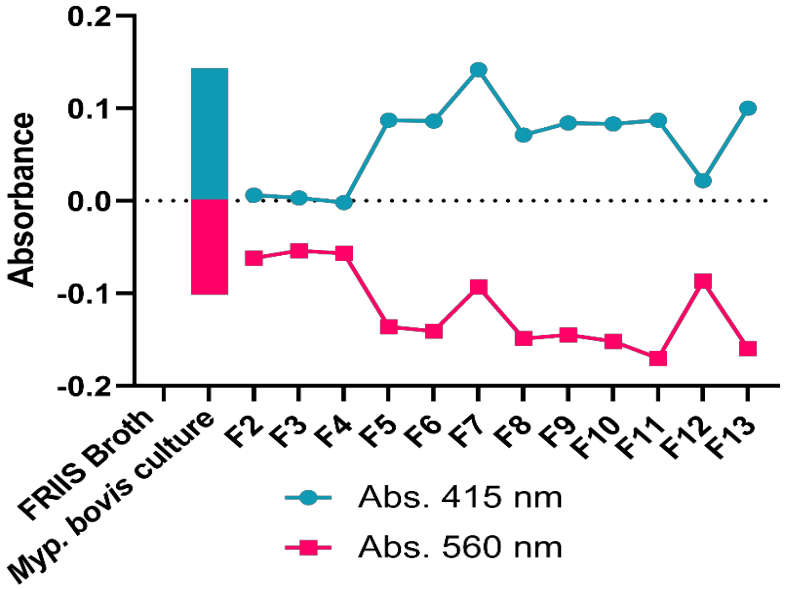

***Figure 9*: Viability of *Mycoplasma bovis* (*M. bovis*) isolate W18_04866 (#1) was assessed following processing by Size Exclusion Chromatography (SEC) columns**

Isolate W18_04866 (#1) of *M. bovis* was processed using a qEV10 35 nm Size Exclusion Chromatography (**SEC**) column, with all fractions (**F2–F13**) inoculated into Friis Broth (**FB**) to assess the growth of *M. bovis*.

An uninoculated FB control alongside a positively infected *M. bovis* culture was used to normalise colour change using light absorbance spectrophotometry at wavelengths of 415 nm and 560 nm.

Isolate W18_04866 (#1) of *M. bovis* remained viable following processing by a SEC column.

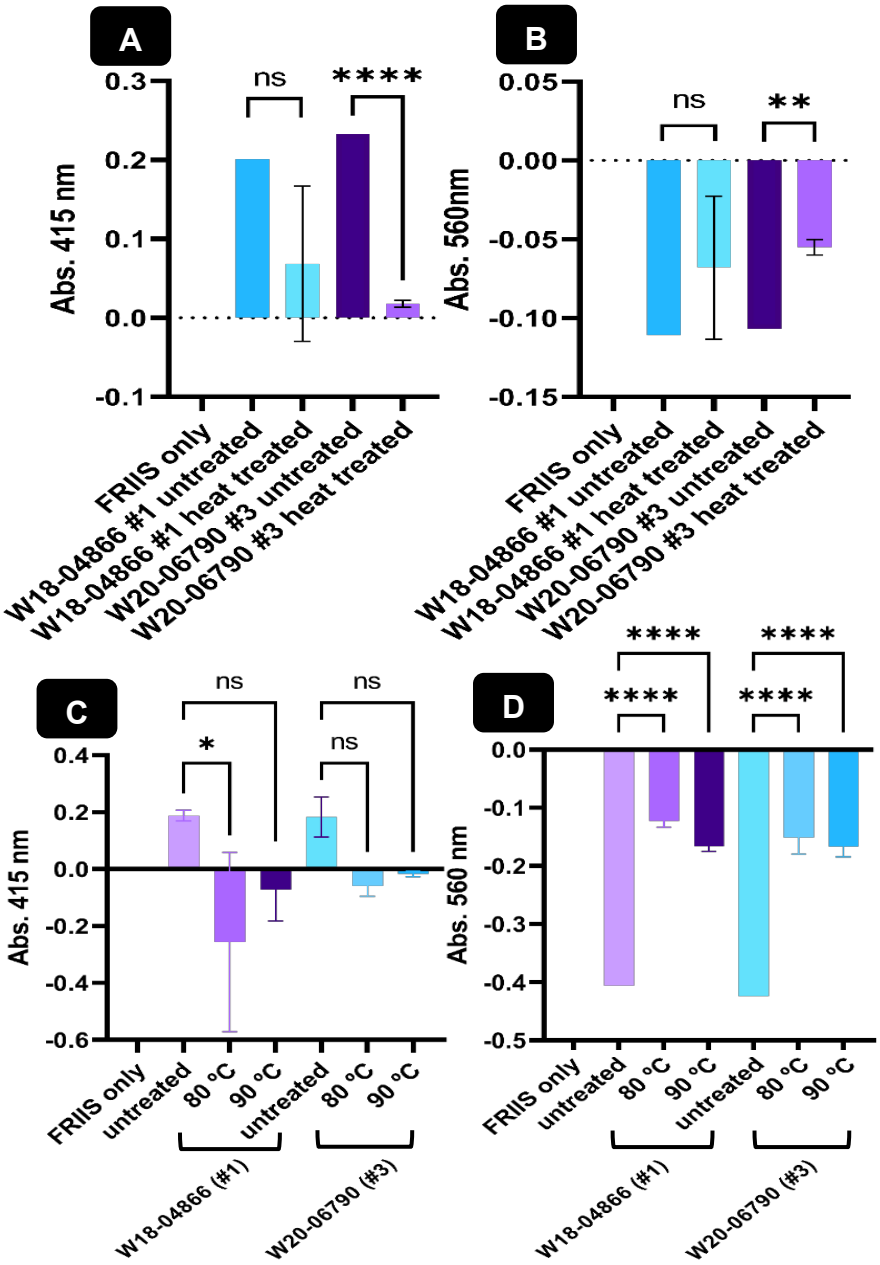

***Figure 10*: Viability of two isolates of *Mycoplasma bovis* (*M. bovis*) was assessed following heat treatment at three different temperatures**

Isolates W18_04866 (#1) and W20_06790 (#3) of *M. bovis* were heat–treated separately at 56 °C for two hours (**A** and **B**), or 80 °C and 90 °C (**C** and **D**) for ten minutes.

Heat–treated isolates were inoculated into Friis Broth and were normalised to an uninoculated Friis Broth (**FRIIS only**) (negative control) and a positive/untreated isolate control (**untreated**) using light absorbance spectrophotometry at wavelengths of 415 nm (**A** and **C**) and 560 nm (**B** and **D**).

Analyses were performed using a One–Way ANOVA.

The significance values are indicated as * = $p < 0.05$, ** = $p < 0.01$, **** = $p < 0.00001$, or ns = not significant.

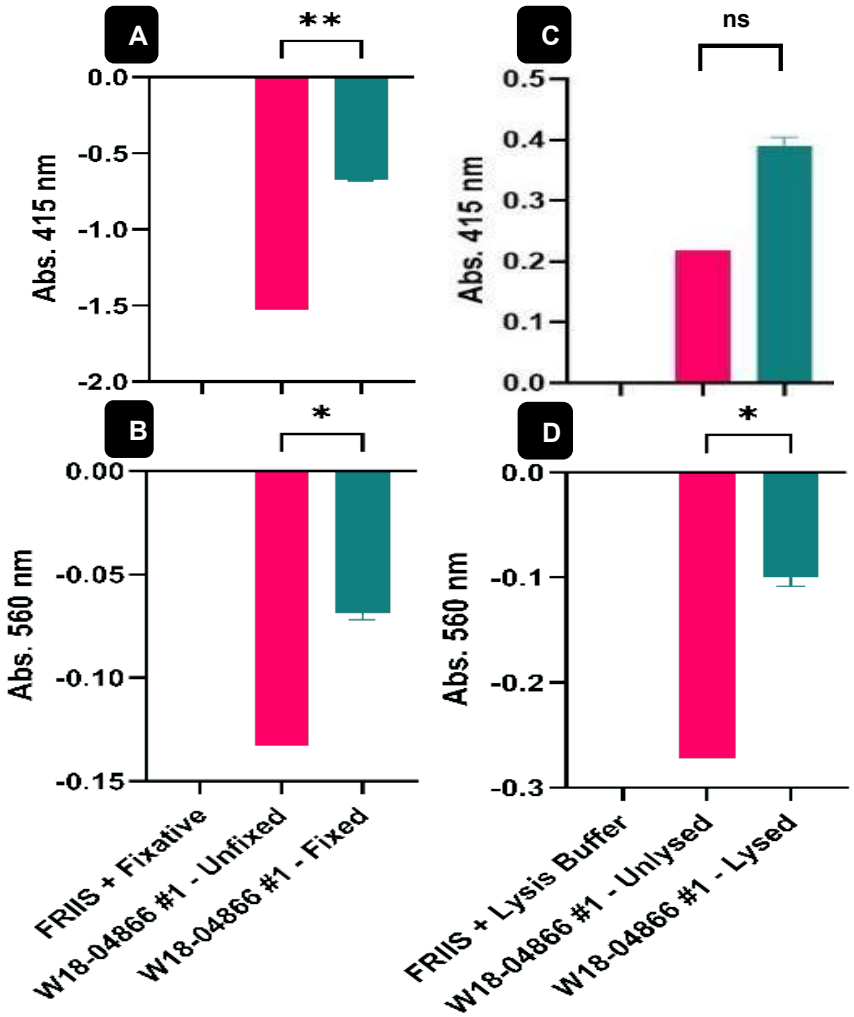

***Figure 11*: Viability of *Mycoplasma bovis* (*M. bovis*) isolates were assessed following fixation or lysis**

Isolate W18_04866 (#1) of *M. bovis* was combined with a fixative of 3 % (v/v) glutaraldehyde/0.1 M sodium cacodylate (**SDC**) buffer (**A** and **B**).

Isolate W18_04866 (#1) was lysed using 7 M Urea, 2 M Thiourea, and 1 % SDC in 100 mM Ammonium bicarbonate buffer (**C** and **D**).

All inactivated samples were normalised to an uninoculated Friis Broth containing the solution used for treatment (**FRIIS + Fixative or FRIIS + Lysis Buffer**) (negative control) and were compared to an untreated *M. bovis* control.

Isolate growth was assessed four–days post fixation using light absorbance spectrophotometry at wavelengths of 415 nm and 560 nm.

Analyses were performed using an unpaired students t–test.

The significance values are indicated as * = $p < 0.05$, ** = $p < 0.01$, or ns = not significant.

3.1.6 During the entirety of culturing, *M. bovis* was present within the co–culture bioreactor

To investigate the effects of *M. bovis* on bEEL-cells, a continuous presence of *M. bovis* within the co–culture bioreactor flask was necessary and was confirmed using PCR (**Figure 12**).

Harvests from each bioreactor were repeatedly assessed for presence of *Mycoplasma* ssp., with the bEEL control bioreactor assessed more frequently than the co–culture bioreactor to ensure unwanted *Mycoplasma* ssp. had not contaminated the cell culture.

Comparing the control bEEL bioreactor *(lane 7)* to the positive mycoplasma control (*lane 2*) demonstrated that all nineteen *Mycoplasma* ssp., including *M. bovis*, tested by the LookOut Mycoplasma PCR Detection kit were not present in the control bioreactor harvests.

Sterile technique was confirmed by a continued absence of any *Mycoplasma* ssp. in the control bioreactor flask (as *lane 7* represented DNA from bEEL cells seeded directly from the control bioreactor).

In harvests 1, 6 and 7 (*lanes 4, 5, and 6*) of the co–culture bioreactor, two bands indicated presence of a *Mycoplasma* sp. Bands in these lanes likely represented *M. bovis* as the first harvest of the co–culture bioreactor was taken a week after the initial inoculation, and the final harvest of the co–culture bioreactor was taken seven weeks after the initial inoculation of *M. bovis*.

An additional inoculation of *M. bovis* between the first and final harvest did not occur, meaning that detection of a *Mycoplasma* sp. within later bioreactor harvests was indicative that the initial inoculation of *M. bovis* had remained over seven weeks of co–culturing.

Band intensity at ~250 bp, as compared to band intensity at ~500 bp, indicated differences in the presence of a *Mycoplasma* sp. (as demonstrated in the example provided by the LookOut Mycoplasma PCR Detection kit). In *lanes 4, 5, and 6*, a greater intensity of the band at ~250 bp, compared to the band intensity at ~500 bp, was representative of a substantial presence of a *Mycoplasma* sp. in culture.

It was not required to assess presence of *Mycoplasma ssp.* in the T75 cell culture flasks containing *M. bovis* medium controls. Colour change of FB and aRPMI was indicative that W18_04866 (#1) was growing. Further evidence of *M. bovis* growth was indicated by observation of a biofilm that formed two–weeks post inoculation in FB.

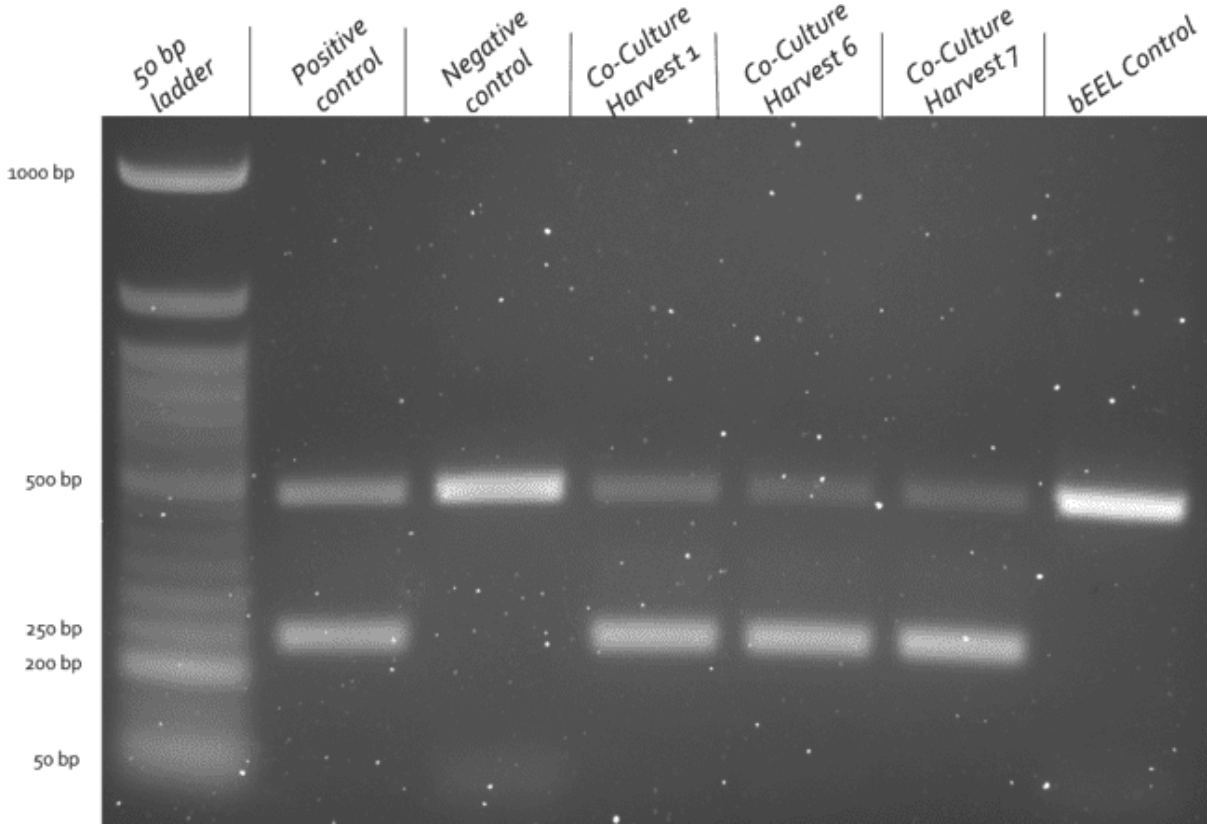

Figure 12: **Presence or absence of *Mycoplasma bovis* (*M. bovis*) in bioreactor flasks was confirmed by deoxyribonucleic acid (DNA) amplification**

Deoxyribonucleic acid (**DNA**) was amplified from three harvests of the co–culture flask (containing a bovine endometrial epithelial cell line (**bEEL cells**) and *M. bovis* isolate W18_04866 (#1)) (*lanes 4–6)* and a single harvest of the bEEL control bioreactor (*lane 7*).

A pre–included positive (*lane 2*) and negative control (*lane 3*) from the LookOut Mycoplasma Polymerase Chain Reaction Detection kit were run alongside a GeneRuler 50 bp DNA ladder (*lane 1*).

A single band (at ~500 bp) confirmed the detection kit was functioning, a second band (at ~250 bp) confirmed presence of a *Mycoplasma* sp.

Agarose gels (1.5 %) were run for fifty minutes at 100 V. Gels were imaged using a ChemiDoc MP Imaging System.

3.1.7 Infection of bEEL cells using *M. bovis* occurs through adherence and intercellular infection

To investigate the ability of *M. bovis* to infect bEEL cells, a gentamicin protection assay was designed to compare adherence of *M. bovis* and intracellular infection by *M. bovis* (**Figure 3**).

Initially, the assay was established using *M. ovi.* In wells not treated with gentamicin, *M. ovi* successfully proliferated. Growth of *M. ovi* was inhibited by gentamicin treatment at ≥ 50 µg/mL, indicating that adherence of *M. ovi* to bEEL cells was more likely to occur than intracellular infection. There was no clear evidence in three consecutive assays using the same infection conditions that *M. ovi* intracellularly invades bEEL cells (**Table 2**).

In contrast, intracellular infection of bEEL cells was more likely using *M. bovis* than *M. ovi*. Three consecutive replicates of the same infection conditions were created, with use of W18_04866 (#1) and W20_06790 (#3) providing two biological replicates for the gentamicin protection assays.

Intracellular *M. bovis* were protected at a gentamicin concentration of 100 µg/mL as compared to treated control *M. bovis* (**Table 2**).

As no growth was observed at 200 µg/mL (independent of *M. bovis* location), intracellular infection of *M. bovis* was only indicated by the protection assays as there was greater potential for extracellular *M. bovis* to cause colour change of FB at lesser gentamicin concentration.

***Table 2*: Recovery of *Mycoplasma* ssp. following inclusion within a gentamicin protection assay**

Concentration of gentamicin used	*Mycoplasma ssp.* used for infection of bEEL cells				
		Mycoplasma bovis isolate W18_04866	*Mycoplasma bovis* isolate W20_06790	2x isolates of *Mycoplasma bovis*	*Mycoplasma ovipneumoniae*
	200 µg/mL	✗	✗	NA	✗
	100 µg/mL	✓	✓	✓	✗
	50 µg/mL	✓	✓	NA	✗
	25 µg/mL	✓	✓	NA	✓
	No gentamicin	✓	✓	✓	✓

Footnote: Abbreviations = Species plural (**ssp.**), bovine endometrial epithelial cell line (**bEEL cells**) micrograms/millilitre (**µg/mL**), not applicable (**NA**), growth of the *Mycoplasma* spp. after gentamicin treatment (✓), no growth of the *Mycoplasma* spp. after gentamicin treatment (✗).

3.1.8 Pre–stained *M. bovis* was present in post–infected bEEL cells, with differences in fluorescence dependent on the presence of *M. bovis*

To further investigate adherence of *M. bovis* and intracellular infection by *M. bovis*, epi– fluorescent microscopy was performed to visualise the positioning of pre–stained *M. bovis* within bEEL cells (**Figure 13**).

Staining with R18 only occurred in the presence of *M. bovis* isolate W18_04866 (#1) (**Figure 13A**).

In dye–only controls, R18 was absent (**Figure 13B**). The fluorescence of R18 detected in the negative controls (dye–only) was minimal.

Infected and uninfected bEEL cells demonstrated typical staining patterns for actin (FITC–Phalloidin) (**Figure 13C**) and nuclei (DAPI) (**Figure 13D**).

Only bEEL cells infected with pre–stained *M. bovis* established distinctive areas of punctate–staining (**Figure 13E**).

Dye–only controls demonstrated minimal presence of R18 (**Figure 13F**).

Red–fluorescent *M. bovis* were observed in co–location with bEEL cells. The fluorescence generated by the stains taken up by bEEL cells were a clear contrast to the fluorescence generated by the stain taken up by *M. bovis*.

It was unclear if isolate W18_04866 (#1) was adherent to the outer membrane of bEEL cells or had been internalised.

However, it was more likely that fluorescent red pre–stained *M. bovis* was internalised by bEEL cells as tended to be centralised around the nucleus.

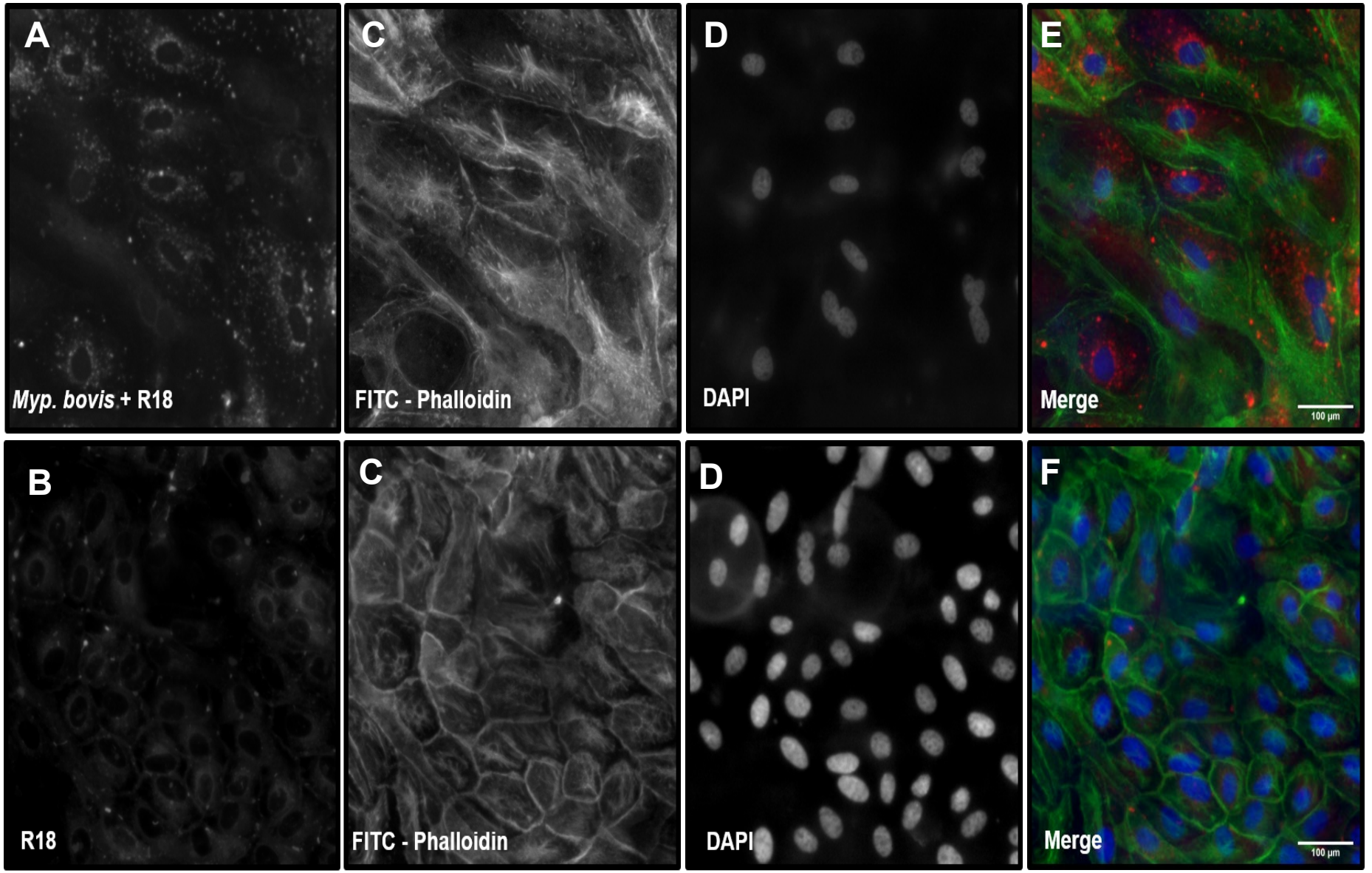
A
Myp. bovis + R18
C
FITC - Phalloidin
D
DAPI
E
Merge
100 µm
B
R18
C
FITC - Phalloidin
D
DAPI
F
Merge
100 µm

***Figure 13*: Epi–fluorescent imaging of a co–culture revealed relative positions of *Mycoplasma bovis* (*M. bovis*) and a bovine endometrial epithelial cell line (bEEL cells)**

Infection of bEEL cells using *M. bovis* isolate W18_04866 (#1) (pre–stained using a red Octadecyl Rhodamine B Chloride (**R18**) stain (diluted to 5 µg/mL from a stock solution (2 mg/mL), at a multiplicity of infection of 100 (**A**).

Control bEEL cells were pre–stained with the same concentration of R18, without an inclusion of *M. bovis* (**B**).

Twenty–four hours post–infection, bEEL cells were fixed with 10 % formalin and permeabilised using 0.05 % (v/v) Triton X–100/1x Phosphate Buffered Saline (**1x PBS**).

Fixed bEEL cells were post–stained with a green Fluorescein isothiocyanate (**FITC**)–Phalloidin stain (**C**) diluted $^{1}/_{500}$ from 0.5 mg/mL and a blue 4′,6–diamidino–2–phenylindole (**DAPI**) stain (**D**) diluted $^{1}/_{1000}$ from 2 mg/mL.

Images were collected using a 20x long–working objective of a Nikon TiU inverted epi–fluorescent microscope coupled with a mercury HBO lamp, using DAPI, FITC, and Texas Red filters.

Images were processed and merged using FIJI (ImageJ) (**E** (pre–stained *M.* bovis included) and **F** (dye–only controls) and a 100 µm scale was included.

3.1.9 A stable, long–term culture in the control bioreactor flask was established using bEEL cells

At each weekly harvest of the control bEEL bioreactor, the media of both compartments was analysed for cell debris to estimate the stability of cell culture in a bioreactor flask. A minimal number of live cells within the media compartment confirmed adherence of bEEL cells to the polyethylene terephthalate matrix within the cell compartment.

Three individual counts were created using the media from each compartment and were averaged to assess bEEL cell viability. Seventy–two hours post initial cell seeding, the cell compartment of the control bEEL bioreactor flask had an averaged live cell count of 13 % and the media compartment had an averaged live cell count of 3 %.

Subsequent weekly checks indicated that bEEL cells remained stable throughout the entirety of culturing in the bioreactor flask. The averaged live cell count of the cell compartment was ~15 % and the averaged live cell count of the media compartment remained ~3 %.

An inability to remove *M. bovis*–containing medium from PC3 without prior inactivation hindered assessing cell debris in the co–culture bioreactor flask, as the successful inactivation methods either fixed or lysed cells.

3.2 Assessment of small Extracellular Vesicles (sEVs)

3.2.1 The use of SEC columns provided a comparable isolation of sEVs

To compare the performance of all SEC columns used to isolate sEVs, each column was evaluated using light absorbance spectrophotometry at wavelengths of 350 nm and 600 nm (**Figure 14**). Slight differences in the estimated abundance of sEVs/proteins were observed, with absorbance measurements captured following the first and fifth use of each SEC column.

Fractions enriched with sEVs were positioned concordantly between bEEL control and co–culture samples. Absorbance did not provide an accurate assessment of sEV abundance/concentration and was used to estimate their positioning in fractions following isolation using SEC columns.

The sEV–containing fractions (fractions 5–7) isolated from harvests of the control bEEL bioreactor flask (**Figure 14A**), the co–culture bioreactor flask (**Figure 14B**), and the *M. bovis* isolate W18_04866 (#1) control grown in FB (**Figure 14C**) were positioned comparably. However, in later fractions, a peak appeared in the W18_04866 (#1) control samples earlier than in bEEL control or co–culture samples. The absorbance of later fractions was representative of a greater concentration of smaller particles/proteins isolated by SEC in the *M. bovis* FB control.

Fractions 2–12, isolated from isolate W18_04866 (#1) control grown in aRPMI (**Figure 14D**), generated minimal absorbance peaks. The absorbance reading at both wavelengths was negative, with the greatest particle abundance within fraction 7. However, using absorbance, it seemed likely that growing W18_04866 (#1) in aRPMI had generated minimal sEVs. Quality control of each SEC column was required prior to the first use of each SEC column as provided a baseline column flow rate. Column flow rate was measured twice consecutively and averaged.

In column 10622, an initial flow rate of 146 drops/minute was reduced to 112.5 drops/minute after five column uses. In column 10621, flow rate was reduced from 100 to 80 drops/minute after five column uses. In column SP719826, flow rate was reduced from 113 to 97 drops/minute after five column uses. In column SP210948, flow rate was reduced from 107 to 89 drops/minute after five column uses. Columns were not reused after five isolations as their flow rate continually decreased after the initial isolation, which was likely representative of increased blockages occurring in the column resin.

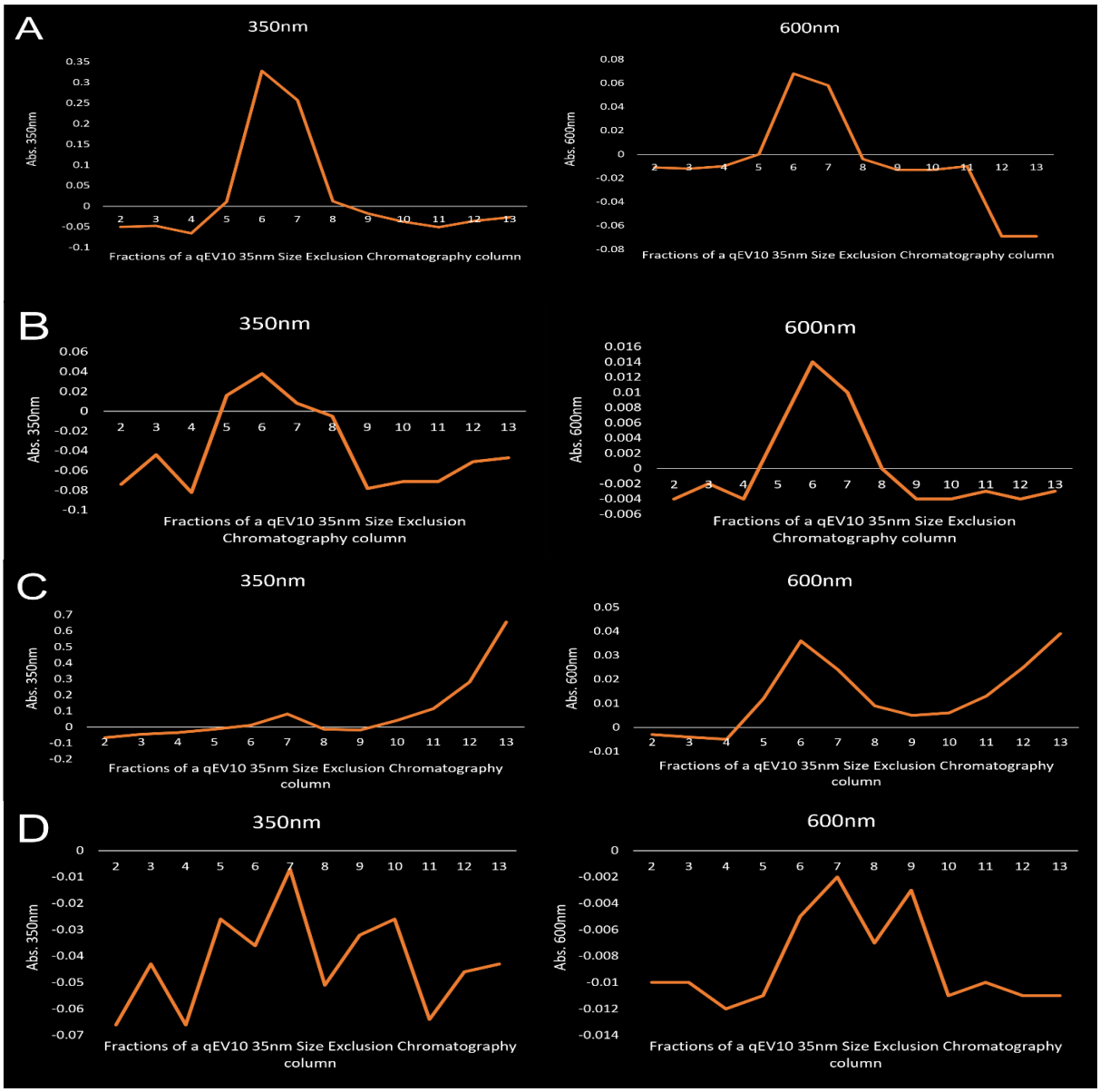

***Figure 14*: Spectrophotometry at 350 nm and 600 nm provided quality control of Size Exclusion Chromatography (SEC) columns**

Use of qEV10 35 nm Size Exclusion Chromatography (**SEC**) columns enabled isolation of small extracellular vesicles (**sEV**s) from 10 mL of clarified medium.

Fractions 2–13 were created using SEC columns and were measured using light absorbance spectrophotometry at wavelengths of 350 nm and 600 nm.

Samples processed using SEC columns included: a control bovine endometrial epithelial cell line (**bEEL cells**) (**A**), a co–culture of bEEL cells and *Mycoplasma bovis* (***M. bovis***) isolate W18_04866 (#1) (**B**), a *M. bovis*–only control grown in Friis Broth (**FB**) (**C**), and a *M. bovis*–only control grown in Advanced Rosewell Park Memorial Institute 1640 (**aRPMI**) medium (**D**).

The first and fifth use of each SEC column were quality controlled in this way.

3.2.2 Measuring sEVs presented similar concentrations and sizes between fractions

To investigate the size and concentration of sEVs within fractions 5–7, TRPS was utilised to measure samples from the control bEEL bioreactor flask. All sEV measurements by TRPS are summarised in **Table 3**and by **Figure 15**.

As demonstrated, the size of sEVs in isolated within fractions 5–7 by SEC columns were comparable. Therefore, each fraction was concentrated together as it maximised the sEVs available for lysis.

Fractions 5–7, isolated from all *M. bovis*–containing samples, could not be analysed by TRPS as sEV aggregation was altered by the heat/chemical inactivation that was required for removal of samples from the PC3 facility.

***Table 3*: Summary statistics of Tunable Resistive Pulse Sensing**

Sample Label	Measurement Date	Mean Dia (nm)	Mode Dia (nm)	d90/d10	Raw Conc (/ml)	Particle Count	Particle Rate (/min)
F5-7 P5	24/05/2021 1:08:47 pm	155	107	2.5e+0	5.71e+012	515	550.7
F5-7 P10	24/05/2021 1:10:20 pm	160	100	2.7e+0	5.71e+012	528	1118.5
F5 P5	24/05/2021 1:27:30 pm	145	103	2.7e+0	2.53e+011	511	216.9
F5 P10	24/05/2021 1:31:57 pm	181	129	2.9e+0	2.53e+011	505	241.1
F6 P5	24/05/2021 1:40:45 pm	172	119	2.8e+0	4.59e+012	582	763.3
F6 P10	24/05/2021 1:42:38 pm	179	118	2.8e+0	4.59e+012	676	1073.7
F7 P5	24/05/2021 3:40:31 pm	144	114	2.0e+0	5.41e+011	580	5321.7
F7 P10	24/05/2021 3:41:26 pm	152	113	2.1e+0	5.41e+011	689	8171.9

Footnote: **Abbreviations** = Fractions 5–7 (**F5–7**) containing small extracellular vesicles (**sEVs**), Fraction 5 (**F5**) containing sEVs, Fraction 6 (**F6**) containing sEVs, Fraction 7 (**F7**) containing sEVs, pressures 5 mbar and 10 mbar (**P5 and P10**), size (**nm**); **d10** is the point in the size distribution where 10% of the sample is contained, **d90** is the point where 90% of the sample is contained, d90/d10 is the ratio of these two values. sEV concentration (**particles/mL**), particle rate (**particles/minute**)

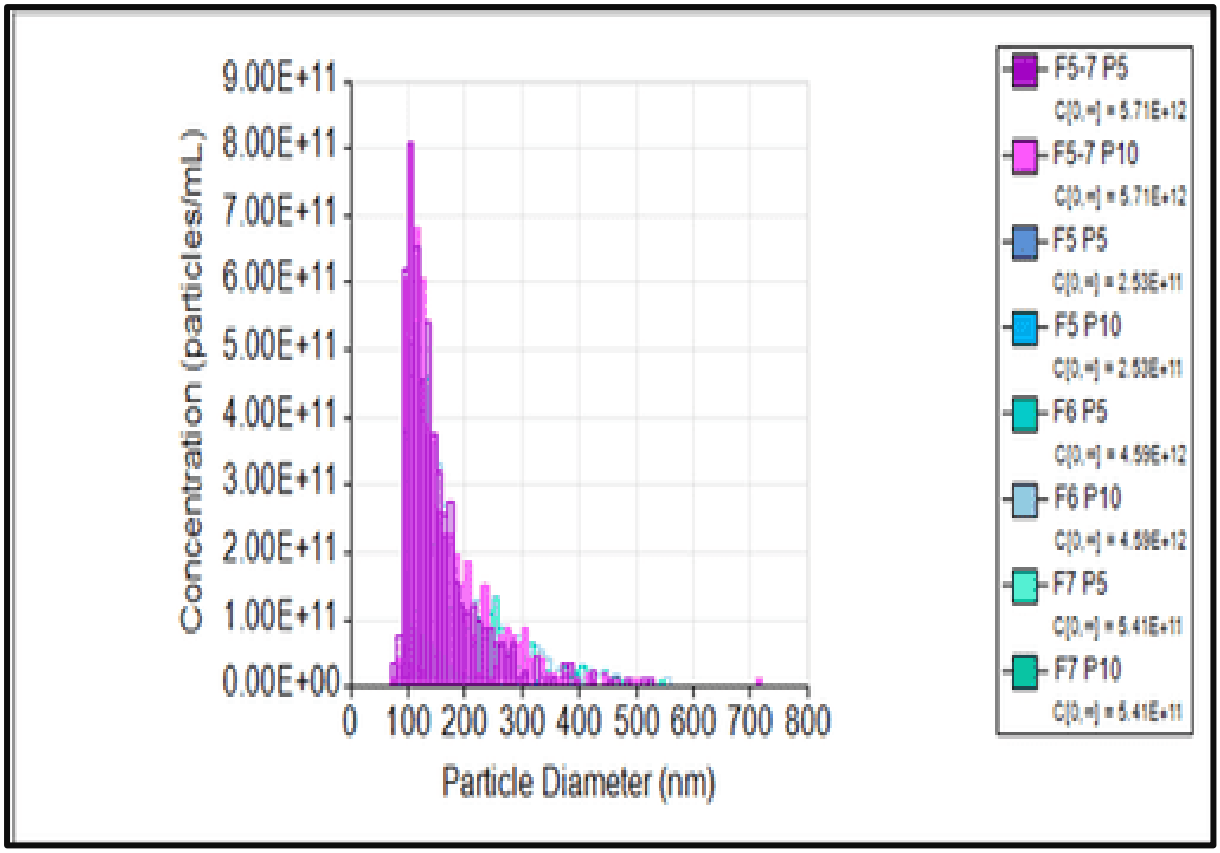

***Figure 15*: Summary statistics of Tunable Resistive Pulse Sensing (TRPS) analysis of small extracellular vesicles (sEVs) isolated from a bovine endometrial epithelial cell line**

Fractions 5–7 (**F5–7**) were measured either individually or concentrated together and were measured using Tunable Resistive Pulse Sensing (**TPRS**).

Control CPC100 (diluted $^{1}/_{1000}$ in Phosphate Buffered Saline (**1x PBS**) particles of 100 nm in size were used to calibrate the qNANO (the machine that utilises TRPS) and enable measurements of small extracellular vesicles (**sEVs**) within samples from a bovine endometrial epithelial cell line (**bEEL cells**).

Two pressures, 5 mbar and 10 mbar (**P5 and P10**), provided a calibrated measure of sEV size (**nm**) and concentration (**particles/mL**).

This distribution graph was generated from all sEVs assessed by TRPS, with the summarised data presented within Table 2.

The total concentration of sEVs was compared against the size of all particles measured by qNANO.

3.2.3 Isolated sEVs were visualised as cup–shaped vesicles using Transmission Electron Microscopy (TEM)

To investigate the presence of sEVs within fractions 5–7, and to correlate bioreactor flasks with sEV production, TEM was performed for visual confirmation (**Figure 16**).

At a magnification of 43,000x (**Figure 16A**) and 135,000x (**Figure 16Ai**), it was clear that cup–shaped vesicles were abundant within fractions 5–7 of a $^{1}/_{5}$ diluted control bEEL sample. As sEVs are formed by a bi–layered membrane, fixation caused dehydration of vesicles and negative staining distinguished their resulting 'cup' shape.

At a magnification of 43,000x (**Figure 16B**) and 135,000x (**Figure 16Bi**), TEM images from co–culture samples were more convoluted than bEEL–only control images. Areas of aggregated particles were more prominent within these grids. Nevertheless, cup–shaped vesicles were evident within TEM grids, meaning that isolation of sEVs from co–culture samples was successful using SEC columns.

The proportion of sEVs available to generate a size distribution was limited and presence of aggregated particles prevented an accurate measurement of sEVs. However, the sEVs within the co–culture samples were of a comparable size to bEEL control sEVs. Ten separate images at a magnification of 43,000x were captured using TEM to assess presence of sEVs in co–culture fractions. Time limitations prevented subsequent repeats of TEM using co–culture sEVs.

Imaging of isolate W18_04866 (#1), cultured in FB (**Figure 16C**) or aRPMI (**Figure 16D**), revealed a stark contrast to previous cultures. Accurately sizing sEVs within these samples was prevented by their seemingly low abundance.

At all magnifications, grids were heavily obscured by a layer of protein or cellular debris in FB samples (**Figure 16C**). However, a small proportion of cup–shaped vesicles were distinguished, and their size was seemingly diminished compared to sEVs from bEEL and co–culture samples.

At a magnification of 43,000x, images of isolate W18_04866, cultured in aRPMI (**Figure 16D**), were less obscured than images of FB cultures. Contrasting the absorbance peaks generated by light absorbance spectrophotometry, a very small proportion of sEVs was evident on TEM grids. The size of sEVs was seemingly diminished compared to sEVs from bEEL and co–culture samples.

If possible, a minimum of fifty sEVs were counted on the grids and were measured to establish a moderately accurate sEV size distribution graph (**Figure 17**).

From the control bEEL bioreactor, the sizes of sEVs were averaged from five separate images captured at the same magnification, with sEVs most frequently measured between 50–80 nm. Time limitations prevented subsequent repeats of TEM using control bEEL sEVs.

Substantial differences were demonstrated between the two sections of a Amicon Ultra–15 Centrifugal Filter Unit with an Ultracel–100 membrane (**Figure 18**).

The retentate captured within these filter units was associated with presence of sEVs. In contrast, the ultrafiltrate was associated with little to no sEVs.

Therefore, sEVs were held within the retentate and were prevented from flowing into the ultrafiltrate by a 100 kDa membrane.

Centrifugation removed contaminants if they were less than 100 kDa in size, meaning that concentrating sEV–rich fractions together provided a cleaner sEV preparation.

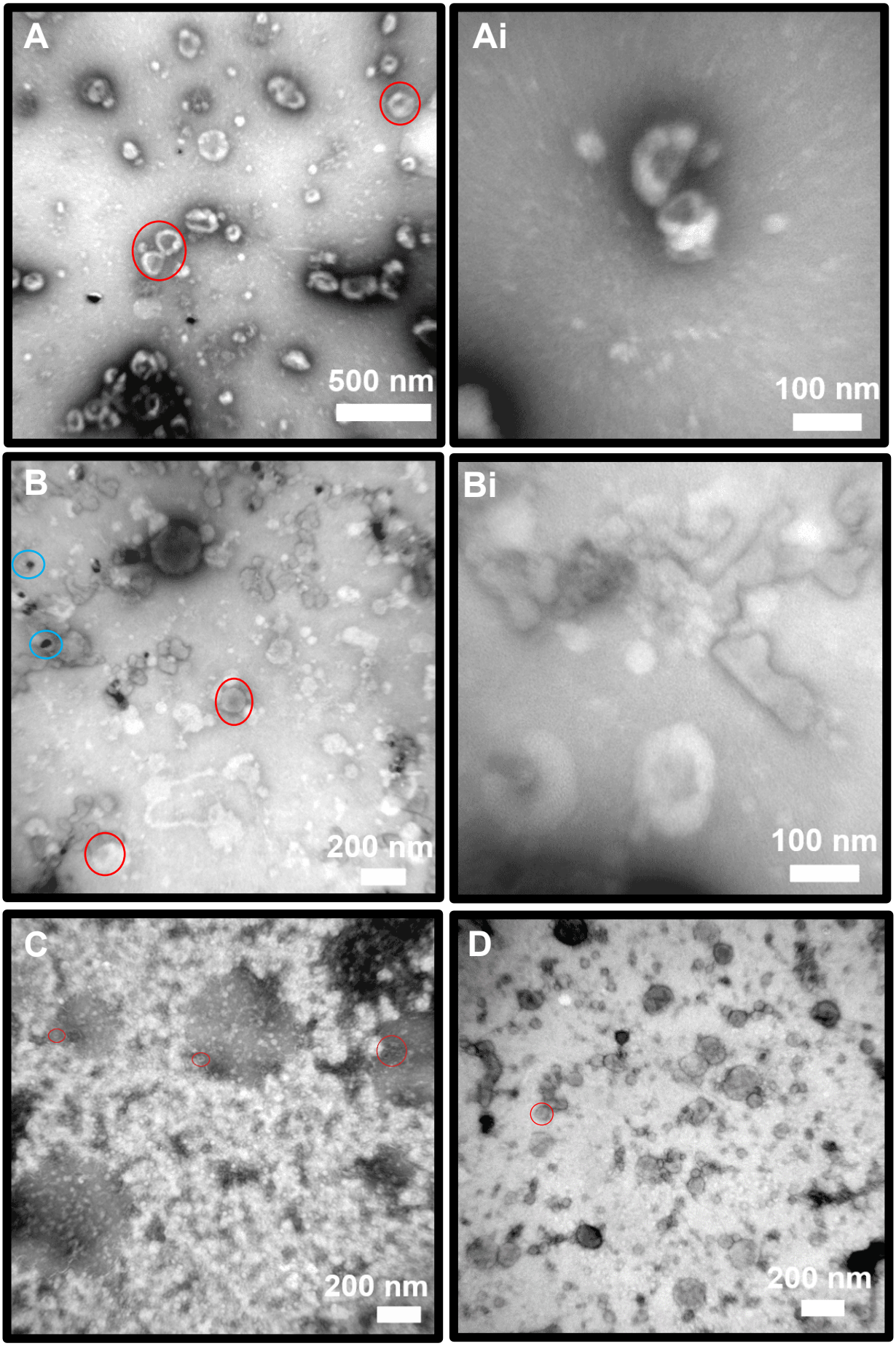
A
500 nm
Ai
100 nm
B
200 nm
Bi
100 nm
C
200 nm
D
200 nm

Figure 16: Transmission Electron Microscopy (TEM) revealed presence of small extracellular vesicles (sEVs) in culture

Pooled fractions 5–7 were isolated using Size Exclusion Chromatography (**SEC**) columns. Samples included: harvests of a control bovine endometrial epithelial cell line (**bEEL cells**) bioreactor flask (**A**), harvest of a co–culture bioreactor flask (**B**) containing bEEL cells and *Mycoplasma bovis* (***M. bovis***) isolate W18_04866 (#1), and a *M. bovis* only control (**D**).

These treatments were cultured in Advanced Rosewell Park Memorial Institute 1640 (**aRPMI**) medium.

A *M. bovis* only control (**C**) cultured in Friis Broth (**FB**) was included.

Fractions 5–7 of each treatment were concentrated using Amicon 100 kDa Ultra–15 Centrifugal Filter Units.

Small extracellular vesicles (**sEV**s) within concentrated fractions 5–7 were fixed for twenty–four hours using 3 % (v/v) glutaraldehyde in 0.1 M sodium cacodylate buffer. Treatments were diluted $^{1}/_{5}$ prior to fixation.

Inversion of 2 mm Formvar/Carbon coated size–200 mesh copper grids onto each fixed sample enabled their transfer.

Grids were negatively stained prior to imaging using an aqueous 4 % (w/v) uranyl acetate solution.

Images were captured using a Tecnai G2 Spirit BioTWIN Transmission Electron Microscope.

Unless specified by an (**i**), all images were captured at a magnification of 43,000x.

An (**i**) denotes a magnification of 135,000x. A 500 nm (**A**), a 200 nm (**B, C** and **D**) and a 100 nm (**Ai** and **Bi**) scale bar was included.

A red circle denotes cup–shaped vesicles (**sEVs**) and a blue circle potentially denotes negatively stained *M. bovis* or *M. bovis*–sEVs.

Dr. Alice Lake must be acknowledged for her considerable efforts in capturing all sEV images using TEM.

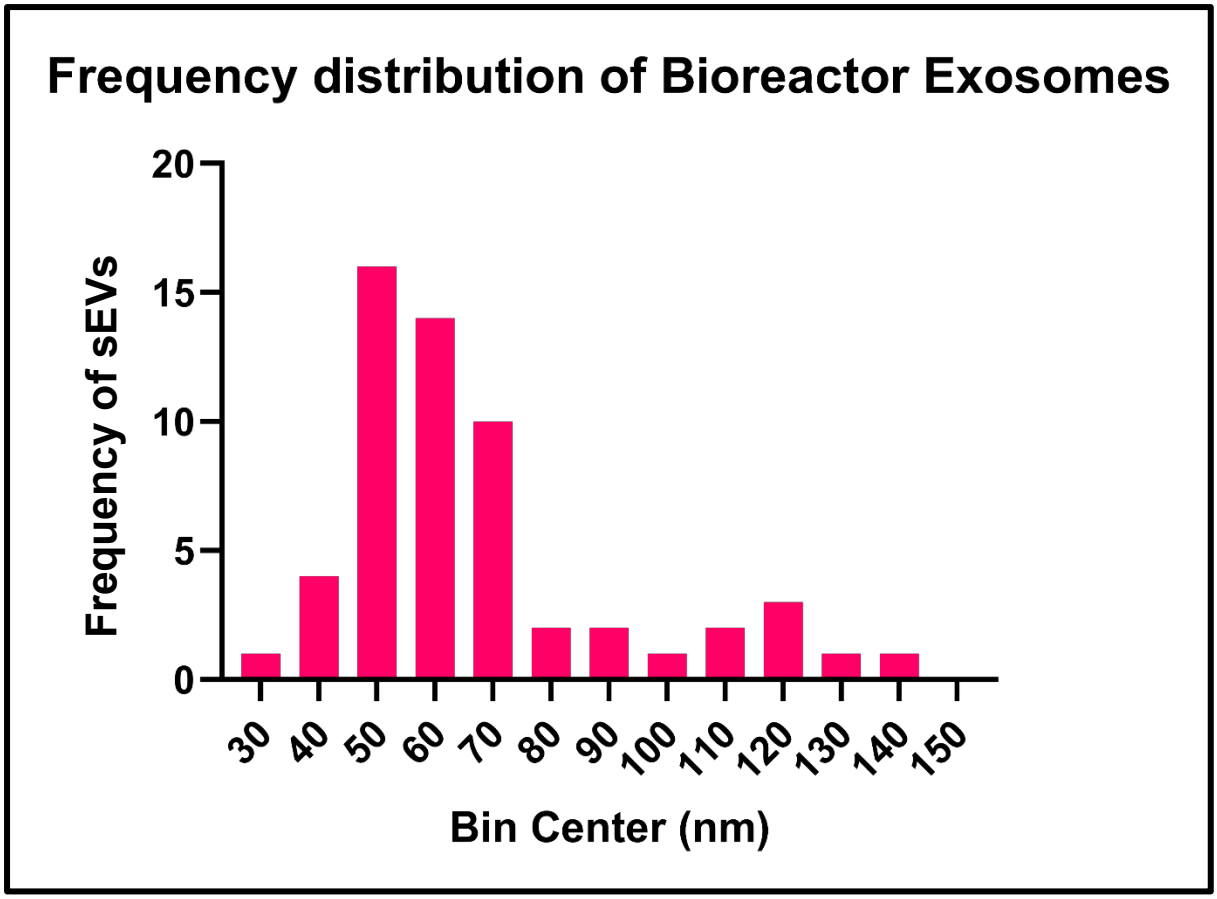

***Figure 17*: Histogram of fixed small extracellular vesicles (sEVs) from a bovine endometrial epithelial cell line (bEEL cells) using Transmission Electron Microscopy (TEM)**

Harvests of the control bovine endometrial epithelial cell line (**bEEL cells**) bioreactor flask were fixed using 3 % glutaraldehyde in 0.1 M sodium deoxycholate solution and were negatively stained prior to imaging using an aqueous 4 % (w/v) uranyl acetate solution.

Transmission Electron Microscopy (**TEM**) images were captured at a magnification of 43,000x and 135,000x.

Measurements of small extracellular vesicles (**sEVs**) were provided using ImageJ (FIJI) and plotted using GraphPad.

The average size of sEVs was created using from three separate TEM images at 43,000x from a control bEEL bioreactor flask and were measured against the scale bar included within the images.

Dr. Alice Lake must be acknowledged for her considerable efforts in capturing all sEV images using TEM.

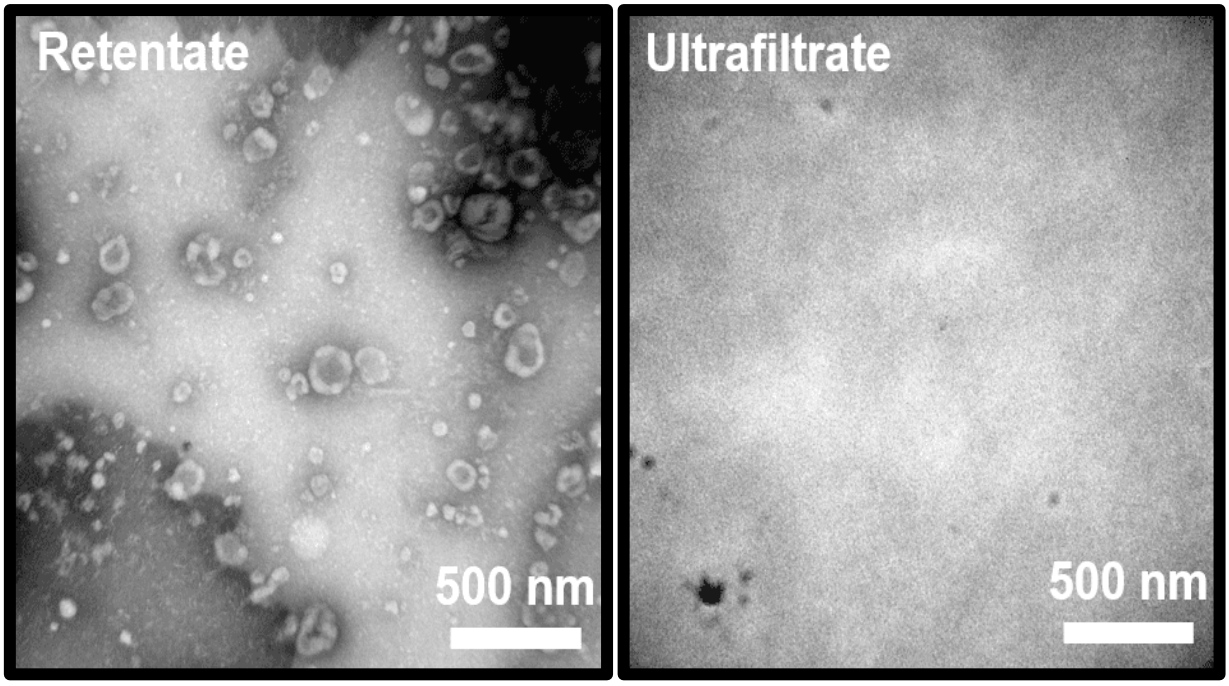

***Figure 18*: Transmission Electron Microscopy (TEM) imaging revealed differences in the presence of small extracellular vesicles (sEVs) within the filter units used to concentrate sEV fractions from Size Exclusion Chromatography columns**

Small extracellular vesicles (**sEVs**) were isolated using Size Exclusion Chromatography (**SEC**) columns from a harvest of the control bovine endometrial epithelial cell line (**bEEL cells**) bioreactor flask.

The sEVs were isolated to fractions 5–7 and were concentrated using an Amicon 100 kDa Ultra–15 Centrifugal Filter Unit.

Images were captured using a Tecnai G2 Spirit BioTWIN Transmission Electron Microscope (**TEM**).

The retentate and ultrafiltrate of the filter units were viewed at a magnification of 43,000x.

A 500 nm scale bar was included on each TEM image.

Dr. Alice Lake must be acknowledged for her considerable efforts in capturing all sEV images using TEM.

3.2.4 Fractions 5–7 contained sEVs and were not contaminated with cellular debris

For characterisation of sEVs isolated using SEC columns, an Exo–Check™ Exosome Antibody Array was used to assess proteins in fractions 5–7 (**Figure 19**).

The Exo–Check was not repeated owing to time constraints and a limit on the concentration of sEV lysates available.

Functional performance of the assay was confirmed by prominent detection of the two Horse–Radish Peroxidase positive control markers.

Of eight sEV–specific protein markers, five could be detected. These included CD63, CD81, ALG–2–interacting protein X (**ALIX**), Intercellular Adhesion Molecule 1 (**ICAM–1**) and Flotillin–1 (**FLOT–1**). Thus, lysates of fractions 5–7 were associated with presence of sEVs.

Tumour susceptibility gene 101 (**TSG–101**) and Annexin A5 (**ANXA5**) were noticeable by a very faint reaction. Epithelial Cellular Adhesion Molecule (**EpCAM**) was not detected.

A cellular contamination protein marker (cis–Golgi–Matrix Protein 130) and a background control were blank. Thus, sEV lysates were correlated with an absence of cellular contamination.

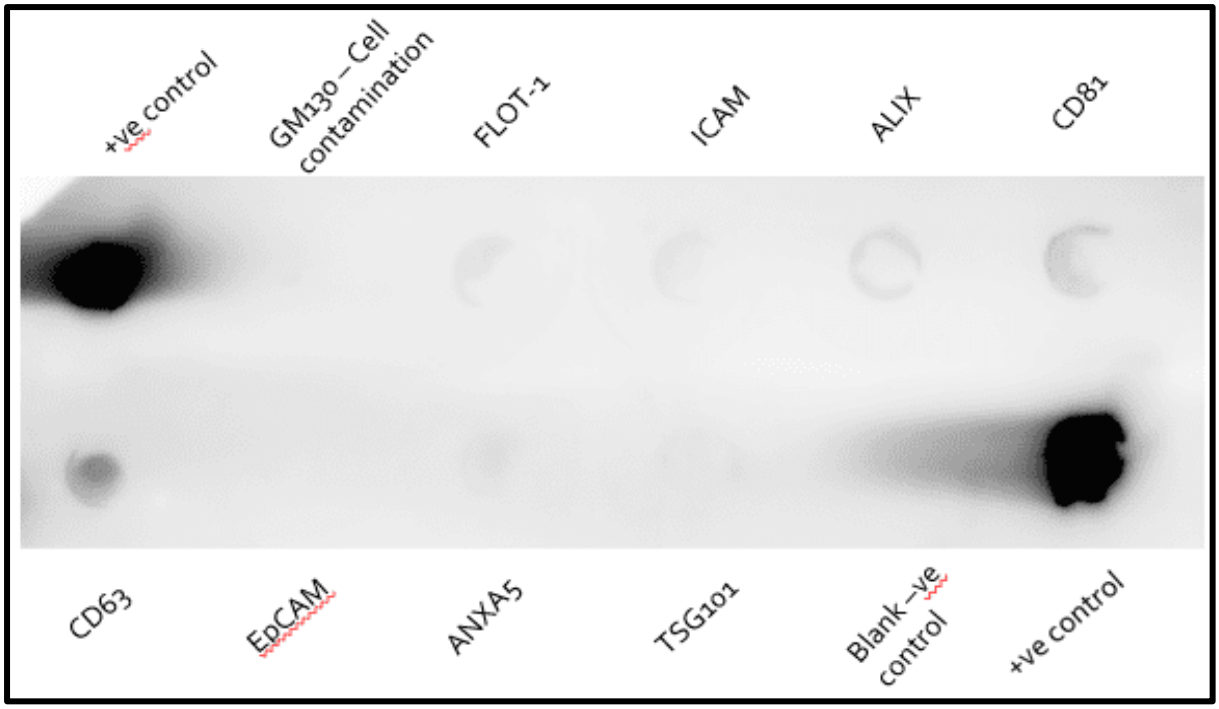

***Figure 19*: A small extracellular vesicle (sEV)–specific antibody array evaluated lysed sEVs isolated from a control bovine endometrial epithelial cell line (bEEL cells)**

Concentrated sEVs from fractions 5–7, isolated using Size Exclusion Chromatography (**SEC**) columns, were lysed and 6 µg of protein processed using an Exo–Check™ Exosome Antibody Array.

Two Horse–Radish Peroxidase positive controls (**+ve control**) were strongly positive on the membrane.

A background negative control (**Blank –ve control**) and a cellular contamination protein marker GM130 (cis–Golgi–Matrix Protein 130; **GM130 – Cell contamination**) were negative on the membrane.

Of the eight sEV–specific protein markers, **CD63** and **CD81** were positive.

ALG–2–interacting protein X (**ALIX**), Intercellular Adhesion Molecule 1 (**ICAM–1**), and Flotillin–1 (**FLOT–1**) were weakly positive on the membrane.

Tumour susceptibility gene 101 (**TSG–101**) and Annexin A5 (**ANXA5**) were very weakly positive on the membrane.

Epithelial Cellular Adhesion Molecule (**EpCAM**) was negative on the membrane.

The membrane was imaged using a ChemiDoc MP Imaging System.

3.2.5 By using SEC columns, sEVs were isolated to Fractions 5–7

Further characterisation of sEVs required lysis of fractions 2–11, with each fraction subsequently probed with a variety of sEV–specific antibodies and a sEV exclusion antibody. Positioning of sEVs and their relevant antigen markers were demonstrated within fractions 2–11, with sEV proteins associated with fractions 5–8 (**Figure 20**).

Syntenin–1 was detected in fractions 4–10, which was indicated by protein bands at the expected molecular mass of ~32 kDa (**Figure 20A**). The greatest intensity bands were evident in fractions 5 and 6. Weaker intensity protein bands were evident in fractions 8, 9 and 10. Bands of smaller sized proteins were likely attributed to non–specific antibody binding or fragmentation.

CD63 was detected in fractions 6–8 at the expected molecular weight of ~26 kDa (**Figure 20B**). The intensity of the band in fraction 7 was relatively stronger than in other fractions. Protein bands detected in fractions 6–8 (at ~50kDa) were approximately double the molecular weight of CD63 and may have been caused by dimerization of the tetraspanin protein (Zimmerman et al., 2016).

Heat–Shock Protein 70 (**HSP70**) was detected in fractions 6–8 at the expected molecular weight between 66–78 kDa (**Figure 20C**), with fraction 6 showing the strongest band intensity.

CD63 and HSP70 antibodies indicated presence of sEVs in fraction 8. However, to prevent potential protein contamination of cellular components that were also present in fraction 8, it was not included when fractions 5–7 were concentrated together.

CD9 was detected in fractions 5–7 at a molecular mass of ~28–30 kDa, which was slightly greater than an expected molecular weight of ~24 kDa (**Figure 20D**). Detection of different size proteins in other fractions may have been caused by antibody–binding to other proteins of the tetraspanin family.

Calnexin was detected in fractions 10 and 11 at ~40 kDa, which was smaller than the expected molecular weight of ~97 kDa (**Figure 20E**). The smaller molecular weight may be attributed to post–translational modifications or protein cleavage. However, bands were not evident in any other fraction demonstrating that this sEV–exclusion antibody was functional.

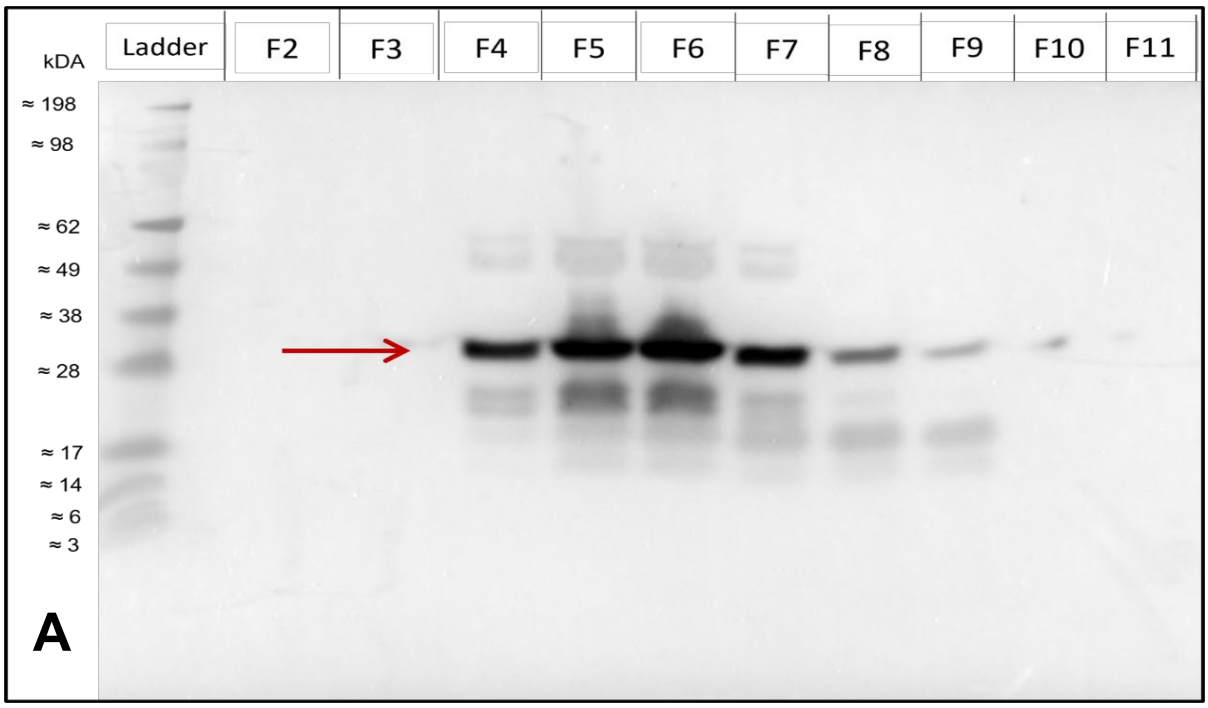
kDA
Ladder
F2
F3
F4
F5
F6
F7
F8
F9
F10
F11
≈ 198
≈ 98
≈ 62
≈ 49
≈ 38
≈ 28
≈ 17
≈ 14
≈ 6
≈ 3
A

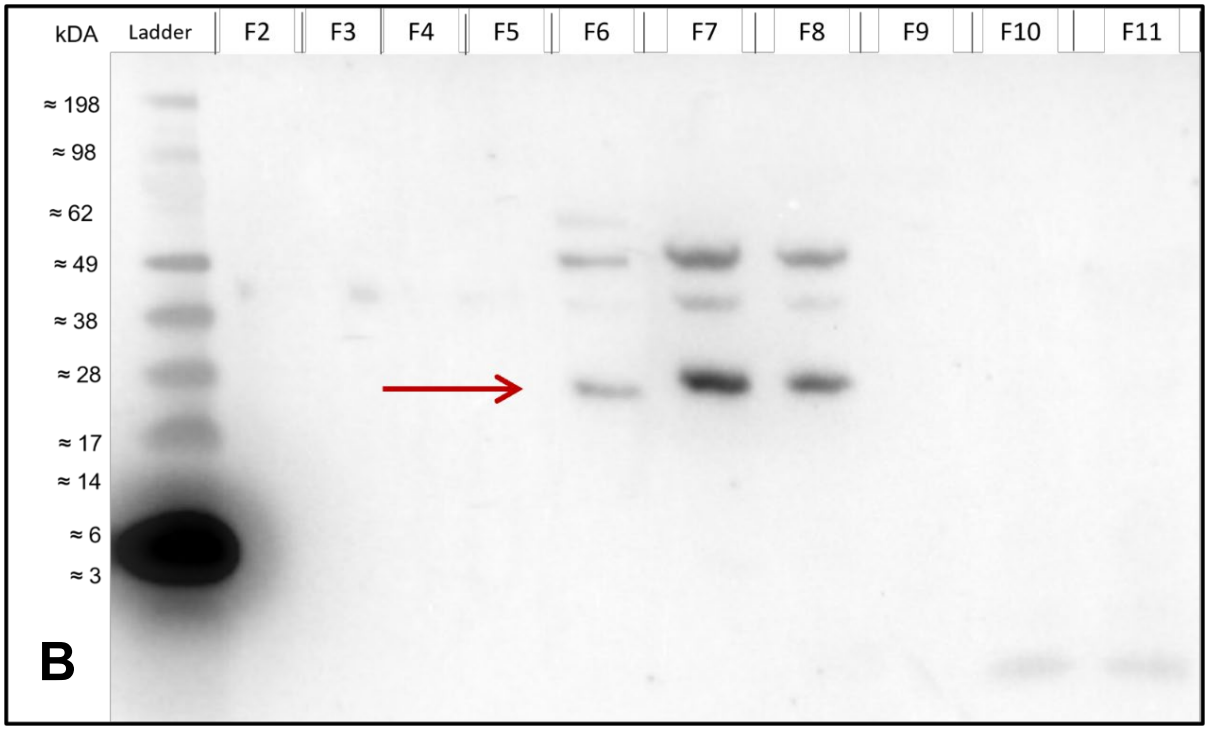
kDA
Ladder
F2
F3
F4
F5
F6
F7
F8
F9
F10
F11
≈ 198
≈ 98
≈ 62
≈ 49
≈ 38
≈ 28
≈ 17
≈ 14
≈ 6
≈ 3
B

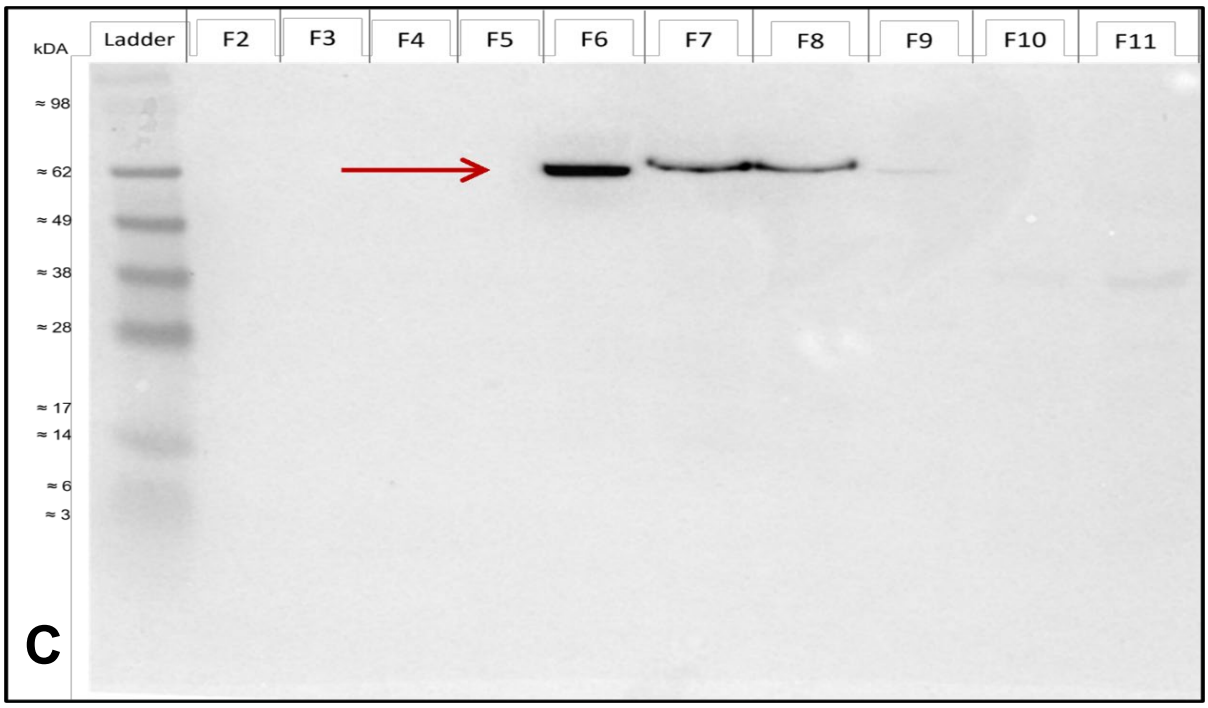
kDA
Ladder
F2
F3
F4
F5
F6
F7
F8
F9
F10
F11
≈ 98
≈ 62
≈ 49
≈ 38
≈ 28
≈ 17
≈ 14
≈ 6
≈ 3
C

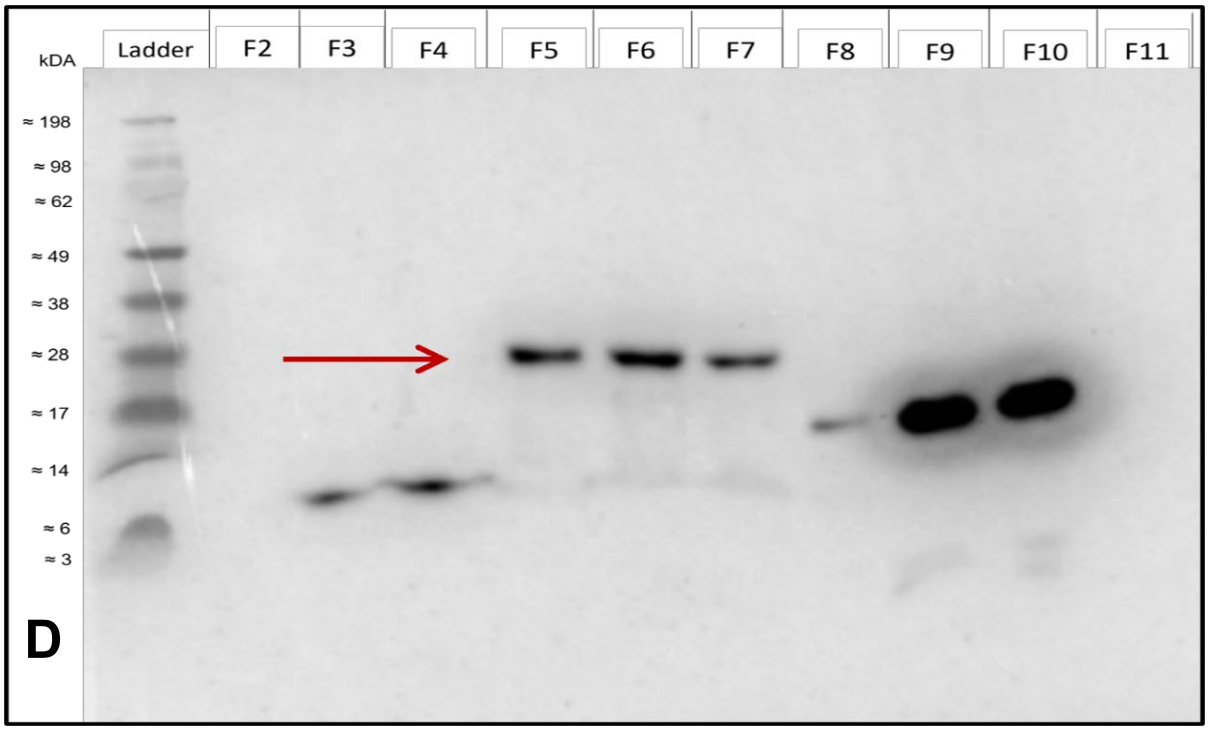
kDA
Ladder
F2
F3
F4
F5
F6
F7
F8
F9
F10
F11
≈ 198
≈ 98
≈ 62
≈ 49
≈ 38
≈ 28
≈ 17
≈ 14
≈ 6
≈ 3
D

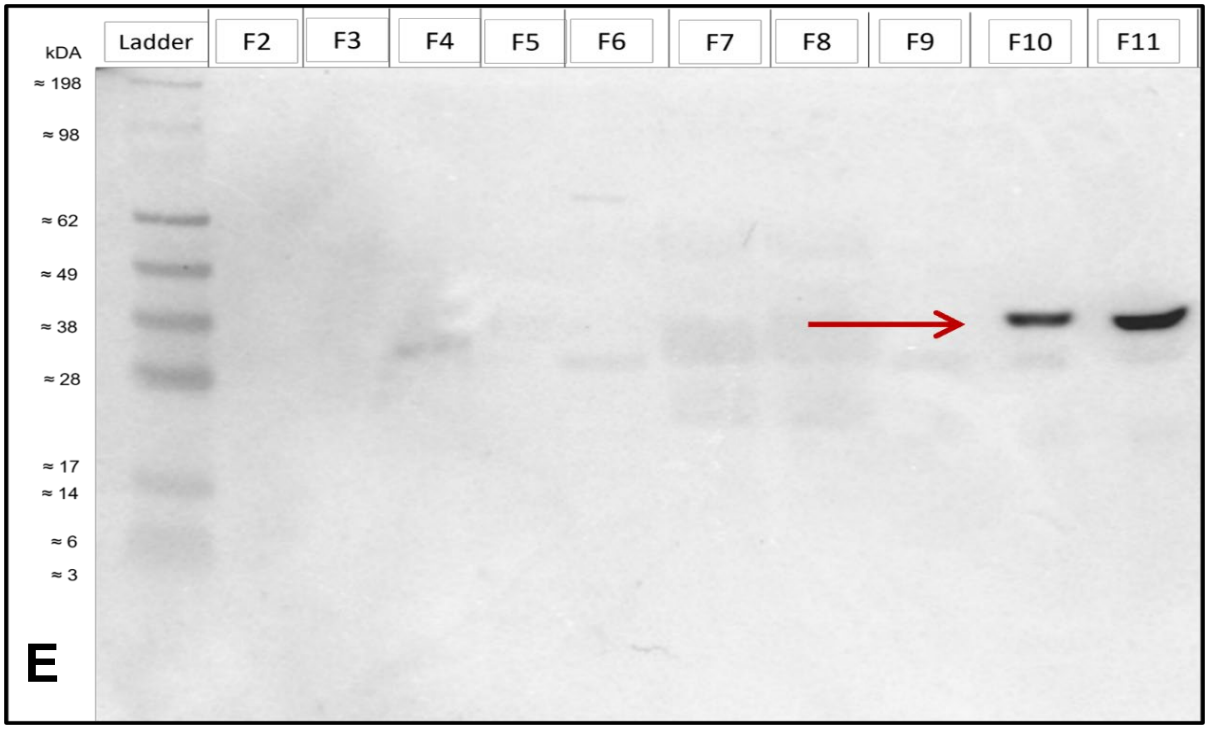

***Figure 20*: Western blotting provided positions of small extracellular vesicles (sEVs)–specific and sEV–exclusion protein markers**

Concentrated sEVs, isolated using Size Exclusion Chromatography (**SEC**) columns, were lysed and concentrated.

Into each well of a 4–12 % Bis–Tris Gel, 10 % from each individual fraction (2–11) (**F2–11**) was loaded.

A SeeBlue™ Plus2 Pre–stained Protein Standard was run in *lane 1* alongside fractions 2–11.

Proteins were separated at 120 V for ninety minutes.

Anti–protein rabbit primary antibodies against Syntenin–1 (expected kDa of ~32) (**A**) CD63 (expected kDa of ~26) (**B**), Heat Shock Protein 70 (expected kDa of 66–78) (**C**), CD9 (**D**) (expected kDa of ~24), and Calnexin (expected kDa of ~98) (**E**), were diluted $^{1}/_{1000}$ in blocking solution.

Membranes were probed for primary antibody using goat anti–rabbit horse radish peroxidase secondary antibody, diluted $^{1}/_{10,000}$ in blocking solution.

Membranes were imaged using a ChemiDoc MP Imaging System using colorimetric (ladder) and chemiluminescence (protein bands) settings.

Bands denoting sEV–specific and exclusion proteins are indicated by a dark red arrow.

Bands evident at unexpected molecular weights could be attributed to dimerization, post–translational modifications or non–specific antibody binding.

3.2.6 Minimal information for studies of extracellular vesicles (2018) (MISEV2018)

The most recent guidelines provided by the Minimal Information for Studies of Extracellular Vesicles (2018) (**MISEV2018**) were summarised to compare with what was achieved within the thesis (Théry et al., 2018).

The conditions provided within the MISEV2018 guidelines that related to cellular generation of sEVs, separation of sEVs, concentration of sEVs, storage of sEVs, characterisation of sEVs, and reporting of sEV metrics were directly comparable to what was achieved within the thesis (**Table 4**).

Conditions provided within the MISEV2018 guidelines relevant to determining function of sEVs were not applicable as the thesis was relevant to biomarker discovery.

***Table 4*: Summary of how the guidelines provided by the minimal information for studies of extracellular vesicles (2018)* compared with what was achieved within the thesis**

Technique	Minimal information for studies of extracellular vesicles (2018)*	Experimentally achieved in thesis
Culturing and Harvesting Conditions	All details regarding medium composition and preparation are required. Medium must be either serum–free or serum must be sEV–depleted.	All details regarding composition of aRPMI medium and Friis Broth were included. Within the aRPMI medium was a commercially generated 'exosome–depleted Foetal Bovine Serum' to reduce contaminating bovine sEVs. Cells were adapted to a reduced 'exosome–depleted' serum medium over eight weeks.
Separation of sEVs	"Separation of: 1) EVs from other non-EV components of the matrix (conditioned medium, biofluid, tissue) 2) the different types of EVs from each other are achieved to various degrees by the different techniques available" (Théry et al., 2018)* Less pure sEV samples are required when assessing samples for biomarkers, whereas highly purified sEV samples are required when assessing biomarker function.	The cell culture of each experimental and control condition was clarified to remove cellular debris. The clarified cell culture medium was subsequently concentrated from 15 mL to 10 mL. The sEVS from each 10 mL sample of clarified cell culture were separated using IZON qEV10 SEC columns.

Concentration of sEVs	"Concentration is a means to increase numbers of EVs per unit volume, with or without separation" (Théry et al., 2018)*.	All sEV containing fractions were combined and concentrated using pre–primed Amicon Ultra–15 Centrifugal Filter Units with an Ultracel–100 membrane.

Storage of sEVs	• Storage container:
	  ○ Type of storage vessel?
	  ○ What temperature were sEVs stored at?
	  ○ What buffer were sEVs stored in?
	• Further analysis of sEVs:
	  ○ Frozen?
	  ○ How long?
	  ○ Number of freeze thaw and freeze–thaw cycles?
		The supernatant from each cell culture condition was kept frozen at – 20 °C.
		The sEV lysates (sEVs in lysis buffer: 7 M Urea, 2 M Thiourea, 1 % SDC in 100 mM Ammonium bicarbonate and sterile Optima™ LC–MS/MS–grade water) were frozen at – 80 °C following heating each sample at 95 °C for ten minutes.
		Protein LoBind tubes were used to store all sEVs and lysed sEVs.
		The sEV lysates were transferred between facilities using dry ice. Each sEV lysate sample was stored for less than a month before they were assessed using LC–MS/MS.
		The sEV stocks were freeze–thawed twice, once to create an aliquot for initial processing using LC–MS/MS, and the second freeze–thaw enabled the rest of each sEV sample to be processed using LC–MS/MS.
		Samples that were used for TRPS and TEM were kept at 4 °C.
		The samples required for TRPS were stored in PBS and the TEM samples were fixed in 3 % (v/v) glutaraldehyde (Thermo Fisher Scientific) in 0.1 M sodium cacodylate buffer.

Characterisation of sEVs	"Each preparation of sEVs need to be: 1) defined by quantitative measures of the source of sEVs (e.g., number of secreting cells, volume of biofluid, mass of tissue). 2) characterized to the extent possible to determine abundance of sEVs (total particle number and/or protein or lipid content) 3) tested for presence of components associated with sEV subtypes or sEVs generically (at least three positive protein markers of EVs, including at least one transmembrane/lipid-bound protein-cytosolic protein, and at least one negative protein marker) 4) tested for the presence of non–vesicular, co– isolated components" (Théry et al., 2018)*.	An estimate of the number of cells present in each bioreactor was provided, as was the volume of biofluid required for the SEC columns (10 mL). TRPS was used to assess the size and concentration of sEVs that were present within the control bioreactor samples. Nanoparticle tracking analysis was not used as an additional measurement of sEVs as time constraints and availability limited the inclusion of this analysis. TEM was used to assess the size and abundance of sEVs present in all cell culture conditions following their fixation. The sEVs of the control bioreactor were characterised using western blotting. Primary antibodies used were Syntenin–1 (sEV control marker (transmembrane/cytoplasmic protein), CD63, Heat–Shock Protein 70, CD9 and Calnexin (negative sEV control, endoplasmic reticulum marker). Additionally, an Exo–Check Exosome Antibody Array was utilised, which included primary antibody markers such as CD63, CD81, ALIX, ICAM–1, FLOT–1, TSG–101, ANNXA5 and EpCAM. A negative control sEV marker (cis–Golgi–Matrix Protein 130) was included in this antibody array.

Reporting	"ISEV endorses the EV–TRACK knowledgebase as a facilitating and updatable tool for comprehensive reporting of EV experimental studies, which returns an "EV–METRIC" (Théry et al., 2018)*.	Reporting the parameters of this study to the EV–TRACK database provided an EV–METRIC grade of 75 %. The EV–TRACK ID was EV220306 and was linked to the last name of the author (PRATT).
Assessing Function	An inclusion of assays that demonstrate functionality of biomarkers is required dependent on the hypothesis/research question.	Not applicable as our research assessed samples for presence of an sEV biomarker, rather than determining function.

Footnote: **Abbreviations = Small Extracellular Vesicle (sEV), Advanced Rosewell Park Memorial Institute medium (aRPMI), Phosphate Buffered Saline (PBS), Size Exclusion Chromatography (SEC), Sodium deoxycholate (SDC), Liquid Chromatography Tandem Mass Spectrometry (LC–MS/MS) Tunable Resistive Pulse Sensing (TRPS), Transmission Electron Microscopy (TEM), ALG–2–interacting protein X (ALIX), Intercellular Adhesion Molecule 1 (ICAM–1), Flotillin–1 (FLOT–1), Tumour susceptibility gene 101 (TSG–101), Annexin A5 (ANXA5), Epithelial Cellular Adhesion Molecule (EpCAM), Information for Studies of Extracellular Vesicles (ISEV).**

***Théry, C., Witwer, K. W., Aikawa, E., Alcaraz, M. J., Anderson, J. D., Andriantsitohaina, R., Antoniou, A., Arab, T., Archer, F., & Atkin-Smith, G. K. (2018). Minimal information for studies of extracellular vesicles 2018 (MISEV2018): a position statement of the International Society for Extracellular Vesicles and update of the MISEV2014 guidelines. *Journal of Extracellular Vesicles*, 7(1), 1535750.**

3.3 Assessing composition and regulation of sEV proteins using Liquid Chromatography Tandem Mass Spectrometry (LC–MS/MS)

3.3.1 Quality Control

To investigate if there were differences between LC–MS/MS batches and to confirm the extent of instrument variability, identical quality control (**QC_Mix**) samples were spiked within three individual LC–MS/MS injections.

Differences in sample distribution were minimal. Each pair of QC_Mix samples had a strong direct relationship (correlation coefficient > 0.75), demonstrating that there was very little difference in sample distribution between injection batches (**Figure 21**).

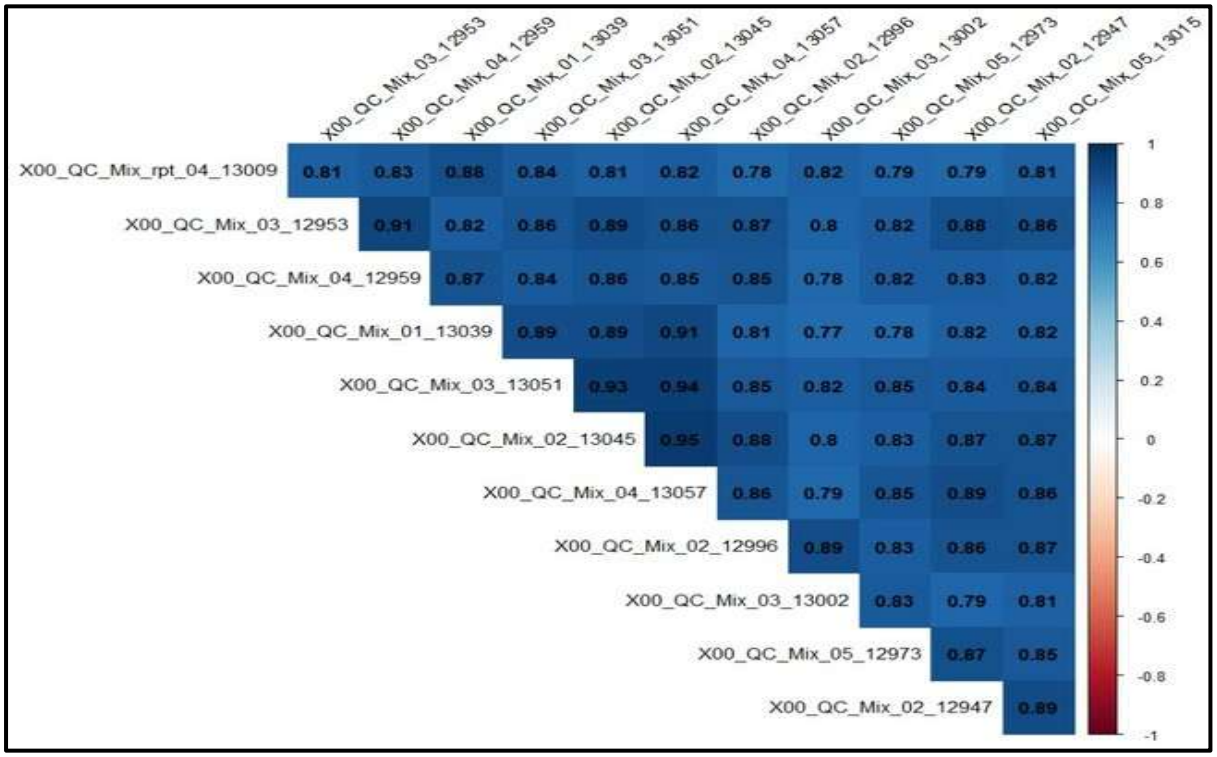

***Figure 21*: Quality control (QC) of each Liquid Chromatography Tandem Mass Spectrometry (LC–MS/MS) injections revealed no batch effect**

Identical quality control mix (X00_QC_Mix_0…) samples were distributed throughout all three separate LC–MS/MS injections forming injection batches. Correlation between the log10 (intensity +1) values were plotted between each pair of samples.

An included scale pair denoted a high value (approaching +1.00) as a strong direct relationship, values near 0.50 are considered moderate and values below 0.30 are considered to show weak relationship.

A low negative value (approaching -1.00) is similarly a strong inverse relationship, and values near 0.00 indicate little, if any, relationship.

Dr. Evelyne Maes and Ancy Thomas must be acknowledged for their outstanding effort in processing all peptide samples for analysis using LC–MS/MS.

Dr. Charles Hefer and Dr. Alasdair Noble must be acknowledged for their considerable efforts in statistically analysing all LC–MS/MS samples.

3.3.2 Correlation of sEV peptide samples

To investigate the comparability of different samples of proteins from lysed sEVs, numerous samples from each of the three injections were assessed. Most samples were highly correlated, with many overlapping samples demonstrated within the Principal Component Analysis (**PCA**) plots (**Figure 22**). Processing each treatment group by LC–MS/MS during different batches of injections did not affect peptide analysis. Variance of all samples across injection batches was minimal.

There were differences between samples from control and treatment groups (**Figure 23A).**

The FB medium only samples and FB–grown *M. bovis* samples were greatly correlated.

Although aRPMI medium only samples and aRPMI–grown *M. bovis* samples were not as greatly overlapped as FB samples, a correlation still occurred between these treatment groups.

Correlation between the co–culture samples and the aRPMI–grown *M. bovis* was clear as half of the co–culture samples overlapped with the aRPMI–grown *M. bovis* samples.

Within **Figure 23A**, the bEEL control samples were correlated with the co–culture samples as more than half of bEEL control samples were overlapping with the co–culture samples.

However, the bEEL control and the co–culture samples were compared specifically, (**Figure 23B**), their correlation was not as clear as only two samples of the co–culture overlapped with the bEEL control samples. The bEEL control samples were more widespread, demonstrating greater variance in the samples, whereas the co–culture samples were less varied and demonstrated a tighter distribution.

A comparison of the aRPMI and FB medium only samples revealed a clear separation and demonstrated that the media used were clearly varied (**Figure 23C**).

Finally, a comparison of the aRPMI–grown *M. bovis* samples and FB–grown *M. bovis* samples revealed a widespread distribution of the aRPMI–grown *M. bovis* samples, whereas the FB–grown *M. bovis* samples were very tightly distributed (**Figure 23D**). The FB–grown *M. bovis* samples were correlated with some of the aRPMI–grown *M. bovis* samples but there was a clear difference in some aRPMI–grown *M. bovis* samples, which contributed to the widespread distribution within the PCA plot.

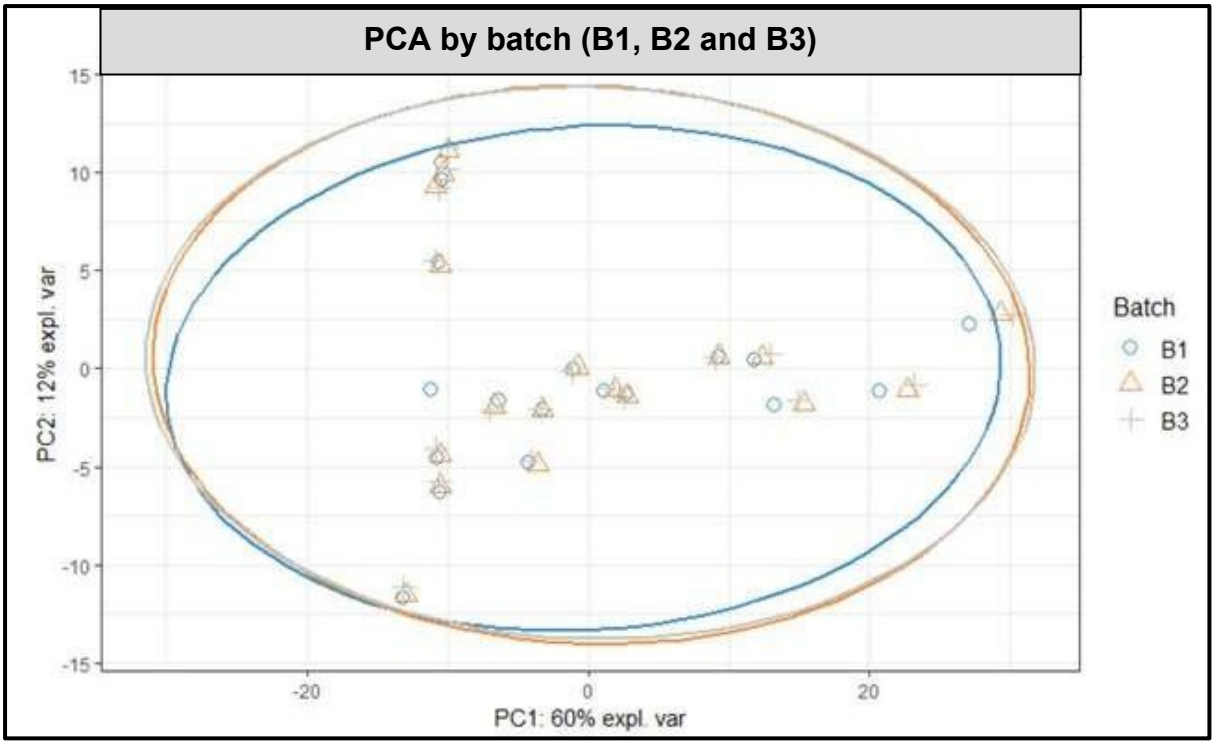

***Figure 22*: A Principal Component Analysis (PCA) revealed no batch effect between three separate injections of Liquid Chromatography Tandem Mass Spectrometry (LC–MS/MS)**

A Principal Component Analysis (**PCA**) plot compared eighteen total samples.

Samples included: harvests from a control bovine epithelial endometrial cell line (**bEEL cells**) bioreactor flask (five samples), harvests from a co–culture bioreactor flask containing bEEL cells and *Mycoplasma bovis* (***M. bovis***) isolate W18_04866 (#1) (five samples), a *M. bovis* only control cultured in Advanced Rosewell Park Memorial Institute 1640 (**aRPMI**) medium (three samples), a *M. bovis* only control cultured in Friis Broth (**FB**) (three samples), and aRPMI and FB media–only controls (one sample each).

Three individual injections of each small extracellular vesicle (**sEV**) peptide sample created three LC–MS/MS batches.

Batch 1 (**B1**) was represented by blue circles, Batch 2 (**B2**) was represented by orange triangles, and Batch 3 (**B3**) was represented by grey pluses.

Principal Component 1 (**PC1**) has an explained variance of 60% and Principal Component 2 (**PC2**) has an explained variance of 12%, which illustrate discrepancies within the dataset.

Dr. Evelyne Maes and Ancy Thomas must be acknowledged for their outstanding effort in processing all sEV peptide samples for analysis using LC–MS/MS.

Dr. Charles Hefer and Dr. Alasdair Noble must be acknowledged for their considerable efforts in statistically analysing all LC–MS/MS samples.

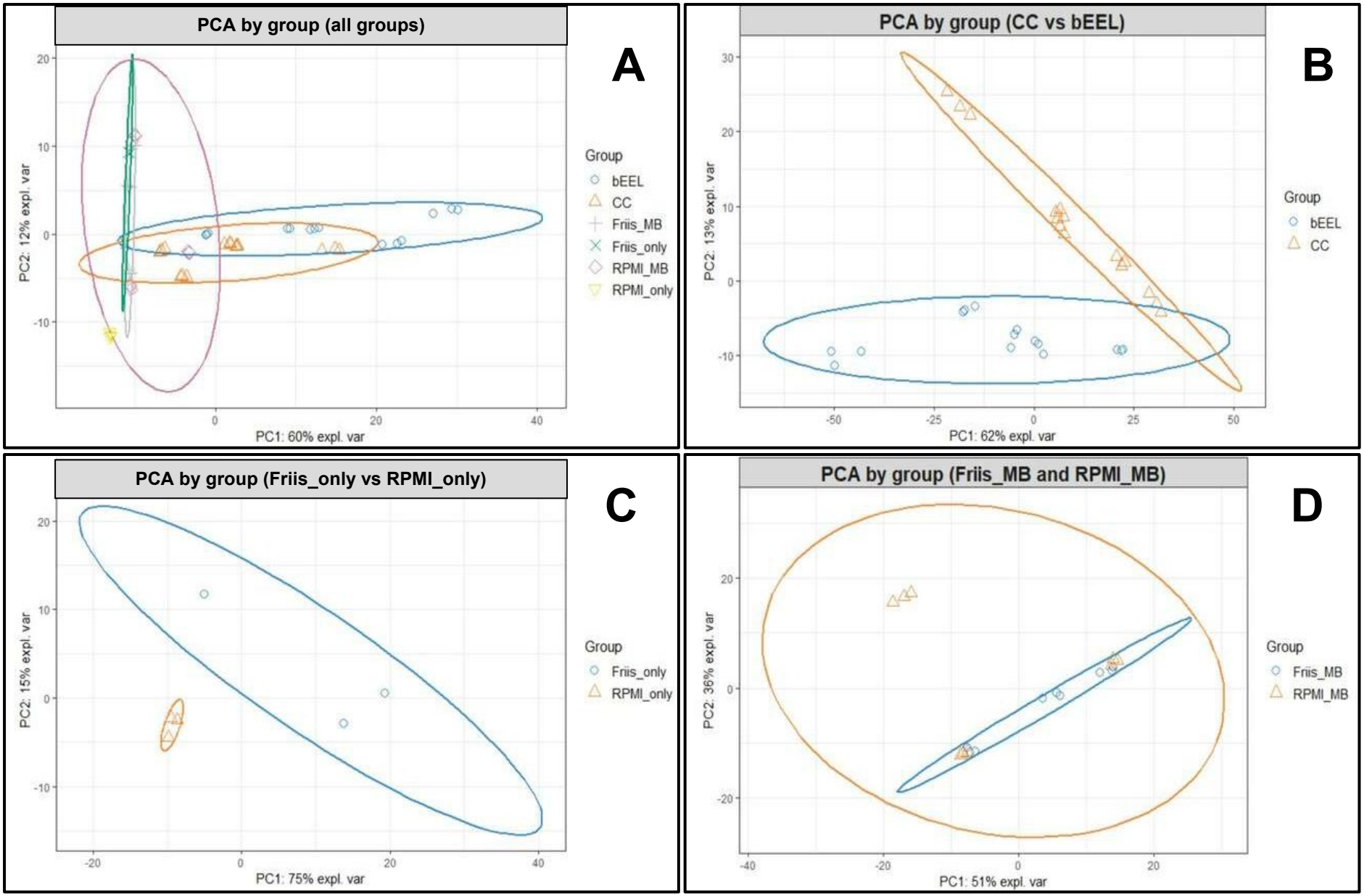
PCA by group (all groups)
A
PC2: 12% expl. var
PC1: 60% expl. var
Group
bEEL
CC
Friis_MB
Friis_only
RPMI_MB
RPMI_only
PCA by group (CC vs bEEL)
B
PC2: 13% expl. var
PC1: 62% expl. var
Group
bEEL
CC
PCA by group (Friis_only vs RPMI_only)
C
PC2: 15% expl. var
PC1: 75% expl. var
Group
Friis_only
RPMI_only
PCA by group (Friis_MB and RPMI_MB)
D
PC2: 36% expl. var
PC1: 51% expl. var
Group
Friis_MB
RPMI_MB

***Figure 23*: A Principal Component Analysis (PCA) of Liquid Chromatography Tandem Mass Spectrometry (LC–MS/MS) data revealed group effects**

Liquid Chromatography Tandem Mass Spectrometry (LC–MS/MS) small extracellular vesicle (**sEV**) peptide samples were analysed using Principal Component Analysis (**PCA**) plots.

All samples from each treatment group (**A**) were compared.

All samples from a control bovine epithelial endometrial cell line (**bEEL cells**)/all samples from a co–culture (**CC**) of bEEL cells and *Mycoplasma bovis* (***M. bovis***) isolate W18_04866 (#1) (**B**) were compared.

All samples from a *M. bovis* only control cultured in Advanced Rosewell Park Memorial Institute 1640 (**aRPMI**) medium (**RPMI_MB**)/a *M. bovis* only control cultured in Friis Broth (**FB**) (**Friis_MB**) (**C**) were compared.

All samples from aRPMI (**RPMI_only**) and FB (**FB_only**) media controls (**D**), were compared.

Principal Component 1 (**PC1**) and Principal Component 2 (**PC2**) have a variety of explained variances within graphs **A–D**, which illustrate discrepancies within the dataset.

Each figure legend was representative of the treatment groups compared within the PCA plot.

Dr. Evelyne Maes and Ancy Thomas must be acknowledged for their outstanding effort in processing all sEV peptide samples using LC–MS/MS.

Dr. Charles Hefer and Dr. Alasdair Noble must be acknowledged for their considerable efforts in statistically analysing all LC–MS/MS samples.

3.3.3 Protein Regulation

To investigate the differences in the sEV proteome of the experimental/control cultures, a $\log_2$–foldchange was used to compare protein regulation of alternative culture conditions.

The main comparison occurred between sEV proteins from the bEEL control and sEV proteins from the co–culture. Subtraction of the $\log_2$ average protein abundance in the co–culture (five biological repeats and three technical replicates) from the $\log_2$ average protein abundance in the bEEL control (five biological repeats and three technical replicates), revealed proteins that were potentially representative of infection.

The average protein abundance in sEVs from culturing *M. bovis* in FB or aRPMI (three biological repeats and three technical replicates) enabled the regulation of *M. bovis*–specific proteins to be compared.

Proteomics analyses revealed numerous proteins that were differently expressed within the *in vitro* infection model. The fifteen most upregulated and fifteen most downregulated proteins for each comparison (relevant to their $\log_2$–foldchange) are listed in **Table 5**, **Table 6**, and **Table 7**.

Although all proteins were considered for their relevance to infection, a $\log_2$ foldchange of proteins between +2 and –2 was explored more thoroughly to assess potential diagnostic markers.

The proteins that were the most biologically relevant to infection are provided/discussed, alongside the most upregulated protein and the most downregulated protein (compared between co–culture sEVs and bEEL control sEVs).

These proteins were used to address the hypothesis that sEV cargo proteins are altered within the infection model, and the relevance of these proteins within a *M. bovis* infection model.

In co–culture, the most upregulated protein was a *M. bovis*–specific protein called Thioredoxin (as compared to bEEL control sEV proteins). In co–culture, the most downregulated proteins were histone proteins (as compared to bEEL control sEV proteins).

There was substantial upregulation of a *M. bovis*–associated L–lactate dehydrogenase in co–culture, with a similar upregulation in sEVs from aRPMI–grown *M. bovis*.

Multiple *Bos taurus*–associated endopeptidase inhibitors were upregulated in co–culture.

Downregulation of an apolipoprotein A–IV protein in co–culture supported the presence of *M. bovis* in culture

Within the sEV proteome, a variety of constitutively expressed proteins were involved in functional cell processes and changes in protein regulation depended on protein function.

However, a pattern of downregulation for a variety of different binding proteins was apparent in the co–culture sEV proteome as compared to the bEEL control sEV proteome.

In **Table 6** and **Table 7**, most differences between the compared sEV proteomes were listed as *Bos taurus* proteins. Therefore, although the concentration of FBS in aRPMI was reduced specifically, the presence of FBS caused a substantial effect on the sEV proteome of aRPMI samples as compared to the sEV proteome of FB samples. However, as FBS originates from a bovine source, there was difficulty in adjusting for this difference in medium content. Whereas the inclusion of *Saccharomyces cerevisiae* in FB could be accounted for and was adjusted out accordingly when comparing sEV proteomes.

***Table 5*: Summary of the fifteen most upregulated and fifteen most downregulated proteins from the small extracellular vesicle (sEV) cargo of a bovine endometrial epithelial cell line (bEEL cells) compared to co–culture (CC) using log_2 foldchange**

Accession Number	Description of Protein	Log2 fold change (bEEL – CC)
A0A2N8U3M2 A0A2N8U3M2_MYCBV	Thioredoxin OS=*Mycoplasma bovis* OX=28903 GN=BBB47_00670 PE=3 SV=1	10.73
A0A2N8U2Q4 A0A2N8U2Q4_MYCBV	L-lactate dehydrogenase OS=*Mycoplasma bovis* OX=28903 GN=MBOVJF4278_00553 PE=3 SV=1	9.70
A0A2N8U1H9 A0A2N8U1H9_MYCBV	Uncharacterized protein OS=*Mycoplasma bovis* OX=28903 GN=MBOVJF4278_00084 PE=4 SV=1	7.29
Q4U0X8 Q4U0X8_MYCBV	BMP family ABC transporter substrate-binding protein OS=*Mycoplasma bovis* OX=28903 GN=p48 PE=3 SV=1	7.26
XP_024848428.1	Pregnancy zone protein isoform X1 [*Bos taurus*]	6.95
A0A2N8U2T2 A0A2N8U2T2_MYCBV	Putative lipoprotein MPN_284 OS=*Mycoplasma bovis* OX=28903 GN=MBOVJF4278_00566 PE=3 SV=1	6.23
A0A2N8U1L8 A0A2N8U1L8_MYCBV	Xylulose-5-phosphate phosphoketolase OS=*Mycoplasma bovis* OX=28903 GN=xpkA PE=3 SV=1	5.75
NP_001015590.2	Inter-alpha-trypsin inhibitor heavy chain H4 precursor [*Bos taurus*]	4.89
NP_001192390.1	Keratin type I cytoskeletal 24 [*Bos taurus*]	4.57
A0A193CK94 A0A193CK94_MYCBV	2-oxoisovalerate dehydrogenase OS=*Mycoplasma bovis* OX=28903 GN=BBB47_02400 PE=4 SV=1	4.36
NP_777095.1	Alpha-2-antiplasmin precursor [*Bos taurus*]	4.04
A0A2N8U3I7 A0A2N8U3I7_MYCBV	Variable surface lipoprotein OS=*Mycoplasma bovis* OX=28903 GN=H0I37_03785 PE=4 SV=1	3.37
NP_001073834.1	Arrestin domain-containing protein 1 [*Bos taurus*]	3.16
G5E5T5 G5E5T5_BOVIN	Uncharacterized protein OS=*Bos taurus* OX=9913 PE=1 SV=2	2.92
A0A2N8U2M4 A0A2N8U2M4_MYCBV	Uncharacterized protein OS=*Mycoplasma bovis* OX=28903 GN=MBOVJF4278_00496 PE=4 SV=1	2.66
NP_001157250.1	Fibronectin precursor [*Bos taurus*]	-2.85
NP_001003900.1	Tubulin beta-2B chain [*Bos taurus*]	-2.90
NP_001015600.1	Keratin type I cytoskeletal 19 [*Bos taurus*]	-3.07
XP_024830882.1	Collagen alpha-1(XVIII) chain isoform X4 [*Bos taurus]*	-3.12
NP_001029865.1	Integrin-linked protein kinase [*Bos taurus*]	-3.23
NP_001015613.1	Creatine kinase B-type [*Bos taurus*]	-3.42
NP_001192286.1	Vacuolar protein sorting-associated protein 37B [*Bos taurus*]	-3.52
XP_024848729.1	Keratin-associated protein 6-1-like [*Bos taurus*]	-4.73
NP_001039711.1	Histone H2B type 1-D [*Bos taurus*]	-4.82
P68401 PA1B2_BOVIN	Platelet-activating factor acetylhydrolase IB subunit beta OS=*Bos taurus* OX=9913 GN=PAFAH1B2 PE=1 SV=1	-4.93
NP_001069674.1	Keratin type II cuticular Hb1 [*Bos taurus*]	-5.17
NP_001178214.2	Collagen alpha-1 (XV) chain precursor [*Bos taurus*]	-5.51
NP_001192525.1	Histone H2A type 1-C [*Bos taurus*]	-6.30
NP_001014411.1	Histone H3.3 [*Bos taurus*]	-6.61
NP_776305.1	Histone H4 [*Bos taurus*]	-7.24

Footnote: Abbreviations = OrganismName (**OS**), OrganismIdentifier (**OX**), GeneName (**GN**), ProteinExistence (**PE**), SequenceVersion (**SV**), Bovine endometrial epithelial cell line (**bEEL**), co – culture (**CC**)

***Table 6*: Summary of the fifteen most upregulated and fifteen most downregulated proteins from the small extracellular vesicle (sEV) cargo of a *Mycoplasma bovis* (*M. bovis*) grown in Friis Broth (FB) compared to *Mycoplasma bovis* (*M. bovis*) grown in Advanced Rosewell Park Memorial Institute 1640 (aRPMI) medium using log_2 foldchange**

Accession Number	Description of Protein	Log2 foldchange (Friis_MB – aRPMI_MB)
NP_001192894.1	Laminin subunit alpha-4 precursor [*Bos taurus*]	9.59
NP_001020740.1	Heat shock protein beta-1 [*Bos taurus*]	7.80
NP_001289593.1	Integrin alpha-3 precursor [*Bos taurus*]	7.66
NP_001095811.1	Galectin-3 [*Bos taurus*]	7.59
NP_001103471.1	GTPase KRas [*Bos taurus*]	6.82
XP_024841789.1	Deleted in malignant brain tumours 1 protein isoform X43 [*Bos taurus*]	6.07
A0A2N8U1H9 A0A2N8U1H9_MYCBV	Uncharacterized protein OS=*Mycoplasma bovis* OX=28903 GN=MBOVJF4278_00084 PE=4 SV=1	5.93
NP_001193746.1	Laminin subunit gamma-1 precursor [*Bos taurus*]	5.59
NP_001074989.1	Lymphocyte antigen 6 complex locus G6E precursor [*Bos taurus*]	5.45
NP_001103451.1	Integrin alpha-6 precursor [*Bos taurus*]	5.37
XP_024840623.1	Major vault protein isoform X1 [Bos taurus]	5.37
NP_001358947.1	Mucin-1 isoform 1 precursor [*Bos taurus*]	4.86
NP_001098943.1	Erythrocyte band 7 integral membrane protein [*Bos taurus*]	4.84
NP_001095673.1	Netrin-4 precursor [*Bos taurus*]	4.79
XP_024836887.1	Guanine nucleotide-binding protein subunit alpha-13 isoform X1 [Bos taurus]	4.76
NP_001137572.1	Tubulin beta-1 chain [*Bos taurus*]	-1.00
NP_001069022.1	Carboxylesterase 1 precursor [*Bos taurus*]	-1.03
A0A3Q1LVM5 A0A3Q1LVM5_BOVIN	Inter-alpha-trypsin inhibitor heavy chain H1 OS=*Bos taurus* OX=9913 GN=ITIH1 PE=1 SV=1	-1.04
NP_001039642.1	Leucine-rich alpha-2-glycoprotein precursor [*Bos taurus*]	-1.06
NP_001077233.1	Myosin regulatory light chain 12B [*Bos taurus*]	-1.11
NP_001193120.1	RAS-related protein Rab-5B [*Bos taurus*]	-1.16
XP_015327157.2	Beta-casein isoform X2 [*Bos taurus*]	-1.31
F1MLD7 F1MLD7_BOVIN	Uncharacterized protein OS=*Bos taurus* OX=9913 GN=EFR3A PE=4 SV=3	-1.50
NP_001039711.1	Histone H2B type 1-D [*Bos taurus*]	-1.57
NP_803482.1	Glutathione S-transferase P [*Bos taurus*]	-1.61
NP_001069381.1	Keratin type II cuticular Hb5 [*Bos taurus*]	-3.40
NP_001069674.1	Keratin type II cuticular Hb1 [*Bos taurus*]	-4.67
NP_001069974.1	Keratin type I cuticular Ha1 [*Bos taurus*]	-5.64
XP_005220820.1	Keratin type I cuticular Ha3-I isoform X1 [*Bos taurus*]	-6.12
XP_005220820.1	Keratin type I cuticular Ha3-I isoform X1 [*Bos taurus*]	-6.12

Footnote: Abbreviations = OrganismName (**OS**), OrganismIdentifier (**OX**), GeneName (**GN**), ProteinExistence (**PE**), SequenceVersion (**SV**) *Mycoplasma bovis* grown in Friis Broth (Friis_MB), *Mycoplasma bovis* grown in Advanced Rosewell Park Memorial Institute 1640 (aRPMI_MB)

***Table 7*: Summary of the fifteen most upregulated and fifteen most downregulated proteins from the small extracellular vesicle (sEV) cargo of a *Mycoplasma bovis*(*M. bovis*) grown in Friis Broth (FB) compared to co–culture (CC) using log_2 foldchange**

Accession Number	Description of Protein	Log2 fold change (FB_MB – CC)
NP_001020740.1	Heat shock protein beta-1 [*Bos taurus*]	10.39
NP_001192894.1	Laminin subunit alpha-4 precursor [*Bos taurus*]	10.04
NP_001095811.1	Galectin-3 [*Bos taurus*]	9.93
NP_001103471.1	GTPase KRas [*Bos taurus*]	9.45
XP_024841789.1	Deleted in malignant brain tumours 1 protein isoform X43 [*Bos taurus*]	9.17
NP_001289593.1	Integrin alpha-3 precursor [*Bos taurus*]	9.10
NP_001074989.1	Lymphocyte antigen 6 complex locus G6E precursor [*Bos taurus*]	8.56
A0A2N8U3M2 A0A2N8U3M2_MYCBV	Thioredoxin OS=*Mycoplasma bovis* OX=28903 GN=BBB47_00670 PE=3 SV=1	8.20
A0A2N8U1H9 A0A2N8U1H9_MYCBV	Uncharacterized protein OS=*Mycoplasma bovis* OX=28903 GN=MBOVJF4278_00084 PE=4 SV=1	8.06
NP_001098943.1	Erythrocyte band 7 integral membrane protein [*Bos taurus*]	7.79
NP_001358947.1	Mucin-1 isoform 1 precursor [*Bos taurus*]	7.67
NP_001095673.1	Netrin-4 precursor [*Bos taurus*]	7.45
NP_001229501.1	Calmodulin-1 [*Bos taurus*]	7.44
NP_001103451.1	Integrin alpha-6 precursor [*Bos taurus*]	7.10
NP_001193746.1	Laminin subunit gamma-1 precursor [*Bos taurus*]	7.10
NP_001039750.1	Complement component C8 alpha chain precursor [*Bos taurus*]	-6.29
NP_001076854.1	Keratin type II cuticular Hb3 [*Bos taurus*]	-6.46
NP_776376.1	Plasminogen precursor [*Bos taurus*]	-6.57
A0A3Q1LZ90 A0A3Q1LZ90_BOVIN	Ig-like domain-containing protein OS=*Bos taurus* OX=9913 PE=4 SV=1	-6.74
NP_001032557.1	Apolipoprotein A-IV precursor [*Bos taurus*]	-6.76
NP_776302.1	Prothrombin precursor [*Bos taurus*]	-6.98
NP_001192237.1	von Willebrand factor precursor [*Bos taurus*]	-7.18
E1BH94 E1BH94_BOVIN	Peptidoglycan recognition protein 2 OS=*Bos taurus* OX=9913 GN=PGLYRP2 PE=4 SV=3	-7.26
NP_001069674.1	Keratin type II cuticular Hb1 [*Bos taurus*]	-7.76
NP_776667.2	Apolipoprotein A-I preproprotein [*Bos taurus*]	-7.83
NP_001091485.1	Inter-alpha-trypsin inhibitor heavy chain H2 precursor [*Bos taurus*]	-7.89
NP_001070018.1	Complement C1s subcomponent precursor [*Bos taurus*]	-8.34
XP_024848729.1	Keratin-associated protein 6-1-like [*Bos taurus*]	-9.32
NP_776304.1	Coagulation factor V precursor [*Bos taurus*]	-9.76
A0A3Q1MJJ4 A0A3Q1MJJ4_BOVIN	Apolipoprotein A-I OS=*Bos taurus* OX=9913 GN=APOA1 PE=1 SV=1	-17.25

Footnote: Abbreviations = OrganismName (**OS**), OrganismIdentifier (**OX**), GeneName (**GN**), ProteinExistence (**PE**), SequenceVersion (**SV**), co–culture (**CC**), *Mycoplasma bovis* grown in Friis Broth (Friis_MB)

4 Discussion

4.1 Co–culture and control bioreactor flasks

The current study established the first *in vitro* model of bEEL cells infected with *M. bovis* in a bioreactor flask and is, therefore, the first study to describe an infection model using a bovine cell line in a bioreactor flask.

To confirm our infection model, using PCR, we assessed the presence of *M. bovis* in the co–culture bioreactor flask and the absence of *M. bovis* in the bEEL control bioreactor flask throughout the three months that bioreactor flasks were cultured. After infection with *M. bovis* isolate W18_04866 (#1), adherence of the bacterium and/or intracellular infection of bEEL cells was observed.

Previous research has investigated the response of cells, e.g., epithelial cells, monocytes, and pluripotent stem cells, to pathogenic bacteria *in vitro* (Zoumpopoulou et al., 2009; Bartfeld et al., 2015; Loss et al., 2020). Additionally, Josi et al. (2018) successfully established co–cultures between other bovine epithelial cell lines and different strains of *M. bovis*. Infection of endometrial primary cells using *M. bovis* has been achieved by Pôrto et al. (2021).

By combining a standard infection model with bioreactor flasks, we were able to increase sEV yield for downstream investigation (Artuyants et al., 2021).

Understanding the relationship between infection and disease is a key factor in developing treatments for diseases such as endometritis, which has a major impact on animal welfare and production in bovine herds (Osawa, 2021).

Post–partum, cattle can develop chronic uterine inflammation as a result of *M. bovis* infection, manifesting as metritis or endometritis, which negatively impacts fertility (Ghanem et al., 2013; Molina-Coto & Lucy, 2018). Uncontrolled influx and growth of microorganisms in the uterus at the time of conception or birth furthers disease symptoms (Kumar & Purohit, 2019; Hazelton et al., 2020a).

In tissue, *M. bovis* can remain hidden for long periods and their ability to avoid elimination by the immune system is a substantial factor in the development of fertility issues (Askar et al., 2021).

Furthermore, *M. bovis* can survive the fertilisation process and cause calves to be infected from birth (Bielanski et al., 2000).

Successful use of a bioreactor flask to co–culture *M. bovis* isolate W18_04866 (#1) with a bovine endometrial cell line provides a model to gain a greater understanding of potential virulence factors that affect fertility in cattle, or that represent *M. bovis* infection through *in vitro* production of sEVs.

Consistency of bioreactor culture conditions were previously demonstrated in pluripotent cell types, such as mesenchymal stromal cells (**MSC**s), with cell growth consistent with characteristics of those grown in traditional *in vitro* culture conditions (Das et al., 2019).

Furthermore, growing cells in 3D in a bioreactor flask, greatly increased output of MSC–derived sEVs in comparison to traditional 2D culture as, in 2D conditions, sEV secretion is limited by cells reaching confluency quicker than in 3D growth conditions (Witwer et al., 2019).

Using bioreactor flasks to generate sEVs has facilitated drug discovery experiments, development of diagnostic tools and, particularly, the use of sEVs as therapeutic agents (Joseph et al., 2018; Bauer & Giebel, 2021).

The sEV output in this study, generated by bEEL control and co–culture conditions, was maximised by utilising the 3D cell growth conditions of a bioreactor flask. Our study has established *M. bovis*–infected bEEL cells as an *in vitro* model to investigate sEV cargo produced during and in response to infection.

4.2 Cargo of sEVs

Infection of bEEL cells with *M. bovis* altered the protein cargo of sEVs, indicating that cellular functions were modulated during infection.

The proteins that were most biologically relevant to infection are provided/discussed, alongside the most upregulated protein and the most downregulated protein (compared between co–culture sEVs and bEEL control sEVs).

These proteins were discussed to address the hypothesis that sEV cargo proteins are altered within the infection model, and to understand the relevance of these proteins within a *M. bovis* infection model.

Future research could explore the other sEV cargo proteins altered within the *M. bovis* infection model to understand their relevance to infection.

4.2.1 Thioredoxin

The greatest upregulation in co–culture sEVs relative to control sEVs was a *M. bovis*–specific protein named thioredoxin. Thioredoxin is present in each domain of life and is essential in redox reactions and many oxidative stress responses (Balsera & Buchanan, 2019). Expression of thioredoxin increases in *M. bovis* strains that are responding to stress, which can occur as a result of changes to growth conditions (Li et al., 2011).

Detection of *M. bovis*–specific thioredoxin in sEVs further confirmed that *M. bovis* was present within the co–culture, which corresponded with PCR results. Although thioredoxin was highly upregulated in co–culture sEVs, the ubiquitous nature of thioredoxin expression makes it unusable as a diagnostic marker.

4.2.2 Histones

The greatest downregulation in co–culture sEVs relative to control sEVs were histone proteins. It is known that negatively charged DNA associates with positively charged histone proteins within sEVs, forming complexes that can alter sEV size accordingly (Vagner et al., 2018).

Whilst not completely understood, histone proteins aid insight into transfer of genetic information between cells as they assist in maintaining DNA integrity within sEVs (Chang et al., 2020).

The downregulation of these proteins in co–culture could indicate that infection by *M. bovis* can reduce exchange of genetic material between cells. In support of this, changes in histone post–translational modifications were observed after infection with other intracellular bacteria (Rennoll-Bankert et al., 2015; Zheng et al., 2016).

Therefore, downregulation of histone proteins within sEVs from other co–cultures indicate that changes in chromatin accessibility occur and a reduced likelihood of forming nucleosome–like complexes within infected cells.

If this is the case, downregulation of histone proteins resulting from infection by *M. bovis* may indicate co–culture sEVs are limited in their ability for DNA–based biomarker exchange as compared with control sEVs.

Future research should assess how histones are specifically packaged within sEVs and if their downregulation prevents packaging of known DNA–based biomarkers for exchange between cells.

An alternative explanation regarding the downregulation of histone proteins within co–culture sEVs could be provided by an altered expression of p53, a master tumour–suppressor protein.

Pathogenic bacteria hijack p53 regulation for increased survival in their host cell, which causes infection–related alterations to apoptosis (Siegl & Rudel, 2015).

For example, infection by *Helicobacter pylori* amplifies development of adenocarcinomas in the gastric tract by modifying post–translational modifications of histones; changes in p53 activity were induced by an intracellularly secreted bacterial virulence factor: cytotoxin–associated gene A protein (Wei et al., 2015).

Downregulating apoptosis in cells infected with pathogenic bacteria through changes in p53 may reduce packaging of histone–DNA complexes within sEVs. Therefore, as histone proteins were downregulated in co–culture sEVs, it is likely that an introduction of *M. bovis* was responsible for altering bEEL cell cycle regulation.

Future experiments should assess differences in p53 mutant cell lines to understand the role of this protein within histone regulation of infected cell lines.

4.2.3 Apolipoproteins

Downregulation of multiple *Bos taurus*–associated apolipoproteins in the proteome of co–culture sEVs relative to control sEVs indicated that *M. bovis* reduced the metabolic capability of bEEL cells.

As *M. bovis* incorporates sterol proteins to regulate fluidity of the cytoplasmic membrane, it requires a supply of lipids from either the host cell or growth medium (Kornspan & Rottem, 2012).

Infection by *M. tuberculosis* reduced or prevented an ability of host macrophages to catabolise cholesterol by inhibiting host enzymes involved in cholesterol metabolism (Wilburn et al., 2018).

Therefore, inhibiting host proteins involved with cholesterol metabolism implies that *M. bovis* uses lipids for its own pathogenesis and growth, which host cells are prevented from utilising (Adamu et al., 2020).

4.2.4 L–lactate dehydrogenase

L–lactate dehydrogenase proteins are utilised by a variety of organisms in gluconeogenesis and DNA metabolism (Farhana & Lappin, 2021). A *M. bovis*–associated L–lactate dehydrogenase was significantly upregulated in the co–culture sEV proteome relative to control sEVs.

Increased L–lactate dehydrogenase expression implies that the metabolic functions of *M. bovis* were increased in the co–culture. However, an upregulation of *M. bovis*–associated L–lactate dehydrogenase within sEVs of aRPMI–grown *M. bovis*, relative to FB–grown *M. bovis*, indicated that *M. bovis* grown in aRPMI without bEEL cells were likely nutrient deprived. The availability of nutrients, for example sterol proteins (provided only from an animal–derived source such as serum), for growth of extracellular *M. bovis* was likely limited in aRPMI as compared with nutrient availability in FB (Beier et al., 2018).

Although an upregulation of L–lactate dehydrogenase was prominent in co–culture sEVs, it likely indicated a presence of metabolically active *M. bovis* instead of nutrient–deficient *M. bovis* as bEEL cells were available for infection within the co–culture.

However, it should be noted that a limitation of the co–culture model is that extracellular bacteria will produce their own sEVs (Tulkens et al., 2020). Therefore, the sEV population we are investigating was mixed, which may have confounded the assessment of L–lactate dehydrogenase as represented different states of *M. bovis* metabolic function.

In a previous study, it was determined that different isoforms of L–lactate dehydrogenase demonstrated use as biomarkers following infection with *Mycoplasma pneumoniae* (Liu et al., 2018b). However, because of issues in specificity, their main use would be to indicate pathogenic presence unless combined with other markers more specific for diagnosing infection (Choi et al., 2019). Furthermore, this research indicates that L–lactate dehydrogenase is not likely to be specific to *M. bovis* infection.

A *Bos taurus*–associated L–lactate dehydrogenase was similarly upregulated in co–culture sEVs relative to control sEVs. Therefore, L–lactate dehydrogenase is not likely to be a useful biomarker for *M. bovis* infection as changes in protein expression likely represent altered cellular metabolism rather than specific diagnosis of *M. bovis*. Instead, changes in expression of L–lactate dehydrogenase appear to be influenced by nutrient availability for *M. bovis* in this study.

4.2.5 Endopeptidase inhibitors

There was an upregulation in multiple *Bos taurus* proteins involved in endopeptidase inhibition within co–culture sEVs relative to control sEVs.

In contrast, there was a downregulation in these proteins in sEVs from *M. bovis* grown in both aRPMI and FB.

When the log_2 fold change from sEVs of *M. bovis* grown in FB was compared to the log_2 fold change of sEVs from the co–culture, an even greater downregulation in these inhibitory proteins was indicated.

This demonstrates that co–culturing bEEL cells with *M. bovis* altered pathways involved in endopeptidase inhibition, with an upregulation of inhibitory proteins unique to co–culture.

Endopeptidases are involved in a variety of functions with their main purpose to cleave peptide bonds at specific non–terminal amino acids to enable further degradation or protein recycling (Gurumallesh et al., 2019).

An upregulation in inhibitory proteins of specific endopeptidases, serine–type and cysteine–type, occurred by co–culturing bEEL cells and *M. bovis*.

Interpreting this regulatory change is difficult because of the limited knowledge of the role of endopeptidase activity in the host response to infection.

Most endopeptidase research within immunity relates to bacterial endopeptidase activity, their role within avoidance of host immune responses or their function within cancer progression (Mallick et al., 2019; Zhang & Lin, 2021).

However, earlier research has provided some understanding regarding inhibition of host endopeptidases. Failure to cleave Toll–like Receptor 9 (**TLR9**) prevents recruitment of the adaptor molecule Myeloid Differentiation Factor 88 (Ewald et al., 2008).

Further, an inhibition of asparagine endopeptidases prevented secretion of pro–inflammatory cytokines following TLR9 stimulation, which demonstrates that endopeptidases are essential in enabling initiation of TLR9 activity in response to antigenic stimulation (Sepulveda et al., 2009).

Comparably, host asparagine endopeptidases were linked with control of Toll–like Receptor 7 activity in response to influenza detection (Maschalidi et al., 2012).

Although asparagine endopeptidases were not directly upregulated in co–culture, it established that endopeptidase activity is linked to host immune responses that intend to reduce infection.

Therefore, an upregulation of proteins that inhibit serine–type and cysteine–type endopeptidases would likely be caused by influence of *M. bovis* on bEEL cells.

Future experiments should test differences in the infective ability of various *Mycoplasma* ssp. to understand effects caused by endopeptidase inhibition within host cells.

4.2.6 Summary

In summary, the protein cargo of sEVs from cells *in vitro* within a bioreactor flask can be used for assessing differences in proteins caused by infection of pathogenic organisms.

Future research should assess whether potential protein biomarkers are representative of infection *in vivo* and if they could be developed further into a *M. bovis*–specific diagnostic test.

4.3 Infection: Intracellular or Adherence?

Co–culturing bEEL cells with two separate *Mycoplasma* ssp. revealed differences in the specificity of infection. Adherence of both *Mycoplasma* ssp. was not specific to the species of animal that cells were derived from, however, intracellular infection only occurred in cells from the animal species that the *Mycoplasma* sp. naturally infects.

Gentamicin protection assays are widely used to assess the ability of pathogenic organisms to intracellularly invade host cells, with examples including *Listeria monocytogenes*, *Salmonella enterica* and a porcine *Mycoplasma* sp.: *Mycoplasma hyopneumoniae* (Birhanu et al., 2018; Raymond et al., 2018; Aviv et al., 2019; Papić et al., 2019).

Two separate *Mycoplasma* ssp., *M. ovi* and *M. bovis*, were used in the current study to assess if intracellular infection of bEEL cells had occurred. When compared, the intracellular infection status of bEEL cells caused by *M. bovis* or *M. ovi* was vastly different.

At all gentamicin concentrations tested, *M. ovi* was not intracellularly protected by the cytoplasmic membrane of bEEL cells. In contrast, not treating the co–culture with gentamicin enabled growth of *M. ovi* to occur and indicated adherence to the cytoplasmic membrane of bEEL cells

Adherence of both isolates of *M. bovis* to bEEL cells was certain as performed comparably to *M. ovi* in the absence of gentamicin. Without the presence of bEEL cells, *M. bovis* did not survive when treated with gentamicin. Antibiotic treatment was consistent with concentrations of gentamicin used in gentamicin protection assays with alternative isolates of *M. bovis* (Bürki et al., 2015).

However, the differences in survival at greater concentrations of gentamicin can be explained by use of different *M. bovis* isolates to infect alternative epithelial cell lines. It remains inconclusive whether *M. bovis* isolate W18_04866 (#1) intracellularly infects host cells.

In a previous study, internalised *Yersinia pestis* did not proliferate when plated following four hours of gentamicin treatment at comparable antibiotic concentrations, questioning the ability of gentamicin to penetrate eukaryotic cell membranes (VanCleave et al., 2017).

Whilst W18_04866 (#1) was treated with gentamicin for only three hours, concentrations greater than 100 µg/mL likely penetrated the cytoplasmic membrane of bEEL cells and prevented survival of intracellular *M. bovis*.

Therefore, the gentamicin protection assay was useful for confirming adherence of *Mycoplasma* ssp. to eukaryotic cell lines. However, in our study, the gentamicin protection assay provided inconclusive results regarding intracellular infection. Different cell types and varied bacterial isolates seemingly have different responses to gentamicin in terms of preventing the growth of intracellular pathogens.

Epi–fluorescent microscopy provided an alternative assessment of bEEL cell infection using W18_04866 (#1). There was clear punctate fluorescence pattern present in bEEL cells infected with pre–stained *M. bovis*, which was not present in bEEL cells treated with stain–only. An obvious reduction in distinctive areas of fluorescent red coincided with uninfected bEEL cells.

The true route of infection by *Mycoplasma* ssp. remains unknown.

However, positioning of fluorescently stained *M. bovis* suggested that intracellular infection had occurred as the majority of pre–stained *M. bovis* tended to converge around the nucleus of bEEL cells. If *M. bovis* isolate W18_04866 (#1) was able to adhere to bEEL cells but not enter them, there would likely be more areas of pre–stained *M. bovis* spread throughout the actin–cytoskeleton rather than being condensed around the nucleus.

However, further investigation using high–resolution microscopy and 3D image construction would be required to support a hypothesis that *M. bovis* isolate W18_04866 (#1) intracellularly infects bEEL cells.

Confocal microscopy of three bovine epithelial cell lines that were different from the one used in the current study demonstrated intracellular infection of *M. bovis* is likely, as gentamicin treatment prior to imaging elicited changes in the position of the bacterium within cells (Josi et al., 2018).

Adherence and intracellular infection of many biologically related *Mycoplasma* ssp. have been demonstrated using a variety of immortalised cell lines and primary cells. For example, invasion of *M. bovis* was demonstrated in bovine synovial cells (Nishi et al., 2021a).

Intriguingly, Nishi et al. (2021a) demonstrated that *M. bovis* utilised the endocytic clathrin–dependent pathway (involved in early endosome formation and subsequent generation of sEVs) for intracellular invasion of bovine synovial cells.

Another example included demonstrating that bovine bronchiolar epithelial cells were successfully infected by *M. bovis* and intracellular infection was less apparent than adherence of *M. bovis* (Nunoya et al., 2020).

In bovine mammary epithelial cells, infection by *M. bovis* resulted in an impaired lysosome function and subsequent prevention of the autophagy of infected cells, indicating a potential effect on sEV processing (Liu et al., 2021).

Prior studies suggest that *Mycoplasma* ssp. follow an infection pathway where adherence and intracellular mechanisms are both utilised by the bacterium for continued survival. Intracellular infection by a *Mycoplasma* sp. tends to be host specific, as in contrast, it was likely that *M. ovi* bound to bEEL cells using membrane adhesin proteins present in many *Mycoplasma* ssp. (Vizarraga et al., 2020).

Protein factors, termed nucleomodulins, are used by gram–positive/negative bacteria and have been linked to modifications of host nuclear processes (Bierne & Pourpre, 2020).

Essential pathways that form nucleotides are minimal in *M. bovis*, which supports the hypothesis that intracellular invasion is required at a point during infection to gain of nucleotide precursors that aid in increased bacterial growth (Sharma et al., 2015).

Furthermore, Zhang et al. (2021) demonstrated that secondary metabolites secreted by *M. bovis* aided virulence.

To prevent detection and potential clearance from host cells, *M. bovis* may modify nuclear processes using these secreted metabolites. Secretion of virulence factors involved in intracellular infection may be different between species, which could explain the varied results of gentamicin protection assays.

Mycoplasma ovipneumoniae may have been compromised in its capability to complete an infection cycle by species cross–reactivity, as compared with the specific infectious ability of *M. bovis* in bEEL cells, as bEEL cells are bovine in origin.

Future experiments should compare the infection ability of different *Mycoplasma* ssp., aiming to understand if specific virulence factors unique to each *Mycoplasma* sp. assist in adherence or are useful in facilitating an intracellular infection of varied cell types.

4.4 Inactivation

Every experimental sample that contained *M. bovis* was assessed for absence of viable *M. bovis* prior to removal from the PC3 facility due to the biosecurity concerns related to *M. bovis* in New Zealand. Our results indicated that *M. bovis* remained viable following heat treatment and/or processing of culture using SEC columns.

A baseline heat treatment protocol of 56 °C for thirty minutes was assessed and this treatment did not kill *M. bovis*; bacterial growth was demonstrated in Friis Broth (**FB**) and on Friis Agar (**FA**). Pasteurisation methods at ~60 °C for thirty minutes are apparently sufficient in treating *M. bovis* contained within discard milk and colostrum, without creating flow–on effects regarding product quality (Parker et al., 2016; Gille et al., 2020). Growth of each isolate after 56 °C–treatment questions if *M. bovis* is fully inactivated at pasteurisation temperatures.

Treatments at 80 °C and 90 °C for ten minutes were assessed and resulted in limited subsequent growth in FB. On FA, *M. bovis* growth was influenced by treatment at 80 °C, with a reduced number of colonies evident on agar compared with untreated controls. However, a reduction in colony numbers is not sufficient to demonstrate complete inactivation (Espinosa et al., 2020). In comparison, heat treatment at 90 °C for ten minutes killed all extracellular *M. bovis* in FB and minimal growth was evident on FA, which was in agreement with the findings of Zbinden et al. (2015).

However, without inclusion of a secondary element such as a lysis buffer, *M. bovis* grown *in vitro* remains viable at the temperatures tested for these time periods, evident by colony growth on FA. Whilst lysis prevented *M. bovis* growth, it prevented assessment of size and concentration of sEVs using TEM and/or qNANO as sEV structure was chemically degraded.

Treatment at high temperatures for extended periods creates issues in terms of protein unfolding/degradation (Lapidus, 2017; Kleinjan et al., 2021). Heat treatment can cause sEV aggregation meaning that it was counterintuitive to heat treat *M. bovis* at 90 °C in samples containing isolated sEVs. Schulz et al. (2020) challenged these ideas but only demonstrated that sEVs are thermo–stable at 37 °C. However, concentration and size of sEVs are altered at temperatures greater than 37 °C. Heat–treating sEV samples for longer periods increased the observed damage to sEVs and sEV–proteins.

Mycoplasma bovis survived SEC isolation, which was indicated by colour change of growth medium after transfer of each fraction to FB. The viability of *M. bovis* after culture was processed using SEC columns meant that samples had to undergo a step to destroy viable bacteria prior to LC–MS/MS.

Only lysis and fixation provided results that met the required biosecurity standard for transfer of *M. bovis*–containing samples as treatment resulted in complete inactivation.

Whilst heat treatment at 90 °C inactivated *M. bovis* in FB, colonies formed on FA and protein degradation was too great to consider including an additional heat treatment step to inactivate *M. bovis* in sEV–containing samples.

The safety of the agricultural industry of New Zealand was an extremely high priority for our study and these inactivation results have major implications for biosecurity.

Our results demonstrate that without fixation or lysis *M. bovis* can survive *in vitro* and, if not contained properly, there is the risk for a substantial outbreak of disease.

When considering using sEVs as diagnostic tools, contaminating microorganisms of comparable sizes can coexist in samples following SEC isolation.

Heat treatment can be used to treat these contaminants, but this has downstream implications regarding sEV biology and potential loss of novel protein markers.

4.5 Limitations

Firstly, our study was limited by sEV biology. Woith et al. (2019) states that all kingdoms of life produce sEVs, meaning that *in vitro* growth of extracellular *M. bovis* likely generated sEVs that complicated analysis of co–culture sEVs. An inclusion of a control for *M. bovis* (grown in FB) did aid in comparing protein cargo to co–culture sEVs. However, this was limited by a reduced concentration of sEVs as *M. bovis* could not be grown in a bioreactor flask.

Future studies will benefit from a greater variation in conditions. These should include creating conditions to replicate the stress on bEEL cells caused by *M. bovis* infection (such as growth of bEEL cells under anoxic conditions), culturing a pathogenic bacterium within its growth media (alongside a co–culture and uninfected control) in a bioreactor flask for longer than three months to provide a greater proportion sEVs, or comparing changes of the sEV transcriptome to the sEV proteome to assess differences caused by *M. bovis* infection.

Secondly, because bEEL cells are adherent, it was difficult to obtain an accurate cell count when they were growing in the bioreactor flasks, which led to limiting our assessment of the MOI that *M. bovis* would infect bEEL cells. Although *M. bovis* was inoculated into the bioreactor flask at an assumed MOI of 5, this ratio may have been greater or lesser depending on the growth of bEEL cells at the point of inoculation.

However, infection of bEEL cells by *M. bovis* was verified by gentamicin protection assays and epi–fluorescent microscopy, with the presence of *M. bovis* in the bioreactor confirmed throughout the life of the co–culture bioreactor flask by PCR. This meant that although an accurate MOI was limited by using a bioreactor flask, we confirmed that infection of bEEL cells with *M. bovis* was highly likely within the co–culture flask.

Thirdly, the LC–MS/MS–based proteome analysis of *M. bovis*–only sEVs was potentially confounded by sEVs introduced by animal serum that was used to supplement the growth medium. The inclusion of an Exosome–Depleted FBS and the adaptation of bEEL cells to a reduced FBS medium minimised contaminating bovine sEVs. However, equine/porcine serum and a yeast extract were used to supplement *M. bovis*, which complicated proteomic analysis of sEVs in *M. bovis*–only control samples.

Therefore, any proteomic analysis of control/treatment sEVs must consider potential contamination by serum and serum sEVs, which could indicate changes in protein regulation that are not representative of infection.

Finally, biosecurity requirements in New Zealand limit direct analysis of sEVs from cultures containing *M. bovis* without prior fixation or lysis.

Measurement of sEV size and concentration from samples that contained *M. bovis* was limited by the inability to safely eradicate live *M. bovis* without using a lysis buffer.

Consequently, common methods to quantify sEVs could not be used. Co–culture sEVs could be fixed and imaged using TEM. However, sEVs were mostly indistinguishable within TEM images of FB–cultured *M. bovis* and meant that fixation prevented an accurate analysis of sEVs from this treatment.

4.6 Conclusion

In conclusion, our study has demonstrated the first use of a bioreactor flask for successful infection of a bovine cell line with *M. bovis*. It is also the first study to use proteomics to assess differences in sEVs (produced within bioreactor flasks) from an *in vitro M. bovis* infection model.

Bioreactor flasks maximised the output of sEVs, which increased the accuracy in comparing proteomic differences in sEVs caused by *M. bovis* infection. Although a specific biomarker was not immediately obvious, the infection model delivered candidate protein markers that might represent *M. bovis* infection.

Future research will continue to investigate whether a diagnostic biomarker of *M bovis* infection can be identified *in vivo*, with the aim of developing a diagnostic test for improving worldwide eradication of *M. bovis*.

Following the use of SEC columns and heat treatment, *M. bovis* remained viable. Complete inactivation of *M. bovis* requires the use of lysis or fixation, which has implications in biosecurity measures for *M. bovis*. Adherence of *M. bovis* to bEEL cells was certain, but intracellular infection remained inconclusive.

Future research can utilise live, pre–stained *M. bovis* for infection of cells. Further experiments using 3D imaging or high–resolution microscopy to follow the infection pathway of *M. bovis* should occur to provide a greater understanding of *M. bovis* infection in host cells.

5 Bibliography

Adamu, J. Y., Wawegama, N. K., Kanci Condello, A., Marenda, M. S., Markham, P. F., Browning, G. F., & Tivendale, K. A. (2020). *Mycoplasma bovis* membrane protein MilA is a multifunctional lipase with novel lipid and glycosaminoglycan binding activity. *Infection and Immunity 88*(6), e00945-00919.

Ageta, H., & Tsuchida, K. (2019). Post-translational modification and protein sorting to small extracellular vesicles including exosomes by ubiquitin and UBLs. *Cellular and Molecular Life Sciences*, *76*(24), 4829-4848.

Ahmadi, M. H. (2021). Resistance to tetracyclines among clinical isolates of *Mycoplasma hominis* and *Ureaplasma* ssp.: a systematic review and meta-analysis. *Journal of Antimicrobial Chemotherapy*, *76*(4), 865-875.

Ahn, J. G., Cho, H.-K., Li, D., Choi, M., Lee, J., Eun, B.-W., Jo, D. S., Park, S. E., Choi, E. H., & Yang, H.-J. (2021). Efficacy of tetracyclines and fluoroquinolones for the treatment of macrolide-refractory *Mycoplasma pneumoniae* pneumonia in children: a systematic review and meta-analysis. *BioMed Central Infectious Diseases*, *21*(1), 1-10.

Al-Farha, A. A.-B., Hemmatzadeh, F., Khazandi, M., Hoare, A., & Petrovski, K. (2017). Evaluation of effects of *Mycoplasma* ssp. mastitis on milk composition in dairy cattle from South Australia. *BioMed Central Veterinary Research*, *13*(1), 1-8.

Alix-Panabieres, C. (2020). The future of liquid biopsy. *Nature*, *579*(7800), S9-S9.

Amram, E., Freed, M., Khateb, N., Mikula, I., Blum, S., Spergser, J., Sharir, B., Ozeri, R., Harrus, S., & Lysnyansky, I. (2013). Multiple locus variable number tandem repeat analysis of *Mycoplasma bovis* isolated from local and imported cattle. *The Veterinary Journal*, *197*(2), 286-290.

Andersson, A.-M., Aspán, A., Wisselink, H. J., Smid, B., Ridley, A., Pelkonen, S., Autio, T., Lauritsen, K. T., Kensø, J., & Gaurivaud, P. (2019). A European inter-laboratory trial to evaluate the performance of three serological methods for diagnosis of *Mycoplasma bovis* infection in cattle using latent class analysis. *BioMed Central Veterinary Research*, *15*(1), 1-10.

Arcangioli, M.-A., Lurier, T., Hauray, K., & Tardy, F. (2021). Large-size fattening calves' lots fed with automatic milk feeders may have an increased risk for *Mycoplasma bovis* infection spread and for antibiotic use. *Animal*, *15*(12), 100397.

Armstrong, D. A., Lee, M. K., Hazlett, H. F., Dessaint, J. A., Mellinger, D. L., Aridgides, D. S., Hendricks, G. M., Abdalla, M. A., Christensen, B. C., & Ashare, A. (2020). Extracellular vesicles from *Pseudomonas aeruginosa* suppress MHC-related molecules in human lung macrophages. *Immunohorizons*, *4*(8), 508-519.

Artuyants, A., Chang, V., Reshef, G., Blenkiron, C., Chamley, L. W., Leung, E., & Hisey, C. L. (2021). Production of extracellular vesicles using a CELLine adherent bioreactor flask. *Methods in Molecular Biology*

Askar, H., Chen, S., Hao, H., Yan, X., Ma, L., Liu, Y., & Chu, Y. (2021). Immune evasion of *Mycoplasma bovis*. *Pathogens*, *10*(3), 297.

Atukorala, I., & Mathivanan, S. (2021). The role of post-translational modifications in targeting protein cargo to extracellular vesicles. In *New Frontiers: Extracellular Vesicles* (pp. 45-60). Springer.

Aviv, G., Cornelius, A., Davidovich, M., Cohen, H., Suwandi, A., Galeev, A., Steck, N., Azriel, S., Rokney, A., & Valinsky, L. (2019). Differences in the expression of SPI-1 genes pathogenicity and epidemiology between the emerging *Salmonella enterica* serovar Infantis and the model *Salmonella enterica* serovar Typhimurium. *The Journal of Infectious Diseases*, *220*(6), 1071-1081.

Awadh, A. A., Le Gresley, A., Forster-Wilkins, G., Kelly, A. F., & Fielder, M. D. (2021). Determination of metabolic activity in planktonic and biofilm cells of *Mycoplasma fermentans* and *Mycoplasma pneumoniae* by nuclear magnetic resonance. *Scientific Reports*, *11*(1), 1-12.

Ayling, R., Gosney, F., & Hlusek, M. (2015). Mycoplasma diagnostics, some results, and what we still don't know about *Mycoplasma bovis* disease. *Cattle Practice*, *23*, 248-251.

Baetz, N. W., & Goldenring, J. R. (2014). Distinct patterns of phosphatidylserine localization within the Rab11a-containing recycling system. *Cellular Logistics*, *4*(2), e28680.

Baietti, M. F., Zhang, Z., Mortier, E., Melchior, A., Degeest, G., Geeraerts, A., Ivarsson, Y., Depoortere, F., Coomans, C., & Vermeiren, E. (2012). Syndecan–syntenin–ALIX regulates the biogenesis of exosomes. *Nature Cell Biology*, *14*(7), 677-685. https://www.nature.com/articles/ncb2502.pdf

Baj-Krzyworzeka, M., Mytar, B., Węglarczyk, K., Szatanek, R., Kijowski, J., & Siedlar, M. (2020). Protumorogenic potential of pancreatic adenocarcinoma-derived extracellular vesicles. *Folia Biologica*, *66*(3), 104-110.

Balsera, M., & Buchanan, B. B. (2019). Evolution of the thioredoxin system as a step enabling adaptation to oxidative stress. *Free Radical Biology and Medicine*, *140*, 28-35.

Bartfeld, S., Bayram, T., van de Wetering, M., Huch, M., Begthel, H., Kujala, P., Vries, R., Peters, P. J., & Clevers, H. (2015). *In vitro* expansion of human gastric epithelial stem cells and their responses to bacterial infection. *Gastroenterology*, *148*(1), 126-136. e126.

Bauer, F. N., & Giebel, B. (2021). Therapeutic potential of mesenchymal stromal cell-derived small extracellular vesicles. *Extracellular Vesicles: Applications to Regenerative Medicine, Therapeutics and Diagnostics*.

Becker, C. A., Ambroset, C., Huleux, A., Vialatte, A., Colin, A., Tricot, A., Arcangioli, M.-A., & Tardy, F. (2020). Monitoring *Mycoplasma bovis* diversity and antimicrobial susceptibility in calf feedlots undergoing a respiratory disease outbreak. *Pathogens*, *9*(7), 593.

Behera, S., Rana, R., Gupta, P., Kumar, D., Rekha, V., Arun, T., & Jena, D. (2018). Development of real-time PCR assay for the detection of *Mycoplasma bovis*. *Tropical Animal Health and Production*, *50*(4), 875-882.

Beier, L. S., Siqueira, F. M., & Schrank, I. S. (2018). Evaluation of growth and gene expression of *Mycoplasma hyopneumoniae* and *Mycoplasma hyorhinis* in defined medium. *Molecular Biology Reports*, *45*(6), 2469-2479.

Bielanski, A., Devenish, J., & Phipps-Todd, B. (2000). Effect of *Mycoplasma bovis* and *Mycoplasma bovigenitalium* in semen on fertilization and association with *in vitro* produced morula and blastocyst stage embryos. *Theriogenology*, *53*(6), 1213-1223.

Bierne, H., & Pourpre, R. (2020). Bacterial factors targeting the nucleus: the growing family of nucleomodulins. *Toxins*, *12*(4), 220.

Biosecurity, N. Z. (2021). *Mycoplasma bovis situation report as at 16 December*. https://www.mpi.govt.nz/biosecurity/mycoplasma-bovis/situation-report/

Biosecurity, O. o. t. M. f. (2020). *Eradicating Mycoplasma bovis – Update and Next Steps*. https://www.mpi.govt.nz/resources-and-forms/publications/

Birhanu, B. T., Park, N.-H., Lee, S.-J., Hossain, M. A., & Park, S.-C. (2018). Inhibition of *Salmonella typhimurium* adhesion, invasion, and intracellular survival via treatment with methyl gallate alone and in combination with marbofloxacin. *Veterinary Research*, *49*(1), 1-11.

Borchsenius, S. N., Vishnyakov, I. E., Chernova, O. A., Chernov, V. M., & Barlev, N. A. (2020). Effects of *Mycoplasma* ssp. on the host cell signaling pathways. *Pathogens*, *9*(4), 308.

Bottinelli, M., Merenda, M., Gastaldelli, M., Picchi, M., Stefani, E., Nicholas, R. A., & Catania, S. (2020). The pathogen *Mycoplasma dispar* shows high minimum inhibitory concentrations for antimicrobials commonly used for bovine respiratory disease. *Antibiotics*, *9*(8), 460.

Breuer, M., Earnest, T. M., Merryman, C., Wise, K. S., Sun, L., Lynott, M. R., Hutchison, C. A., Smith, H. O., Lapek, J. D., & Gonzalez, D. J. (2019). Essential metabolism for a minimal cell. *Elife*, *8*, e36842.

Bridgeman, B. (2021). *Molecular and immunological analysis of New Zealand isolates of Mycoplasma ovipneumoniae: a thesis presented in partial fulfilment of the requirements for the degree of Doctor of Philosophy in Veterinary Science at Massey University, Palmerston North, New Zealand*

Bridgeman, B., Gupta, S., Murray, A., Dukkipati, V., Altermann, E., & Wedlock, D. (2020). Draft genome sequence of a New Zealand isolate of *Mycoplasma ovipneumoniae*. *Microbiology Resource Announcements*, *9*(10), e01375-01319.

Brinkmann, K., Enderle, D., Flinspach, C., Meyer, L., Skog, J., & Noerholm, M. (2018). Exosome liquid biopsies of NSCLC patients for longitudinal monitoring of ALK fusions and resistance mutations. *Journal of Clinical Oncology*, *36*(15).

Bürgi, N., Josi, C., Bürki, S., Schweizer, M., & Pilo, P. (2018). *Mycoplasma bovis* co-infection with bovine viral diarrhea virus in bovine macrophages. *Veterinary Research*, *49*(1), 1-11.

Bürki, S., Gaschen, V., Stoffel, M. H., Stojiljkovic, A., Frey, J., Kuehni-Boghenbor, K., & Pilo, P. (2015). Invasion and persistence of *Mycoplasma bovis* in embryonic calf turbinate cells. *Veterinary Research*, *46*(1), 53.

Burton, G. J., Redman, C. W., Roberts, J. M., & Moffett, A. (2019). Pre-eclampsia: pathophysiology and clinical implications. *British Medical. Journal*, *366*.

Cai, H. Y., McDowall, R., Parker, L., Kaufman, E. I., & Caswell, J. L. (2019). Changes in antimicrobial susceptibility profiles of *Mycoplasma bovis* over time. *Canadian Journal of Veterinary Research*, *83*(1), 34-41.

Calcutt, M., Lysnyansky, I., Sachse, K., Fox, L., Nicholas, R., & Ayling, R. (2018). Gap analysis of *Mycoplasma bovis* disease, diagnosis and control: an aid to identify future development requirements. *Transboundary and Emerging Diseases*, *65*, 91-109. https://onlinelibrary.wiley.com/doi/full/10.1111/tbed.12860

Castellanos-Rizaldos, E., Grimm, D. G., Tadigotla, V., Hurley, J., Healy, J., Neal, P. L., Sher, M., Venkatesan, R., Karlovich, C., & Raponi, M. (2018). Exosome-based detection of EGFR T790M in plasma from non–small cell lung cancer patients. *Clinical Cancer Research*, *24*(12), 2944-2950.

Castro-Garza, J., García-Jacobo, P., Rivera-Morales, L. G., Quinn, F. D., Barber, J., Karls, R., Haas, D., Helms, S., Gupta, T., & Blumberg, H. (2017). Detection of anti-HspX antibodies and HspX protein in patient sera for the identification of recent latent infection by *Mycobacterium tuberculosis*. *Public Library of Science One*, *12*(8), e0181714. https://www.ncbi.nlm.nih.gov/pmc/articles/PMC5558980/pdf/pone.0181714.pdf

Chang, X., Fang, L., Bai, J., & Wang, Z. (2020). Characteristics and changes of DNA in extracellular vesicles. *DNA and Cell Biology*, *39*(9), 1486-1493.

Chauhan, K., Aly, S. S., Lehenbauer, T. W., Tonooka, K. H., Glenn, K., Rossitto, P., & Marco, M. L. (2021). Development of a multiplex qPCR assay for the simultaneous detection of *Mycoplasma bovis*, *Mycoplasma* ssp., and *Acholeplasma laidlawii* in milk. *PeerJ*, *9*, e11881. https://www.ncbi.nlm.nih.gov/pmc/articles/PMC8364749/pdf/peerj-09-11881.pdf

Chen, S., Shiesh, S.-C., Lee, G.-B., & Chen, C. (2020). Two-step magnetic bead-based (2MBB) techniques for immunocapture of extracellular vesicles and quantification of microRNAs for cardiovascular diseases: A pilot study. *Public Library of Science One*, *15*(2), e0229610.

Choi, Y.-J., Jeon, J.-H., & Oh, J.-W. (2019). Critical combination of initial markers for predicting refractory *Mycoplasma pneumoniae* pneumonia in children: a case control study. *Respiratory Research*, *20*(1), 1-9.

Core Team, R. (2013). R: A language and environment for statistical computing. *R Foundation for statistical computing, Vienna*.

Crookenden, M. A. (2020). *To obtain approval for new organisms in containment*.

Cruz, M. D., & Kim, K. (2019). The inner workings of intracellular heterotypic and homotypic membrane fusion mechanisms. *Journal of Biosciences*, *44*(4), 1-14.

Dahiya, B., Khan, A., Mor, P., Kamra, E., Singh, N., Gupta, K. B., Sheoran, A., Sreenivas, V., & Mehta, P. K. (2019). Detection of *Mycobacterium tuberculosis* Lipoarabinomannan and CFP-10 (Rv3874) from urinary extracellular vesicles of tuberculosis patients by immuno-PCR. *Pathogens and disease*, *77*(5), ftz049.

Das, R., Roosloot, R., van Pel, M., Schepers, K., Driessen, M., Fibbe, W. E., de Bruijn, J. D., & Roelofs, H. (2019). Preparing for cell culture scale-out: establishing parity of bioreactor-and flask-expanded mesenchymal stromal cell cultures. *Journal of Translational Medicine*, *17*(1), 1-13.

Deeney, A. S., Collins, R., & Ridley, A. M. (2021). Identification of *Mycoplasma ssp.* and related organisms from ruminants in England and Wales during 2005–2019. *BioMed Central Veterinary Research*, *17*(1), 1-12.

Diaz, G., Wolfe, L. M., Kruh-Garcia, N. A., & Dobos, K. M. (2016). Changes in the membrane-associated proteins of exosomes released from human macrophages after *Mycobacterium tuberculosis* infection. *Scientific Reports*, *6*(1), 1-10.

Dongwen L, S. G. K. J. (2021). *predictmeans: Calculate Predicted Means for Linear Models. R package version 1.0.6.*

Drommelschmidt, K., Serdar, M., Bendix, I., Herz, J., Bertling, F., Prager, S., Keller, M., Ludwig, A.-K., Duhan, V., & Radtke, S. (2017). Mesenchymal stem cell-derived extracellular vesicles ameliorate inflammation-induced preterm brain injury. *Brain, Behavior, and Immunity*, *60*, 220-232.

Dudek, K., Nicholas, R. A., Szacawa, E., & Bednarek, D. (2020). *Mycoplasma bovis* infections—Occurrence, diagnosis and control. *Pathogens*, *9*(8), 640.

Dudek, K., Szacawa, E., & Nicholas, R. A. (2021). Recent developments in vaccines for Bovine Mycoplasmoses caused by *Mycoplasma bovis* and *Mycoplasma mycoides* subsp. *mycoides*. *Vaccines*, *9*(6), 549.

Dumke, R., & Ziegler, T. (2019). Long-term low rate of macrolide-resistant *Mycoplasma pneumoniae* strains in Germany. *Antimicrobial Agents and Chemotherapy*, *63*(5), e00455-00419.

Edgar, J. R., Willén, K., Gouras, G. K., & Futter, C. E. (2015). ESCRTs regulate amyloid precursor protein sorting in multivesicular bodies and intracellular amyloid-β accumulation. *Journal of Cell Science*, *128*(14), 2520-2528.

Elkin, S. R., Lakoduk, A. M., & Schmid, S. L. (2016). Endocytic pathways and endosomal trafficking: a primer. *Vienna Medical Weekly Springer Verlag*, *166*(7), 196-204.

Enabulele, J. E., Chukwumah, N. M., & Enabulele, O. (2020). Tetracycline use in children and knowledge of its oral implications among nursing mothers. *Pediatric Dental Journal*, *30*(3), 224-230.

Espinosa, M. F., Sancho, A. N., Mendoza, L. M., Mota, C. R., & Verbyla, M. E. (2020). Systematic review and meta-analysis of time-temperature pathogen inactivation. *International Journal of Hygiene and Environmental Health*, *230*, 113595.

Estadella, I., Pedrós-Gámez, O., Colomer-Molera, M., Bosch, M., Sorkin, A., & Felipe, A. (2020). Endocytosis: a turnover mechanism controlling ion channel function. *Cells*, *9*(8), 1833.

Ewald, S. E., Lee, B. L., Lau, L., Wickliffe, K. E., Shi, G.-P., Chapman, H. A., & Barton, G. M. (2008). The ectodomain of Toll-like receptor 9 is cleaved to generate a functional receptor. *Nature*, *456*(7222), 658-662.

Farhana, A., & Lappin, S. (2021). Biochemistry, Lactate Dehydrogenase. *Treasure Island (FL): StatPearls Publishing*.

Fitzgerald, W., Freeman, M. L., Lederman, M. M., Vasilieva, E., Romero, R., & Margolis, L. (2018). A system of cytokines encapsulated in extracellular vesicles. *Scientific Reports*, *8*(1), 1-11.

Foddai, A., Idini, G., Fusco, M., Rosa, N., De la Fe, C., Zinellu, S., Corona, L., & Tola, S. (2005). Rapid differential diagnosis of *Mycoplasma agalactiae* and *Mycoplasma bovis* based on a multiplex-PCR and a PCR-RFLP. *Molecular and Cellular Probes*, *19*(3), 207-212.

Forrellad, M. A., Klepp, L. I., Gioffré, A., Sabio y Garcia, J., Morbidoni, H. R., Santangelo, M. D. L. P., Cataldi, A. A., & Bigi, F. (2013). Virulence factors of the *Mycobacterium tuberculosis* complex. *Virulence*, *4*(1), 3-66.

Fortier, M., Guilbault, L., & Grasso, F. (1988). Specific properties of epithelial and stromal cells from the endometrium of cows. *Reproduction*, *83*(1), 239-248.

Fox, L. K., Muller, F. J., Wedam, M. L., Schneider, C. S., & Biddle, M. K. (2008). Clinical *Mycoplasma bovis* mastitis in prepubertal heifers on 2 dairy herds. *The Canadian Veterinary Journal*, *49*(11), 1110.

Garcia-Morante, B., Dors, A., León-Kempis, R., De Rozas, A. P., Segalés, J., & Sibila, M. (2018). Assessment of the in vitro growing dynamics and kinetics of the non-pathogenic J and pathogenic 11 and 232 *Mycoplasma hyopneumoniae* strains. *Veterinary Research*, *49*(1), 1-11.

Gauthier, S. A., Pérez-González, R., Sharma, A., Huang, F.-K., Alldred, M. J., Pawlik, M., Kaur, G., Ginsberg, S. D., Neubert, T. A., & Levy, E. (2017). Enhanced exosome secretion in Down syndrome brain-a protective mechanism to alleviate neuronal endosomal abnormalities. *Acta Neuropathologica Communications*, *5*(1), 1-13.

Gautier-Bouchardon, A. V. (2018). Antimicrobial resistance in *Mycoplasma* spp. *Microbiology Spectrum*, *6*(4), 6.4. 07.

Geller, L. T., Barzily-Rokni, M., Danino, T., Jonas, O. H., Shental, N., Nejman, D., Gavert, N., Zwang, Y., Cooper, Z. A., & Shee, K. (2017). Potential role of intratumor bacteria in mediating tumor resistance to the chemotherapeutic drug gemcitabine. *Science*, *357*(6356), 1156-1160.

Ghanem, M. E., Higuchi, H., Tezuka, E., Ito, H., Devkota, B., Izaike, Y., & Osawa, T. (2013). *Mycoplasma* ssp. infection in the uterus of early postpartum dairy cows and its relation to dystocia and endometritis. *Theriogenology*, *79*(1), 180-185.

Gille, L., Evrard, J., Callens, J., Supré, K., Grégoire, F., Boyen, F., Haesebrouck, F., Deprez, P., & Pardon, B. (2020). The presence of *Mycoplasma bovis* in colostrum. *Veterinary Research*, *51*(1), 1-4.

Gireud-Goss, M., Reyes, S., Tewari, R., Patrizz, A., Howe, M. D., Kofler, J., Waxham, M. N., McCullough, L. D., & Bean, A. J. (2020). The ubiquitin ligase UBE4B regulates amyloid precursor protein ubiquitination, endosomal trafficking, and amyloid β42 generation and secretion. *Molecular and Cellular Neuroscience*, *108*, 103542. https://www.ncbi.nlm.nih.gov/pmc/articles/PMC7530133/pdf/nihms-1622647.pdf

Giri, P. K., & Schorey, J. S. (2008). Exosomes derived from *Mycoplasma bovis* BCG infected macrophages activate antigen-specific CD4+ and CD8+ T cells *in vitro* and *in vivo*. *Public Library of Science One*, *3*(6), e2461.

Goetzl, E. J., Boxer, A., Schwartz, J. B., Abner, E. L., Petersen, R. C., Miller, B. L., & Kapogiannis, D. (2015). Altered lysosomal proteins in neural-derived plasma exosomes in preclinical Alzheimer disease. *Neurology*, *85*(1), 40-47.

Golding, B., Luu, A., Jones, R., & Viloria-Petit, A. M. (2018). The function and therapeutic targeting of anaplastic lymphoma kinase (ALK) in non-small cell lung cancer (NSCLC). *Molecular Cancer*, *17*(1), 1-15.

Gopalakrishnan, V., Spencer, C. N., Nezi, L., Reuben, A., Andrews, M., Karpinets, T., Prieto, P., Vicente, D., Hoffman, K., & Wei, S. (2018). Gut microbiome modulates response to anti–PD-1 immunotherapy in melanoma patients. *Science*, *359*(6371), 97-103.

Government, N. Z. (2017). *Analysis of risk pathways for the introduction of Mycoplasma bovis into New Zealand*. https://www.mpi.govt.nz/dmsdocument/28050-Pathways-Report-Redacted.pdf

Government, N. Z. (2018). *Mycoplasma bovis science plan* https://www.mpi.govt.nz/dmsdocument/32713-Mycoplasma-bovis-science-plan

Guerreiro, E. M., Vestad, B., Steffensen, L. A., Aass, H. C. D., Saeed, M., Øvstebø, R., Costea, D. E., Galtung, H. K., & Søland, T. M. (2018). Efficient extracellular vesicle isolation by combining cell media modifications, ultrafiltration, and size-exclusion chromatography. *Public Library of Science One*, *13*(9), e0204276.

Guo, M., Wang, G., Lv, T., Song, X., Wang, T., Xie, G., Cao, Y., Zhang, N., & Cao, R. (2014). Endometrial inflammation and abnormal expression of extracellular matrix proteins induced by Mycoplasma bovis in dairy cows. *Theriogenology*, *81*(5), 669-674.

Gurumallesh, P., Alagu, K., Ramakrishnan, B., & Muthusamy, S. (2019). A systematic reconsideration on proteases. *International Journal of Biological Macromolecules*, *128*, 254-267.

Haapala, V., Pohjanvirta, T., Vähänikkilä, N., Halkilahti, J., Simonen, H., Pelkonen, S., Soveri, T., Simojoki, H., & Autio, T. (2018). Semen as a source of *Mycoplasma bovis* mastitis in dairy herds. *Veterinary Microbiology*, *216*, 60-66.

Hale, H., CF, H., & WN, P. (1962). Bovine mastitis caused by a *Mycoplasma* sp. *The Cornell Veterinarian*, *52*, 582-591.

Hasegawa, Y., Futamata, H., & Tashiro, Y. (2015). Complexities of cell-to-cell communication through membrane vesicles: implications for selective interaction of membrane vesicles with microbial cells. *Frontiers in Microbiology*, *6*, 633. https://www.ncbi.nlm.nih.gov/pmc/articles/PMC4490254/pdf/fmicb-06-00633.pdf

Hassanpour, M., Rezaie, J., Nouri, M., & Panahi, Y. (2020). The role of extracellular vesicles in COVID-19 virus infection. *Infection, Genetics and Evolution*, *85*, 104422.

Hata, E., Harada, T., & Itoh, M. (2019). Relationship between antimicrobial susceptibility and multilocus sequence type of *Mycoplasma bovis* isolates and development of a method for rapid detection of point mutations involved in decreased susceptibility to macrolides, lincosamides, tetracyclines, and spectinomycin. *Applied and Environmental Microbiology*, *85*(13), e00575-00519.

Hazelton, M., Morton, J., Bosward, K., Sheehy, P., Parker, A., Dwyer, C., Niven, P., & House, J. (2020a). *Mycoplasma* ssp. in vaginas of dairy cows before and after exposure to bulls and their association with conception. *Journal of Dairy Science*, *103*, 11705-11805. https://doi.org/10.3168/jds.2020-18758

Hazelton, M., Morton, J., Parker, A., Bosward, K., Sheehy, P., Dwyer, C., Niven, P., & House, J. (2020b). *Mycoplasma bovis* and other Mollicutes in replacement dairy heifers from *Mycoplasma bovis*-infected and uninfected herds: A 2-year longitudinal study. *Journal of Dairy Science*, *103*(12), 11844-11856.

Hazelton, M., Sheehy, P., Bosward, K., Parker, A., Morton, J., Dwyer, C., Niven, P., & House, J. (2018). Shedding of *Mycoplasma bovis* and antibody responses in cows recently diagnosed with clinical infection. *Journal of Dairy Science*, *101*(1), 584-589.

Hazelton, M. S., Morton, J. M., Parker, A. M., Sheehy, P. A., Bosward, K. L., Malmo, J., & House, J. K. (2020c). Whole dairy herd sampling to detect subclinical intramammary *Mycoplasma bovis* infection after clinical mastitis outbreaks. *Veterinary Microbiology*, *244*, 108662. https://doi.org/https://doi.org/10.1016/j.vetmic.2020.108662

Held, P. (2018). Using phenol red to assess pH in tissue culture media. *BioTek Application Note* 1-7.

Heller, M., Schwarz, R., Noe, G., Jores, J., Fischer, A., Schubert, E., & Sachse, K. (2015). First human case of severe septicaemia associated with *Mycoplasma capricolum* subsp. *capricolum* infection. *Journal of Medical Microbiology Case Reports*, *2*(5), e000101.

Hoelzle, K., Ade, J., & Hoelzle, L. E. (2020). Persistence in Livestock Mycoplasmas—a Key Role in Infection and Pathogenesis. *Current Clinical Microbiology Reports*, 1-9.

Homma, Y., Hiragi, S., & Fukuda, M. (2021). Rab family of small GTPases: an updated view on their regulation and functions. *The Federation of European Biochemical Societies Journal*, *288*(1), 36-55.

Horgan, C. P., Hanscom, S. R., Jolly, R. S., Futter, C. E., & McCaffrey, M. W. (2010). Rab11-FIP3 links the Rab11 GTPase and cytoplasmic dynein to mediate transport to the endosomal-recycling compartment. *Journal of Cell Science*, *123*(2), 181-191.

Hosokawa, K., Ishimaru, H., Watanabe, T., & Fujimuro, M. (2020). The lysosome pathway degrades CD81 on the cell surface by poly-ubiquitination and clathrin-mediated endocytosis. *Biological and Pharmaceutical Bulletin*, *43*(3), 540-545.

Huang, Y., Ma, T., Lau, P. K., Wang, J., Zhao, T., Du, S., Loy, M. M., & Guo, Y. (2019). Visualization of protein sorting at the trans-Golgi network and endosomes through super-resolution imaging. *Frontiers in Cell and Developmental Biology*, *7*, 181. https://www.ncbi.nlm.nih.gov/pmc/articles/PMC6733968/pdf/fcell-07-00181.pdf

Hui, W. W., Hercik, K., Belsare, S., Alugubelly, N., Clapp, B., Rinaldi, C., & Edelmann, M. J. (2018). *Salmonella enterica* serovar Typhimurium alters the extracellular proteome of macrophages and leads to the production of proinflammatory exosomes. *Infection and Immunity*, *86*(2), e00386-00317.

Ignatiadis, M., Sledge, G. W., & Jeffrey, S. S. (2021). Liquid biopsy enters the clinic—Implementation issues and future challenges. *Nature Reviews Clinical Oncology*, 1-16.

Javeed, N., Sagar, G., Dutta, S. K., Smyrk, T. C., Lau, J. S., Bhattacharya, S., Truty, M., Petersen, G. M., Kaufman, R. J., & Chari, S. T. (2015). Pancreatic cancer–derived exosomes cause paraneoplastic β-cell dysfunction. *Clinical Cancer Research*, *21*(7), 1722-1733. https://clincancerres.aacrjournals.org/content/clincanres/21/7/1722.full.pdf

Johnson, K. K., & Pendell, D. L. (2017). Market impacts of reducing the prevalence of bovine respiratory disease in United States beef cattle feedlots. *Frontiers in Veterinary Science*, *4*, 189.

Johnstone, R. M., Adam, M., Hammond, J., Orr, L., & Turbide, C. (1987). Vesicle formation during reticulocyte maturation. Association of plasma membrane activities with released vesicles (exosomes). *Journal of Biological Chemistry*, *262*(19), 9412-9420.

Jones, S., King, P. J., Antonescu, C. N., Sugiyama, M. G., Bhamra, A., Surinova, S., Angelopoulos, N., Kragh, M., Pedersen, M. W., & Hartley, J. A. (2020). Targeting of EGFR by a combination of antibodies mediates unconventional EGFR trafficking and degradation. *Scientific Reports*, *10*(1), 1-19.

Joseph, J. S., Malindisa, S. T., & Ntwasa, M. (2018). Two-dimensional (2D) and three-dimensional (3D) cell culturing in drug discovery. *Cell Culture*, *2*, 1-22.

Josi, C., Burki, S., Stojiljkovic, A., Wellnitz, O., Stoffel, M. H., & Pilo, P. (2018). Bovine Epithelial in vitro Infection Models for *Mycoplasma bovis*. *Frontiers in Cellular and Infection Microbiology*, *8*, 329. https://doi.org/10.3389/fcimb.2018.00329

Kakiuchi, T., Miyata, I., Kimura, R., Shimomura, G., Shimomura, K., Yamaguchi, S., Yokoyama, T., Ouchi, K., & Matsuo, M. (2021). Clinical evaluation of a novel point-of-care assay to detect *Mycoplasma pneumoniae* and associated macrolide resistant mutations. *Journal of Clinical Microbiology*, JCM. 03245-03220.

Karim, M. A., Samyn, D. R., Mattie, S., & Brett, C. L. (2018). Distinct features of multivesicular body-lysosome fusion revealed by a new cell-free content-mixing assay. *Traffic*, *19*(2), 138-149. https://onlinelibrary.wiley.com/doi/10.1111/tra.12543

Kaur, G., & Lakkaraju, A. (2018). Early endosome morphology in health and disease. *Retinal Degenerative Diseases*, 335-343.

Khaledi, M., Afkhami, H., Atani, Z. R., Sepehrnia, S., Atani, F. R., & Ahmadi, M. H. (2022). Novel Perspective for Treatment of *Mycoplasma* ssp. Infections: A Promising Future. *International Journal of Peptide Research and Therapeutics*, *28*(1), 1-11.

Kleinjan, M., van Herwijnen, M. J., Libregts, S. F., van Neerven, R. J., Feitsma, A. L., & Wauben, M. H. (2021). Regular industrial processing of bovine milk impacts the integrity and molecular composition of extracellular vesicles. *The Journal of Nutrition*, *151*(6), 1416-1425.

Kneipp, M. M. M. (2021). Defining and diagnosing infectious bovine keratoconjunctivitis. *Veterinary Clinics of North America - Food Animal Practice*, *37*(2), 237-252.

Kornspan, J. D., & Rottem, S. (2012). The phospholipid profile of *Mycoplasma* ssp. *Journal of Lipids*.

Kruh-Garcia, N. A., Wolfe, L. M., Chaisson, L. H., Worodria, W. O., Nahid, P., Schorey, J. S., Davis, J. L., & Dobos, K. M. (2014). Detection of *Mycobacterium tuberculosis* peptides in the exosomes of patients with active and latent *Mycobacterium tuberculosis* infection using MRM-MS. *Public Library of Science One*, *9*(7), e103811. https://www.ncbi.nlm.nih.gov/pmc/articles/PMC4117584/pdf/pone.0103811.pdf

Kumar, D., & Purohit, G. (2019). A discussion on risk factors, therapeutic approach of endometritis and metritis in cattle. *International Journal of Current Microbiology and Applied Sciences*, *8*, 403-421.

Labroussaa, F., Lebaudy, A., Baby, V., Gourgues, G., Matteau, D., Vashee, S., Sirand-Pugnet, P., Rodrigue, S., & Lartigue, C. (2016). Impact of donor–recipient phylogenetic distance on bacterial genome transplantation. *Nucleic Acids Research*, *44*(17), 8501-8511.

Lakshmi, S., Essa, M. M., Hartman, R. E., Guillemin, G. J., Sivan, S., & Elumalai, P. (2020). Exosomes in Alzheimer's disease: Potential role as pathological mediators, biomarkers and therapeutic targets. *Neurochemical Research*, 1-7.

Lapidus, L. J. (2017). Protein unfolding mechanisms and their effects on folding experiments. *F1000Research*, *6*.

Ledger, L., Eidt, J., & Cai, H. Y. (2020). Identification of antimicrobial resistance-associated genes through whole genome sequencing of *Mycoplasma bovis* isolates with different antimicrobial resistances. *Pathogens*, *9*(7), 588.

Li, H., Ouyang, Y., Sadovsky, E., Parks, W. T., Chu, T., & Sadovsky, Y. (2020). Unique microRNA signals in plasma exosomes from pregnancies complicated by preeclampsia. *Hypertension*, *75*(3), 762-771.

Li, R., Wang, J., Sun, X., Liu, L., Wang, J., & Yuan, W. (2021). Direct and rapid detection of *Mycoplasma bovis* in bovine milk samples by recombinase polymerase amplification assays. *Frontiers in Cellular and Infection Microbiology*, *11*, 59.

Li, Y., Zheng, H., Liu, Y., Jiang, Y., Xin, J., Chen, W., & Song, Z. (2011). The complete genome sequence of *Mycoplasma bovis* strain Hubei-1. *Public Library of Science One*, *6*(6), e20999.

Liu, C., Xu, X., Li, B., Situ, B., Pan, W., Hu, Y., An, T., Yao, S., & Zheng, L. (2018a). Single-exosome-counting immunoassays for cancer diagnostics. *Nano Letters*, *18*(7), 4226-4232. https://pubs.acs.org/doi/pdf/10.1021/acs.nanolett.8b01184

Liu, T.-Y., Lee, W.-J., Tsai, C.-M., Kuo, K.-C., Lee, C.-H., Hsieh, K.-S., Chang, C.-H., Su, Y.-T., Niu, C.-K., & Yu, H.-R. (2018b). Serum lactate dehydrogenase isoenzymes 4 plus 5 is a better biomarker than total lactate dehydrogenase for refractory *Mycoplasma pneumoniae* pneumonia in children. *Pediatrics & Neonatology*, *59*(5), 501-506.

Liu, Y., Deng, Z., Xu, S., Liu, G., Lin, Y., Khan, S., Gao, J., Qu, W., Kastelic, J. P., & Han, B. (2021). *Mycoplasma bovis* subverts autophagy to promote intracellular replication in bovine mammary epithelial cells cultured *in vitro*. *Veterinary Research*, *52*(1), 1-16.

Loss, H., Aschenbach, J. R., Ebner, F., Tedin, K., & Lodemann, U. (2020). Inflammatory responses of porcine MoDC and intestinal epithelial cells in a direct-contact co-culture system following a bacterial challenge. *Inflammation*, *43*(2), 552-567.

Lysnyansky, I., & Borovok, I. (2021). A GC-rich prophage-Llike genomic region of *Mycoplasma bovirhinis* HAZ141_2 carries a gene cluster encoding resistance to kanamycin and neomycin. *Antimicrobial Agents and Chemotherapy*, *65*(2), e01010-01020.

Macías, M., Alegre, E., Díaz-Lagares, A., Patiño, A., Perez-Gracia, J. L., Sanmamed, M., López-López, R., Varo, N., & González, A. (2018). Liquid biopsy: from basic research to clinical practice. *Advances in Clinical Chemistry*, *83*, 73-119.

Mallick, S., Das, J., Verma, J., Mathew, S., Maiti, T. K., & Ghosh, A. S. (2019). Role of *Escherichia coli* endopeptidases and DD-carboxypeptidases in infection and regulation of innate immune response. *Microbes and Infection*, *21*(10), 464-474.

Malm, T., Loppi, S., & Kanninen, K. M. (2016). Exosomes in Alzheimer's disease. *Neurochemistry International*, *97*, 193-199.

Malmberg, J. L., O'Toole, D., Creekmore, T., Peckham, E., Killion, H., Vance, M., Ashley, R., Johnson, M., Anderson, C., Vasquez, M., Sandidge, D., Mildenberger, J., Hull, N., Bradway, D., Cornish, T., Register, K. B., & Sondgeroth, K. S. (2020). *Mycoplasma bovis* infections in free-ranging pronghorn, Wyoming, USA. *Emerging Infectious Diseases*, *26*(12), 2807-2814. https://doi.org/10.3201/eid2612.191375

Maschalidi, S., Hässler, S., Blanc, F., Sepulveda, F. E., Tohme, M., Chignard, M., van Endert, P., Si-Tahar, M., Descamps, D., & Manoury, B. (2012). Asparagine endopeptidase controls anti-influenza virus immune responses through TLR7 activation. *Public Library of Science Pathogens*, *8*(8), e1002841-e1002841.

Matet, A., Le Flèche-Matéos, A., Doz, F., Dureau, P., & Cassoux, N. (2020). Ocular *Spiroplasma ixodetis* in newborns in France. *Emerging Infectious Diseases*, *26*(2), 340.

Mathieu, M., Martin-Jaular, L., Lavieu, G., & Théry, C. (2019). Specificities of secretion and uptake of exosomes and other extracellular vesicles for cell-to-cell communication. *Nature Cell Biology*, *21*(1), 9-17.

Maunsell, F. P., & Donovan, G. A. (2009). *Mycoplasma bovis* infections in young calves. *Veterinary Clinics of North America: Food Animal Practice*, *25*(1), 139-177.

McCarthy, M.-C., O'Grady, L., McAloon, C. G., & Mee, J. F. (2021). Longitudinal prevalence of antibodies to endemic pathogens in bulk tank milk samples from dairy herds engaged or not in contract heifer rearing. *Frontiers in Veterinary Science*, *8*.

Mehmet Akan, Hamit Kaan, M., Orkun BABACAN,, Taner ÖNCEL, & TORUN, E. (2014). Diagnosis of *Mycoplasma bovis* infection in cattle by ELISA and PCR. *Journal of Kafkas University Faculty of Veterinary Medicine*, *20*(2).

Mir, B., & Goettsch, C. (2020). Extracellular vesicles as delivery vehicles of specific cellular cargo. *Cells*, *9*(7), 1601.

Molina-Coto, R., & Lucy, M. C. (2018). Uterine inflammation affects the reproductive performance of dairy cows: A review. *Agronomía Mesoamericana*, *29*(2), 449-468.

Nicholas, R. A., Fox, L. K., & Lysnyansky, I. (2016). Mycoplasma mastitis in cattle: To cull or not to cull. *The Veterinary Journal*, *216*, 142-147.

Nishi, K., Gondaira, S., Fujiki, J., Katagata, M., Sawada, C., Eguchi, A., Iwasaki, T., Iwano, H., & Higuchi, H. (2021a). Invasion of *Mycoplasma bovis* into bovine synovial cells utilizing the clathrin-dependent endocytosis pathway. *Veterinary Microbiology*, *253*, 108956.

Nishi, K., Gondaira, S., Okamoto, M., Matsuda, K., Sato, A., Kato, T., Sasagawa, M., Tanaka, T., & Higuchi, H. (2021b). Inflammatory cytokine mRNA and protein levels in the synovial fluid of Mycoplasma arthritis calves. *Journal of Veterinary Medical Science*, 20-0491.

Nunoya, T., Omori, T., Tomioka, H., Umeda, F., Suzuki, T., & Uetsuka, K. (2020). Intracellular localization of *Mycoplasma bovis* in the bronchiolar epithelium of experimentally infected calves. *Journal of Comparative Pathology*, *176*, 14-18.

O'Connor, H. D. (2020, 22 July 2020). *Mycoplasma bovis eradication makes gains three years on from detection* https://www.beehive.govt.nz/release/mbovis-eradication-makes-gains-three-years-detection

Oliveira, T. E. S., Pelaquim, I. F., Flores, E. F., Massi, R. P., Valdiviezo, M. J. J., Pretto-Giordano, L. G., Alfieri, A. A., Saut, J. P. E., & Headley, S. A. (2020). *Mycoplasma bovis* and viral agents associated with the development of bovine respiratory disease in adult dairy cows. *Transboundary and Emerging Diseases*, *67*, 82-93.

Oliveira, T. E. S., Scuisato, G. S., Pelaquim, I. F., Cunha, C. W., Cunha, L. S., Flores, E. F., Pretto-Giordano, L. G., Lisbôa, J. A. N., Alfieri, A. A., & Saut, J. P. E. (2021). The participation of a malignant catarrhal fever virus and *Mycoplasma bovis* in the development of single and mixed infections in beef and dairy cattle with bovine respiratory disease. *Frontiers in Veterinary Science*, *8*.

Osawa, T. (2021). Predisposing factors, diagnostic and therapeutic aspects of persistent endometritis in postpartum cows. *Journal of Reproduction and Development*.

Øverbye, A., Skotland, T., Koehler, C. J., Thiede, B., Seierstad, T., Berge, V., Sandvig, K., & Llorente, A. (2015). Identification of prostate cancer biomarkers in urinary exosomes. *Oncotarget*, *6*(30), 30357. https://www.oncotarget.com/article/4851/pdf/

Palade, G. E. (1955a). A small particulate component of the cytoplasm. *The Journal of Cell Biology*, *1*(1), 59-68.

Palade, G. E. (1955b). Studies on the endoplasmic reticulum: II. Simple dispositions in cells *in situ*. *The Journal of Biophysical and Biochemical Cytology*, *1*(6), 567.

Pan, B.-T., & Johnstone, R. M. (1983). Fate of the transferrin receptor during maturation of sheep reticulocytes in vitro: selective externalization of the receptor. *Cell*, *33*(3), 967-978.

Papić, B., Golob, M., Kušar, D., Pate, M., & Zdovc, I. (2019). Source tracking on a dairy farm reveals a high occurrence of subclinical mastitis due to hypervirulent *Listeria monocytogenes* clonal complexes. *Journal of applied microbiology*, *127*(5), 1349-1361.

Parker, A., House, J., Hazelton, M., Bosward, K., Mohler, V., Maunsell, F., & Sheehy, P. (2016). Milk acidification to control the growth of *Mycoplasma bovis* and *Salmonella dublin* in contaminated milk. *Journal of Dairy Science*, *99*(12), 9875-9884.

Parker, A. M., Sheehy, P. A., Hazelton, M. S., Bosward, K. L., & House, J. K. (2018). A review of *Mycoplasma* diagnostics in cattle. *Journal of Veterinary Internal Medicine*, *32*(3), 1241-1252.

Peippo, J., Vähänikkilä, N., Mutikainen, M., Lindeberg, H., Pohjanvirta, T., Simonen, H., Pelkonen, S., & Autio, T. (2020). 110 Absence of transmission of *Mycoplasma bovis* via naturally contaminated semen during *in vitro* fertilization. *Reproduction, Fertility and Development*, *32*(2), 182-182.

Pereyre, S., & Tardy, F. (2021). Integrating the Human and Animal sides of *Mycoplasma* ssp. Resistance to Antimicrobials. *Antibiotics*, *10*(10), 1216.

Perez-Casal, J. (2020). Pathogenesis and Virulence of *Mycoplasma bovis*. *Veterinary Clinics: Food Animal Practice*, *36*(2), 269-278.

Pérez-Cruz, C., Delgado, L., López-Iglesias, C., & Mercade, E. (2015). Outer-inner membrane vesicles naturally secreted by gram-negative pathogenic bacteria. *Public Library of Science One*, *10*(1), e0116896.

Perl, D. P. (2010). Neuropathology of Alzheimer's disease. *Mount Sinai Journal of Medicine: A Journal of Translational and Personalized Medicine*, *77*(1), 32-42. https://www.ncbi.nlm.nih.gov/pmc/articles/PMC2918894/pdf/nihms-223765.pdf

Petersen, M. B., Wawegama, N. K., Denwood, M., Markham, P. F., Browning, G. F., & Nielsen, L. R. (2018). *Mycoplasma bovis* antibody dynamics in naturally exposed dairy calves according to two diagnostic tests. *BioMed Central Veterinary Research*, *14*(1), 1-10.

Pettersson, B., Uhlen, M., & Johansson, K.-E. (1996). Phylogeny of some *Mycoplasma* ssp. from ruminants based on 16S rRNA sequences and definition of a new cluster within the hominis group. *International Journal of Systematic and Evolutionary Microbiology*, *46*(4), 1093-1098.

Pham, O. H., & McSorley, S. J. (2015). Protective host immune responses to Salmonella infection. *Future Microbiology*, *10*(1), 101-110.

Pillay, P., Maharaj, N., Moodley, J., & Mackraj, I. (2016). Placental exosomes and pre-eclampsia: maternal circulating levels in normal pregnancies and, early and late onset pre-eclamptic pregnancies. *Placenta*, *46*, 18-25.

Pleguezuelos-Manzano, C., Puschhof, J., Huber, A. R., van Hoeck, A., Wood, H. M., Nomburg, J., Gurjao, C., Manders, F., Dalmasso, G., & Stege, P. B. (2020). Mutational signature in colorectal cancer caused by genotoxic pks+ *Escherichia coli*. *Nature*, *580*(7802), 269-273.

Porter, K. R. (1953). Observations on a submicroscopic basophilic component of cytoplasm. *The Journal of Experimental Medicine*, *97*(5), 727-750.

Porter, K. R., Claude, A., & Fullam, E. F. (1945). A study of tissue culture cells by electron microscopy: methods and preliminary observations. *The Journal of Experimental Medicine*, *81*(3), 233.

Pôrto, R. N. G., Junqueira-Kipnis, A. P., de Oliveira Viu, M. A., Teixeira, R. C., & Gambarini, M. L. (2021). Evaluation of activation of bovine endometrial and vaginal epithelial and blood mononuclear cells to produce nitric oxide in response to *Mycoplasma bovis, Mycoplasma bovigenitalium* and *Ureaplasma diversum*. *Acta Veterinaria*, *71*(2), 137-146.

Punyapornwithaya, V., Fox, L., Hancock, D., Gay, J., & Alldredge, J. (2010). Association between an outbreak strain causing *Mycoplasma bovis* mastitis and its asymptomatic carriage in the herd: a case study from Idaho, USA. *Preventive Veterinary Medicine*, *93*(1), 66-70.

Raiborg, C., & Stenmark, H. (2009). The ESCRT machinery in endosomal sorting of ubiquitylated membrane proteins. *Nature*, *458*(7237), 445-452.

Raymond, B., Turnbull, L., Jenkins, C., Madhkoor, R., Schleicher, I., Uphoff, C., Whitchurch, C., Rohde, M., & Djordjevic, S. (2018). *Mycoplasma hyopneumoniae* resides intracellularly within porcine epithelial cells. *Scientific Reports*, *8*(1), 1-13.

Razin, S. (2018). The Mycoplasma membrane. In *Organization of Prokaryotic Cell Membranes* (pp. 165-250). CRC Press.

Reclusa, P., Laes, J.-F., Malapelle, U., Valentino, A., Rocco, D., Gil-Bazo, I., & Rolfo, C. (2019). EML4-ALK translocation identification in RNA exosomal cargo (ExoALK) in NSCLC patients: a novel role for liquid biopsy. *Translational Cancer Research*.

Reese, M., & Dhayat, S. A. (2021). Small extracellular vesicle non-coding RNAs in pancreatic cancer: molecular mechanisms and clinical implications. *Journal of Hematology & Oncology*, *14*(1), 1-27.

Register, K. B., Boatwright, W. D., Gesy, K. M., Thacker, T. C., & Jelinski, M. D. (2018). Mistaken identity of an open reading frame proposed for PCR-based identification of *Mycoplasma bovis* and the effect of polymorphisms and insertions on assay performance. *Journal of Veterinary Diagnostic Investigation*, *30*(4), 637-641.

Register, K. B., Jelinski, M. D., Waldner, M., Boatwright, W. D., Anderson, T. K., Hunter, D. L., Hamilton, R. G., Burrage, P., Shury, T., & Bildfell, R. (2019). Comparison of multilocus sequence types found among North American isolates of *Mycoplasma bovis* from cattle, bison, and deer, 2007–2017. *Journal of Veterinary Diagnostic Investigation*, *31*(6), 899-904.

Rennoll-Bankert, K. E., Garcia-Garcia, J. C., Sinclair, S. H., & Dumler, J. S. (2015). Chromatin-bound bacterial effector ankyrin A recruits histone deacetylase 1 and modifies host gene expression. *Cellular Microbiology*, *17*(11), 1640-1652.

Rohart, F., Gautier, B., Singh, A., & Lê Cao, K.-A. (2017). mixOmics: An R package for 'omics feature selection and multiple data integration. *Public Library of Science Computational Biology*, *13*(11), e1005752.

Roier, S., Zingl, F. G., Cakar, F., Durakovic, S., Kohl, P., Eichmann, T. O., Klug, L., Gadermaier, B., Weinzerl, K., & Prassl, R. (2016). A novel mechanism for the biogenesis of outer membrane vesicles in gram-negative bacteria. *Nature Communications*, *7*(1), 1-13.

Rosenberg, E., DeLong, E. F., Lory, S., Stackebrandt, E., & Thompson, F. (2014). *The Prokaryotes: Actinobacteria*. Springer.

Russano, M., Napolitano, A., Ribelli, G., Iuliani, M., Simonetti, S., Citarella, F., Pantano, F., Dell'Aquila, E., Anesi, C., & Silvestris, N. (2020). Liquid biopsy and tumor heterogeneity in metastatic solid tumors: the potentiality of blood samples. *Journal of Experimental & Clinical Cancer Research*, *39*, 1-13.

Rydström, A., & Wick, M. J. (2007). Monocyte recruitment, activation, and function in the gut-associated lymphoid tissue during oral Salmonella infection. *The Journal of Immunology*, *178*(9), 5789-5801.

Sabir, S. R., Yeoh, S., Jackson, G., & Bayliss, R. (2017). EML4-ALK variants: biological and molecular properties, and the implications for patients. *Cancers*, *9*(9), 118.

Schibrowski, M. L., Barnes, T. S., Wawegama, N. K., Vance, M. E., Markham, P. F., Mansell, P. D., Marenda, M. S., Kanci, A., Perez-Casal, J., & Browning, G. F. (2018). The performance of three immune assays to assess the serological status of cattle experimentally exposed to *Mycoplasma bovis*. *Veterinary Sciences*, *5*(1), 27.

Schultz, K., Strait, E., Erickson, B., & Levy, N. (2012). Optimization of an antibiotic sensitivity assay for *Mycoplasma hyosynoviae* and susceptibility profiles of field isolates from 1997 to 2011. *Veterinary Microbiology*, *158*(1-2), 104-108.

Schulz, E., Karagianni, A., Koch, M., & Fuhrmann, G. (2020). Hot EVs–how temperature affects extracellular vesicles. *European Journal of Pharmaceutics and Biopharmaceutics*, *146*, 55-63.

Sepulveda, F. E., Maschalidi, S., Colisson, R., Heslop, L., Ghirelli, C., Sakka, E., Lennon-Duménil, A.-M., Amigorena, S., Cabanie, L., & Manoury, B. (2009). Critical role for asparagine endopeptidase in endocytic Toll-like receptor signaling in dendritic cells. *Immunity*, *31*(5), 737-748.

Shang, D., Xie, C., Hu, J., Tan, J., Yuan, Y., Liu, Z., & Yang, Z. (2020). Pancreatic cancer cell–derived exosomal microRNA-27a promotes angiogenesis of human microvascular endothelial cells in pancreatic cancer via BTG2. *Journal of Cellular and Molecular Medicine*, *24*(1), 588-604.

Sharma, S., Tivendale, K. A., Markham, P. F., & Browning, G. F. (2015). Disruption of the membrane nuclease gene (MBOVPG45_0215) of *Mycoplasma bovis* greatly reduces cellular nuclease activity. *Journal of Bacteriology*, *197*(9), 1549-1558.

Shekhawat, S. D., Purohit, H. J., Taori, G. M., Daginawala, H. F., & Kashyap, R. S. (2016). Evaluation of heat shock proteins for discriminating between latent tuberculosis infection and active tuberculosis: A preliminary report. *Journal of Infection and Public Health*, *9*(2), 143-152.

Sheridan, C. (2016). Exosome cancer diagnostic reaches market. *Nature Biotechnology*, *34*(4), 359-360. https://doi.org/10.1038/nbt0416-359

Shinde, S. R., & Maddika, S. (2018). Post translational modifications of Rab GTPases. *Small GTPases*, *9*(1-2), 49-56.

Shirejini, S. Z., & Inci, F. (2021). The Yin and Yang of exosome isolation methods: Conventional practice, microfluidics, and commercial kits. *Biotechnology Advances*, 107814.

Siegl, C., & Rudel, T. (2015). Modulation of p53 during bacterial infections. *Nature Reviews Microbiology*, *13*(12), 741-748.

Skog, J., Würdinger, T., Van Rijn, S., Meijer, D. H., Gainche, L., Curry, W. T., Carter, B. S., Krichevsky, A. M., & Breakefield, X. O. (2008). Glioblastoma microvesicles transport RNA and proteins that promote tumour growth and provide diagnostic biomarkers. *Nature Cell Biology*, *10*(12), 1470-1476.

Smith, V. L., Cheng, Y., Bryant, B. R., & Schorey, J. S. (2017). Exosomes function in antigen presentation during an *in vivo Mycobacterium tuberculosis* infection. *Scientific Reports*, *7*(1), 1-12.

Sork, H., Corso, G., Krjutskov, K., Johansson, H. J., Nordin, J. Z., Wiklander, O. P., Lee, Y. X. F., Westholm, J. O., Lehtiö, J., & Wood, M. J. (2018). Heterogeneity and interplay of the extracellular vesicle small RNA transcriptome and proteome. *Scientific Reports*, *8*(1), 1-12.

Stuffers, S., Sem Wegner, C., Stenmark, H., & Brech, A. (2009). Multivesicular endosome biogenesis in the absence of ESCRTs. *Traffic*, *10*(7), 925-937. https://onlinelibrary.wiley.com/doi/10.1111/j.1600-0854.2009.00920.x

Sulyok, K. M., Bekő, K., Kreizinger, Z., Wehmann, E., Jerzsele, Á., Rónai, Z., Turcsányi, I., Makrai, L., Szeredi, L., & Jánosi, S. (2018). Development of molecular methods for the rapid detection of antibiotic susceptibility of *Mycoplasma bovis*. *Veterinary Microbiology*, *213*, 47-57.

Sung, H., Ferlay, J., Siegel, R. L., Laversanne, M., Soerjomataram, I., Jemal, A., & Bray, F. (2021). Global cancer statistics 2020: GLOBOCAN estimates of incidence and mortality worldwide for 36 cancers in 185 countries. *CA: A Cancer Journal for Clinicians*, *71*(3), 209-249. https://acsjournals.onlinelibrary.wiley.com/doi/10.3322/caac.21660

Szacawa, E., Szymańska-Czerwińska, M., Niemczuk, K., Dudek, K., Bednarek, D., & Ayling, R. D. (2016). Comparison of serological, molecular and cultural diagnostic methods for the detection of *Mycoplasma bovis* infections in cattle. *Animal Science Papers & Reports*, *34*(4).

Takahashi, K., Ota, Y., Kogure, T., Suzuki, Y., Iwamoto, H., Yamakita, K., Kitano, Y., Fujii, S., Haneda, M., & Patel, T. (2020). Circulating extracellular vesicle-encapsulated HULC is a potential biomarker for human pancreatic cancer. *Cancer Science*, *111*(1), 98-111.

Théry, C., Witwer, K. W., Aikawa, E., Alcaraz, M. J., Anderson, J. D., Andriantsitohaina, R., Antoniou, A., Arab, T., Archer, F., & Atkin-Smith, G. K. (2018). Minimal information for studies of extracellular vesicles 2018 (MISEV2018): a position statement of the International Society for Extracellular Vesicles and update of the MISEV2014 guidelines. *Journal of Extracellular Vesicles*, *7*(1), 1535750.

Thomas, A., Dizier, I., Trolin, A., Mainil, J., & Linden, A. (2002). Comparison of sampling procedures for isolating pulmonary *Mycoplasma* ssp. in cattle. *Veterinary Research Communications*, *26*(5), 333-339.

Timonen, A. A., Katholm, J., Petersen, A., Mõtus, K., & Kalmus, P. (2017). Within-herd prevalence of intramammary infection caused by *Mycoplasma bovis* and associations between cow udder health, milk yield, and composition. *Journal of Dairy Science*, *100*(8), 6554-6561.

Tulkens, J., De Wever, O., & Hendrix, A. (2020). Analyzing bacterial extracellular vesicles in human body fluids by orthogonal biophysical separation and biochemical characterization. *Nature protocols*, *15*(1), 40-67.

Tully, J. (2012). *The Mycoplasmas V2: Human and Animal Mycoplasmas*. Elsevier.

Tutrone, R., Donovan, M. J., Torkler, P., Tadigotla, V., McLain, T., Noerholm, M., Skog, J., & McKiernan, J. (2020). Clinical utility of the exosome based ExoDx Prostate (IntelliScore) EPI test in men presenting for initial biopsy with a PSA 2–10 ng/mL. *Prostate Cancer and Prostatic Diseases*, *23*(4), 607-614.

Uddin, M., Kabir, M., Jeandet, P., Mathew, B., Ashraf, G. M., Perveen, A., Bin-Jumah, M. N., Mousa, S. A., & Abdel-Daim, M. M. (2020). Novel anti-Alzheimer's therapeutic molecules targeting amyloid precursor protein processing. *Oxidative Medicine and Cellular Longevity*, *2020*.

Vagner, T., Spinelli, C., Minciacchi, V. R., Balaj, L., Zandian, M., Conley, A., Zijlstra, A., Freeman, M. R., Demichelis, F., & De, S. (2018). Large extracellular vesicles carry most of the tumour DNA circulating in prostate cancer patient plasma. *Journal of Extracellular Vesicles*, *7*(1), 1505403.

Vähänikkilä, N., Pohjanvirta, T., Haapala, V., Simojoki, H., Soveri, T., Browning, G., Pelkonen, S., Wawegama, N., & Autio, T. (2019). Characterisation of the course of *Mycoplasma bovis* infection in naturally infected dairy herds. *Veterinary Microbiology*, *231*, 107-115.

Valadi, H., Ekström, K., Bossios, A., Sjöstrand, M., Lee, J. J., & Lötvall, J. O. (2007). Exosome-mediated transfer of mRNAs and microRNAs is a novel mechanism of genetic exchange between cells. *Nature Cell Biology*, *9*(6), 654-659. https://www.nature.com/articles/ncb1596.pdf

van de Graaf, S. F., Rescher, U., Hoenderop, J. G., Verkaart, S., Bindels, R. J., & Gerke, V. (2008). TRPV5 is internalized via clathrin-dependent endocytosis to enter a Ca2+-controlled recycling pathway. *Journal of Biological Chemistry*, *283*(7), 4077-4086.

Van Niel, G., d'Angelo, G., & Raposo, G. (2018). Shedding light on the cell biology of extracellular vesicles. *Nature Reviews Molecular Cell Biology*, *19*(4), 213-228. https://www.nature.com/articles/nrm.2017.125.pdf

VanCleave, T. T., Pulsifer, A. R., Connor, M. G., Warawa, J. M., & Lawrenz, M. B. (2017). Impact of gentamicin concentration and exposure time on intracellular *Yersinia pestis*. *Frontiers in Cellular and Infection Microbiology*, *7*, 505.

Venables, W. N., & Ripley, B. D. (2013). Modern applied statistics with S-PLUS. *Springer Science & Business Media*.

Verdera, H. C., Gitz-Francois, J. J., Schiffelers, R. M., & Vader, P. (2017). Cellular uptake of extracellular vesicles is mediated by clathrin-independent endocytosis and macropinocytosis. *Journal of Controlled Release*, *266*, 100-108.

Vizarraga, D., Kawamoto, A., Matsumoto, U., Illanes, R., Pérez-Luque, R., Martín, J., Mazzolini, R., Bierge, P., Pich, O. Q., & Espasa, M. (2020). Immunodominant proteins P1 and P40/P90 from human pathogen *Mycoplasma pneumoniae*. *Nature Communications*, *11*(1), 1-16.

Wawegama, N. K., Browning, G. F., Kanci, A., Marenda, M. S., & Markham, P. F. (2014). Development of a recombinant protein-based enzyme-linked immunosorbent assay for diagnosis of *Mycoplasma bovis* infection in cattle. *Clinical and Vaccine Immunology*, *21*(2), 196-202.

Wawegama, N. K., Markham, P. F., Kanci, A., Schibrowski, M., Oswin, S., Barnes, T. S., Firestone, S. M., Mahony, T. J., & Browning, G. F. (2016). Evaluation of an IgG enzyme-linked immunosorbent assay as a serological assay for detection of *Mycoplasma bovis* infection in feedlot cattle. *Journal of Clinical Microbiology*, *54*(5), 1269-1275. https://www.ncbi.nlm.nih.gov/pmc/articles/PMC4844740/pdf/zjm1269.pdf

Wei, D., Zhan, W., Gao, Y., Huang, L., Gong, R., Wang, W., Zhang, R., Wu, Y., Gao, S., & Kang, T. (2021). RAB31 marks and controls an ESCRT-independent exosome pathway. *Cell Research*, *31*(2), 157-177.

Wei, J., Noto, J. M., Zaika, E., Romero-Gallo, J., Piazuelo, M. B., Schneider, B., El-Rifai, W., Correa, P., Peek, R. M., & Zaika, A. I. (2015). Bacterial CagA protein induces degradation of p53 protein in a p14ARF-dependent manner. *Gut*, *64*(7), 1040-1048.

Wilburn, K. M., Fieweger, R. A., & VanderVen, B. C. (2018). Cholesterol and fatty acids grease the wheels of *Mycobacterium tuberculosis* pathogenesis. *Pathogens and Disease*, *76*(2), fty021.

Wisselink, H. J., Smid, B., Plater, J., Ridley, A., Andersson, A.-M., Aspán, A., Pohjanvirta, T., Vähänikkilä, N., Larsen, H., & Høgberg, J. (2019). A European interlaboratory trial to evaluate the performance of different PCR methods for *Mycoplasma bovis* diagnosis. *BioMed Central Veterinary Research*, *15*(1), 1-12.

Witwer, K. W., Van Balkom, B. W., Bruno, S., Choo, A., Dominici, M., Gimona, M., Hill, A. F., De Kleijn, D., Koh, M., & Lai, R. C. (2019). Defining mesenchymal stromal cell (MSC)-derived small extracellular vesicles for therapeutic applications. *Journal of Extracellular Vesicles*, *8*(1), 1609206.

Woith, E., Fuhrmann, G., & Melzig, M. F. (2019). Extracellular vesicles—connecting kingdoms. *International Journal of Molecular Sciences*, *20*(22), 5695.

Yang, D., Zhang, W., Zhang, H., Zhang, F., Chen, L., Ma, L., Larcher, L. M., Chen, S., Liu, N., & Zhao, Q. (2020). Progress, opportunity, and perspective on exosome isolation-efforts for efficient exosome-based theranostics. *Theranostics*, *10*(8), 3684.

Yin, Y.-D., Wang, R., Zhuo, C., Wang, H., Wang, M.-G., Xie, C.-M., She, D.-Y., Yuan, X., Wang, R.-T., & Cao, B. (2017). Macrolide-resistant *Mycoplasma pneumoniae* prevalence and clinical aspects in adult patients with community-acquired pneumonia in China: a prospective multicenter surveillance study. *Journal of Thoracic Disease*, *9*(10), 3774.

Yoshida, A., Sakai, N., Uekusa, Y., Imaoka, Y., Itagaki, Y., Suzuki, Y., & Yoshimura, S. H. (2018). Morphological changes of plasma membrane and protein assembly during clathrin-mediated endocytosis. *Public Library of Science Biology*, *16*(5), e2004786.

Yu, W., Hurley, J., Roberts, D., Chakrabortty, S., Enderle, D., Noerholm, M., Breakefield, X., & Skog, J. (2021). Exosome-based liquid biopsies in cancer: Opportunities and challenges. *Annals of Oncology*.

Zbinden, C., Pilo, P., Frey, J., Bruckmaier, R. M., & Wellnitz, O. (2015). The immune response of bovine mammary epithelial cells to live or heat-inactivated *Mycoplasma bovis*. *Veterinary Microbiology*, *179*(3-4), 336-340.

Zhang, H., Hu, G., Lu, D., Zhao, G., Zhang, Y., Zubair, M., Chen, Y., Hu, C., Chen, X., & Chen, J. (2021). Comparative secretome analyses of *Mycoplasma bovis* virulent and attenuated strains revealed MbovP0145 as a promising diagnostic biomarker. *Frontiers in Veterinary Science*, *8*.

Zhang, W., & Lin, Y. (2021). The mechanism of asparagine endopeptidase in the progression of malignant tumors: A review. *Cells*, *10*(5), 1153.

Zheng, L., Leung, E. T., Wong, H., Lui, G., Lee, N., To, K.-F., Choy, K., Chan, R. C., & Ip, M. (2016). Unraveling methylation changes of host macrophages in *Mycobacterium tuberculosis* infection. *Tuberculosis*, *98*, 139-148.

Zhou, B., Xu, K., Zheng, X., Chen, T., Wang, J., Song, Y., Shao, Y., & Zheng, S. (2020). Application of exosomes as liquid biopsy in clinical diagnosis. *Signal Transduction and Targeted Therapy*, *5*(1), 1-14.

Zhu, J., Cai, L., Yang, H., Wen, Y., Wang, J., Rong, T., Shao, J., & Zhang, L. (2014). Echinoderm microtubule-associated protein-like 4-anaplastic lymphoma kinase rearrangement and epidermal growth factor receptor mutation coexisting in Chinese patients with lung adenocarcinoma. *Thoracic Cancer*, *5*(5), 411-416.

Zimmerman, B., Kelly, B., McMillan, B. J., Seegar, T. C., Dror, R. O., Kruse, A. C., & Blacklow, S. C. (2016). Crystal structure of a full-length human tetraspanin reveals a cholesterol-binding pocket. *Cell*, *167*(4), 1041-1051. e1011.

Zoumpopoulou, G., Tsakalidou, E., Dewulf, J., Pot, B., & Grangette, C. (2009). Differential crosstalk between epithelial cells, dendritic cells and bacteria in a co-culture model. *International Journal of Food Microbiology*, *131*(1), 40-51.